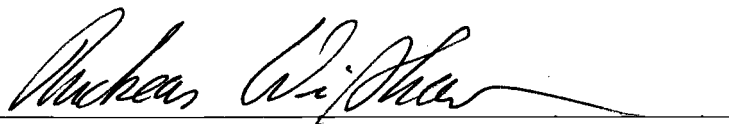


AN ABSTRACT OF THE DISSERTATION OF

Iva Orhanovic for the degree of Doctor of Philosophy in Electrical and Computer Engineering presented on May 28, 2004.

Title: Processing Sequences of Chromatophore Images with Application to Signal Transduction Pathway Modeling.

Abstract approved:



---

Andreas Weisshaar

Systems biology is becoming increasingly important for the study of living organisms. It focuses on the mathematical understanding of biological systems. Cells, the basic units of all living creatures, are biological systems of major interest. Considerable work is being done towards modeling cells as mathematical systems.

At the same time, great effort has been made in an attempt to use chromatophore cells as biosensors for various substances. The results of changes in these cells induced by various substances can be seen under the microscope. Therefore, efficient digital image and video processing algorithms are required to help extract these changes.

This dissertation establishes a link between the biological aspect of chromatophores and digital image/video processing techniques used for chromatophore characterization. A complete model of the  $G_s$ -AC-PKA-granule motion signal transduction pathway is proposed, starting from the input ligand and ending in features extracted from the microscope image. The model is developed by extending an existing system biology differential equation based model of the  $G_s$ -AC-PKA transduction pathway obtained from the Database of Quantitative Cellular Signaling (DQCS). The extension of the

model is founded on physical assumptions about the dynamic behavior of pigment granules as well as on image feature extraction. Several image and video processing methods have been either newly developed or adapted for the characterization of pigment granule distribution images. Examples are presented to demonstrate the effectiveness of the developed image processing methods and of the proposed system model.

Processing Sequences of Chromatophore Images with Application to Signal  
Transduction Pathway Modeling

by  
Iva Orhanovic

A DISSERTATION  
submitted to  
Oregon State University

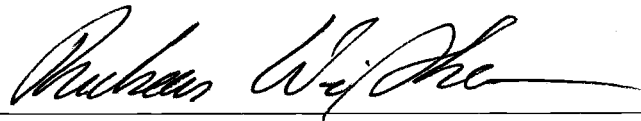
in partial fulfillment of  
the requirements for the  
degree of

Doctor of Philosophy

Presented May 28, 2004  
Commencement June 2005

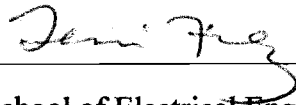
Doctor of Philosophy dissertation of Iva Orhanovic presented on May 28, 2004.

APPROVED:



---

Major Professor, representing Electrical and Computer Engineering



---

Director of the School of Electrical Engineering and Computer Science



---

Dean of the Graduate School

I understand that my dissertation will become part of the permanent collection of Oregon State University libraries. My signature below authorizes release of my dissertation to any reader upon request.



---

Iva Orhanovic, Author

## ACKNOWLEDGMENTS

I carried out my Ph. D. research while staying at home with two young daughters.

I would like to express my sincere thanks to Dr. Regis J. Crinon, my thesis advisor, for many helpful discussions, suggestions, his time and patience during this research.

I also extend thanks to Prof. Wojtek J. Kolodziej for introducing me to the Cytosensor project, his advice and directions on this research.

I wish to thank Prof. Frank W. R. Chaplen for his invaluable biology input.

I am also very grateful to Prof. Andreas Weisshaar for replacing Dr. Kolodziej (after his leave) as the major Professor.

I would also like to thank Prof. Gabor Temes and Prof. Yun-Shik Lee for being my committee members.

Thanks to everyone from the Cytosensor team who helped.

Very special thanks to my husband Neven.

Special thanks as well to my mother Visnja Henc-Bartolic, my childhood English teacher Vera Arbanas-Smolkovic, and Dejan Senic who helped in an indirect way.

## TABLE OF CONTENTS

	<u>Page</u>
1 Introduction .....	1
2 Pigment Granule Transport in Fish Chromatophores .....	5
2.1 Introduction .....	5
2.2 Chromatophores .....	5
2.3 Microtubule Motors and Transport .....	7
2.4 Signal Transduction .....	10
2.4.1 Introduction .....	10
2.4.2 G-protein Mediated Pathway .....	13
2.4.2.1 G-protein Linked Receptors .....	13
2.4.2.2 Heterotrimeric G-protein .....	14
2.4.2.3 Adenylyl Cyclase Enzyme .....	17
2.4.2.4 Cyclic AMP – a Second Messenger .....	17
2.4.3 Protein Phosphorylation/Dephosphorylation .....	19
2.4.3.1 Protein Kinase A – cAMP Dependant Kinase .....	19
2.4.3.2 Protein Phosphatase .....	21
2.4.4 Signal Transduction in Fish Chromatophores .....	21
3 Image and Video Processing of Pigment Granule Distribution Sequences in Fish Chromatophores .....	23
3.1 Introduction .....	23
3.2 Chromatophore Perception and Acquisition .....	24
3.3 Color to Gray Scale Conversion Using Principal Component Analysis ...	27
3.4 Global Motion Estimation Using Optical Flow Equation Model .....	31
3.4.1 Introduction .....	31
3.4.2 Optical Flow Equation Methods .....	31
3.4.2.1 Limitations .....	32

## TABLE OF CONTENTS (Continued)

	<u>Page</u>
3.4.2.2 Additional Constraints .....	32
3.4.3 Lucas – Kanade Model .....	33
3.4.4 Shifted Chromatophore Pigment Distribution Experiment .....	34
3.4.5 Iterative Correction .....	36
3.4.6 Global Motion Estimation Using the Corrected Lucas–Kanade Model	36
3.4.6.1 Test 3-1 .....	36
3.4.6.2 Test 3-1 Results .....	37
3.5 Segmentation of Chromatophore Pigment Granule Distribution Images ..	38
3.5.1 Introduction .....	38
3.5.2 Fundamental Ideas Behind Proposed Segmentation Approach .....	40
3.5.3 Proposed Segmentation Method .....	42
3.5.3.1 Overview of Thresholding Procedure .....	43
3.5.3.2 Statistical Parameter .....	45
3.5.3.3 Interpolation Function .....	46
3.5.3.4 Rectangle Selection .....	46
3.5.3.5 Stopping Criterion of the Square Growth .....	46
3.5.3.6 Error Evaluation at the Image Center .....	48
3.5.3.7 Subdivision of the Image into Smaller Images .....	48
3.5.3.8 First Segmentation .....	49
3.5.3.9 Repeated Segmentation .....	49
3.5.4 Segmentation Examples .....	50
3.5.4.1 Example 3-1 .....	50
3.5.4.2 Example 3-2 .....	55
3.5.4.3 Example 3-3 .....	57
3.6 Feature Extraction of Chromatophore Pigment Granule Distributions by Fitting an Analytical Model .....	59

## TABLE OF CONTENTS (Continued)

	<u>Page</u>
3.6.1 Introduction .....	59
3.6.2 Analytical Model of Chromatophore Pigment Granule Distributions	60
3.6.3 Pigment Granule Distribution Model Equations .....	61
3.6.4 Finding the Pigment Granule Distribution Center .....	64
3.6.5 Pigment Granule Distribution Modeling Example .....	66
4 Mathematical Model of the $G_s$ -AC-PKA Signal Transduction Pathway from the Chemical Reception Signal to the Image Sequence .....	69
4.1 Introduction .....	69
4.2 Fundamentals of Chemical Reaction Modeling .....	69
4.2.1 Simple Reactions .....	70
4.2.2 Model Variables; Units of Measurement; Notation .....	71
4.2.3 Rates of Reactions; The Rate Law .....	72
4.2.4 Stoichiometric Networks; Graph Representation .....	73
4.2.5 Graphical Representation of Biochemical Reactions; Signaling Pathways .....	74
4.3 DQCS Database .....	75
4.4 $G_s$ -AC-PKA Pathway Model .....	75
4.4.1 G-protein Activation .....	76
4.4.2 AC Pathway .....	76
4.4.3 PKA Pathway .....	77
4.5 Mathematical Model of $G_s$ -AC-PKA Pathway .....	78
4.5.1 $G_s$ -AC-PKA Pathway Differential Equations and Nonzero Initial Conditions .....	78
4.5.2 $G_s$ -AC-PKA Pathway Response .....	81
4.6 Link Between Pathway and Visual Image .....	83
4.6.1 Model of Pigment granule Motion: Average Cell Approach .....	84



## TABLE OF CONTENTS (Continued)

	<u>Page</u>
4.6.1.1 Model Initial Conditions .....	86
4.6.1.2 Model Calibration .....	86
4.6.2 Modeling Example 4-1: Average Cell Approach .....	87
4.6.3 Model of Pigment Granule Motion: Individual Cell Approach .....	90
4.6.4 Modeling Example 4-2: Individual Cell Approach .....	93
4.6.5 Average Cell Modeling Approach Applied to Single Cell .....	96
5 Conclusion .....	97
Bibliography .....	99

## LIST OF FIGURES

<u>Figure</u>		<u>Page</u>
2-1	Movement of pigment granules: dispersed and aggregated pigment granules in chromatophores .....	6
2-2	Centrosome with attached microtubules .....	7
2-3	ATP hydrolysis .....	8
2-4	Microtubule motor protein (kinesin) .....	9
2-5	The movement of the motor protein (kinesin) along microtubules .....	10
2-6	Chemical structure of ATP .....	11
2-7	Signaling by phosphorylation/dephosphorylation .....	13
2-8	A schematic drawing of a G-protein-linked receptor .....	14
2-9	GTP (guanosine-5'-triphosphate) .....	15
2-10	GTP-GDP exchange .....	15
2-11	The G-protein activation/inactivation cycle .....	16
2-12	Cyclic AMP .....	18
2-13	The pathway by which a G-protein-linked cell-surface receptor generates a cAMP second messenger .....	18
2-14	The synthesis and degradation of cAMP .....	19
2-15	The activation of cAMP dependent PKA .....	20
2-16	The signal transduction pathway in fish chromatophores .....	22
3-1	Block diagram of methods presented in Chapter 3 .....	23
3-2	A sequence of pictures from a biological experiment that results in the movement of pigment granules in chromatophores .....	25

## LIST OF FIGURES (Continued)

<u>Figure</u>	<u>Page</u>
3-19	Final result after passing the segmented image of Figure 3-16 Through a simple filter of isolated patches ..... 54
3-20	Result after filtering the noisiest segmented image of Figure 3-18 ..... 55
3-21	Original image 2 ..... 56
3-22	Image 2 after performing proposed segmentation without filtering ..... 56
3-23	Original image 3 ..... 57
3-24	Image 3 after segmentation ..... 58
3-25	Segmented and filtered image 3 ..... 58
3-26	Pigment granule distribution of a single cell: (a) Intensity $I(x,y)$ ; (b) $1-I(x,y)$ 60
3-27	Pigment distribution function $g(x,y)$ and its model $f(x,y)$ ..... 61
3-28	Variation of intensity $I(x,y)$ for typical fish chromatophore: original grayscale image; (b) image filtered with $20 \times 20$ pixel half wave cosine filter, $\text{filter}(I(x,y))$ ; (c) surface plot of $1 - I(x,y)$ ; (d) surface plot of $1 - \text{filter}(I(x,y))$ ..... 66
3-29	Chromatophore pigment granule distribution modeling: (a) Original image with calculated positions of pigment distribution centers shown as white dots; (b) Image plot of $b$ coefficient calculated for every point of the image; (a) Image plot of $a = \sqrt{a_1^2 + a_2^2}$ , (d) Image plot of $b \sqrt{a}$ ..... 67
4-1	Two simplified graphical views of chemical reaction (4) ..... 74
4-2	Graphical representation of biochemical reactions along pathways: (a) reaction catalyzed by an enzyme; (b) main and side substrates ..... 74
4-3	Layout of G-protein activation pathway ..... 76
4-4	Layout of AC pathway ..... 77

## LIST OF FIGURES (Continued)

<u>Figure</u>	<u>Page</u>
4-5	Layout of PKA pathway ..... 77
4-6	Summary of $G_s$ -AC-PKA pathway ..... 78
4-7	Pathway model response for input ligand concentration $10^5 L_0$ ..... 81
4-8	Pathway model response for input ligand concentration of $10^2 L_0$ ..... 82
4-9	Pathway model response for input ligand concentration of $L_0$ ..... 82
4-10	Model of average pigment granule distribution with selected pigment granules marking the outer border of the visible pigment distribution: (a) at the time $t$ , (b) at $t+\Delta t$ ..... 84
4-11	First image in 150 image sequence of Example 4-1 ..... 87
4-12	Middle image in 150 image sequence of Example 4-1 ..... 88
4-13	Last image in 150 image sequence of Example 4-1 ..... 88
4-14	Area of pigment granules from pathway model and from measurement ... 89
4-15	Pathway substrate response for Example 4-1 ..... 90
4-16	Definition of effective width of $f(0,y)$ ..... 91
4-17	Image for calibrating individual cell model ( $t = 0$ s) ..... 94
4-18	Image for calibrating individual cell model ( $t = 59$ s) ..... 94
4-19	Image for calibrating individual cell model ( $t = 103$ s) ..... 95
4-20	Comparison of model widths predicted by pathway model (system model) And computed directly from the image sequence (measured) ..... 95
4-21	Comparison of pigmented areas predicted by pathway model (system model) and computed directly from the image sequence (measured) ..... 96

## Abbreviations

AC	adenylyl cyclase
ADP	adenosine diphosphate
ATP	adenosine triphosphate
cAMP	adenosine 3',5'-cyclic monophosphate
DQCS	Database of Quantitative Cellular Signaling
GDP	guanosine diphosphate
G-protein	guanosine triphosphate binding regulatory protein
G <sub>i</sub> -protein	inhibitory guanosine triphosphate binding regulatory protein
G <sub>s</sub> -protein	stimulatory guanosine triphosphate binding regulatory protein
GTP	guanosine triphosphate
H or L	ligand
KL	Karhunen-Loeve transform
MTOC	microtubule organizing center
PCA	principal component analysis
P <sub>i</sub>	inorganic phosphate group
PKA	protein kinase A
R	receptor

## **Chapter 1**

### **Introduction**

Systems biology is a new science field that combines classical molecular and cell biology with systems theory and focuses on the new forms of behavior that emerge when systems of genes and proteins are studied in a unified way. This “kind” of biology is computer-based in order to construct explicit models of biological systems [1], [2].

Cells are biological systems. They are unique systems because of their small size and high system complexity. Cells are small membrane-bounded compartments filled with a concentrated aqueous solution of chemicals. All living creatures are made of these systems including such complex organisms as the human being [3].

The ultimate aim of system biology is the development of a “virtual organism”. In order to reach this aim, it is necessary to develop a “virtual cell” by constructing explicit models of the cell’s intricate signal transduction pathways. The challenge in modeling a cell is that a “virtual cell” should resemble a real cell. At this time, enough is known about cells so that system modeling is possible. Nevertheless, there is no obvious limit on how much more needs to be learned to fully understand cells. As a consequence, modeling is a process in constant progress. In other words, the more that is learned about cells, the more needs to be taken into account in the model. System biology cell modeling is a joint work of a large number of researchers in different fields (e.g., biology, bioengineering, chemical engineering, physics, mechanical engineering, electrical engineering, computer engineering, mathematics, statistics, computer science).

Current models of cells are constructed at different levels of sophistication and at a variety of scales. Modeling takes a number of forms from the description of the network

interaction topology (network graphs), through models that take into account the Boolean interactions between molecules or other entities, to quantitative modeling using sets of differential equations. These models encapsulate the current understanding of a cell system and a living creature as a whole system. They enable predictions of how these systems should respond, and help in the design of experiments to improve the current understanding. System biology modeling will advance medicine, pharmacology, toxicology, genetics, and other disciplines.

This dissertation deals with the biological systems of chromatophores. Chromatophores are colored cells whose color intensity changes are brought about by an active redistribution of pigment-containing organelles. Transfections of these systems with selected receptors enable the detection of various substances [4]. Also, the effect of an applied drug can be detected by means of the induced color intensity change in the system and it can be used for toxicological and pharmacological studies. Redistribution of pigment is easily seen under the microscope.

A lot of research has been done on chromatophores involving several scientific fields. This includes a substantial number of different biological studies which identify the  $G_s$ -AC-PKA (stimulatory guanosine triphosphate binding regulatory protein-adenylyl cyclase-protein kinase A) signal transduction pathway (e.g., [3]–[7]). The use of chromatophores as biosensors has been examined in [4]. Substantial research towards the development of biological sensors using signal processing in sensor arrays has been done [8]. Microtubule dependent dispersion and aggregation of pigment granules in chromatophores has been studied, identifying kinesin and dynein as motor proteins [3], [9]. A differential equation based model of the  $G_s$ -AC-PKA signal transduction pathway has been proposed in [10]. Nevertheless, a complete, unified model of the  $G_s$ -AC-PKA-pigment granule motion pathway has not been developed to this date.

The main goal of this dissertation is to develop a system level model of a fish chromatophore cell that relates the applied chemical to features of a microscope image.

The model is constructed through a link between the biological aspect of chromatophores and digital image/video processing techniques developed for sequences of chromatophore microscope images. The link is established in the form of an extension to an existing system biology differential equation based model of the  $G_s$ -AC-PKA pathway. This differential equation based model is obtained from the Database of Quantitative Cellular Signaling (DQCS) [10]. Differential equation based models of biological reaction pathways are the most detailed quantitative pathway models available at this time. They contain a time domain mathematical relationship between concentrations of the chemicals involved in the reaction pathway. The current knowledge of the main chromatophore signal transduction pathway provides an incomplete model that is disconnected from motor transport proteins (kinesin, dynein), which are thought to be involved in pigment granule motion [3]. The missing connection is built in this work based on a physical model that makes simple assumptions about the shape of an average pigment distribution and about the velocities of the pigment granules.

The second goal of this work is the development of digital image and video processing algorithms for chromatophore image sequences. Color to gray-scale conversion using principal component analysis has been performed. A segmentation algorithm for poorly illuminated chromatophore pigment granule distribution images has been developed. Also, global motion estimation using the optical flow equation method has been applied to sequences of chromatophore pigment granule distribution images. Furthermore, the study of feature extraction of chromatophore pigment granule distribution by an analytical model has been performed.

In Chapter 2 of this dissertation, the biological background material on pigment granule in fish chromatophores has been provided. It covers chromatophores, microtubule motors, transport, and signal transduction. Chapter 3 presents image and video processing techniques that have been developed for pigment granule distribution sequences in fish chromatophores. In Chapter 4, the mathematical model of the  $G_s$ -AC-PKA signal



transduction pathway is described and linked with the image processing techniques of Chapter 3. Finally, in Chapter 5, concluding remarks on this work are made.

## **Chapter 2**

### **Pigment Granule Transport in Fish Chromatophores**

#### **2.1 Introduction**

This chapter introduces the biological background needed for understanding the visible behavior of fish chromatophores. It also illustrates the basic chemical mechanisms behind pigment granule transport in fish chromatophore cells. The theory presented here is provided both for completeness and for easier understanding of the ideas that appear in later chapters.

#### **2.2 Chromatophores**

Some vertebrates such as fish, amphibians, and reptiles, and many invertebrates, have adaptable color patterned integument (skin). Chromatophores are specialized pigment cells in the integument that mediate the color. They synthesize and store pigments. Chromatophores possess thousands of pigment granules, membrane bound organelles which contain color pigment. Changes in the distribution of pigment granules permit an animal to display variations in color.

The color of the integument is a result of absorption and reflection of light rays of certain wavelengths. The coloration can change quickly in response to changes in the environment, such as photic or thermal variations. An adaptable color pattern integument can for instance be used for camouflage, sun protection, thermoregulation, and social interactions.

The morphology of the chromatophores varies from highly dendritic to discoid shape, depending on the location in the animal and on animal species.

There are six kinds of chromatophores, each recognized by its color. They are the melanophores (black), erythrophores (red), cyanophores (blue), xanthophores (yellow), leucophores (white), and iridophores (metallic). Leucophores and iridophores lack color.

When variations in the environment are detected, the animal regulates its colors and patterns via communicating nerve cells and hormones in the blood stream, which affect the chromatophores. Hormones and neurotransmitters act on transmembrane receptors located on the chromatophore cell surface. For example, the drugs clonidine, neurotoxin, nonrepeneprine, and melanocorticotrophic hormone can induce movement of color-filled pigment granules. In response to these hormonal or neural stimulations, the pigment granules are transported along parts of the cell's cytoskeleton (along microtubules) at rates of about  $1 \mu\text{m/s}$ , either towards or away from the cell center. When pigment granules are dispersed throughout the cell, the cell is uniformly color pigmented. The chromatophores hide the color of background cells and the animal bearing such cells appears darkly colored. On the other hand, when pigment granules are aggregated in the cell center, most of the cell is unpigmented, and colors from underneath are exposed (Figure 2-1). An animal bearing such cells would appear lightly colored.

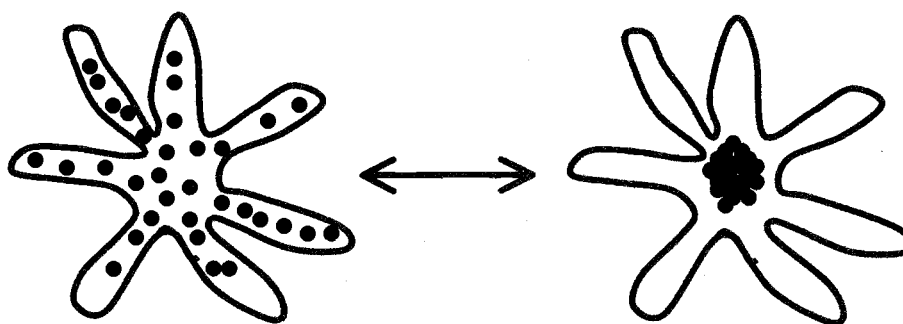


Figure2-1: Movement of pigment granules: dispersed and aggregated pigment granules in chromatophores.

Fish chromatophores are about  $100 \mu\text{m}$  in diameter, located mostly in the dermal layer of the integument but can also be found in the epidermal layer.

In this dissertation, the movement of pigment granules in fish chromatophores is studied *in vitro* and modeled.

### 2.3 Microtubule Motors and Transport

The cytoskeleton is a complex network of protein filaments that extends throughout the cytoplasm. The existence of the cytoskeleton is one of the characteristics of the eukaryotic fish chromatophore cell. It enables the cell to adopt a variety of shapes and to carry out coordinated and directed movements.

There are three types of protein filaments that comprise the cytoskeleton. They are: actin filaments, microtubules, and intermediate filaments. Each type of filament is formed from a different protein subunit: actin for actin filaments, tubulin for microtubules, and fibrous proteins for intermediate filaments.

Chromatophores, like many eukaryotic cells, contain a radial array of microtubules. Microtubules are attached to a single microtubule organizing center (MTOC) called a centrosome. They are polar structures. This means that one end (plus end) is capable of rapid growth, while the other end (the minus end) tends to lose subunits and it is embedded in a structure called the centrosome. The centrosome stabilizes the minus end (Figure 2-2).

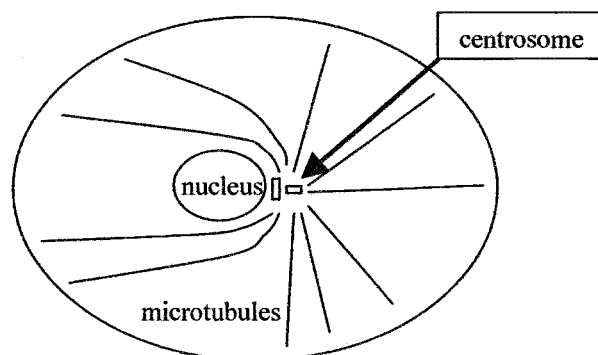


Figure 2-2: A centrosome with attached microtubules.

The pigment granules in chromatophores are attached to microtubules. They either aggregate in the center of the cell or disperse through the cytoplasm along the microtubules.

The movements of pigment granules in fish chromatophores are generated by motor proteins, which use energy derived from repeated cycles of ATP hydrolysis (Figure 2-3) to move steadily along the microtubule.

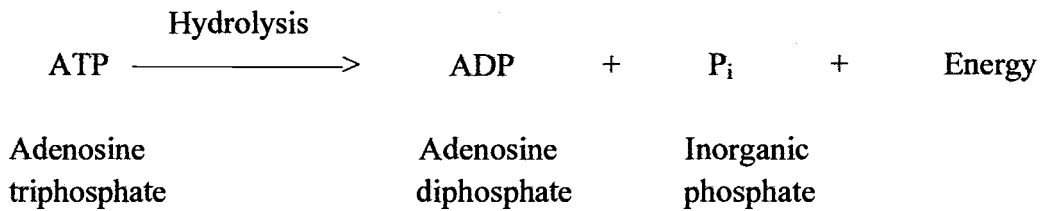


Figure 2-3: ATP hydrolysis.

Motor proteins belong to one of two families: the kinesins and the dyneins. Both the cytoplasmic dyneins and the kinesins are composed of two heavy chains plus several light chains. Each heavy chain contains a conserved, globular, ATP-binding head and a tail composed of a string of rod like domains. The two head domains are ATPase motors that bind to microtubules, while the tails generally bind to specific cell components and thereby specify the type of cargo that the protein transports (Figure 2-4).

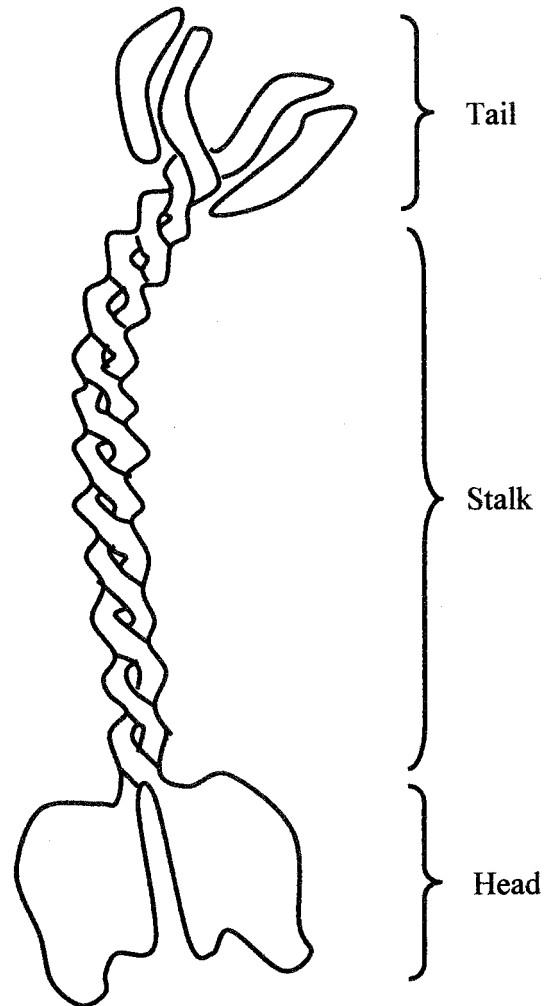


Figure 2-4: Microtubule motor protein (kinesin).

Movement of pigment granules in fish chromatophores towards the center of the cell (aggregation) is believed to involve the activation of the associated dynein motors. Movement towards the cell periphery (dispersion) is believed to involve the associated kinesin motors [3] (Figure 2-5).

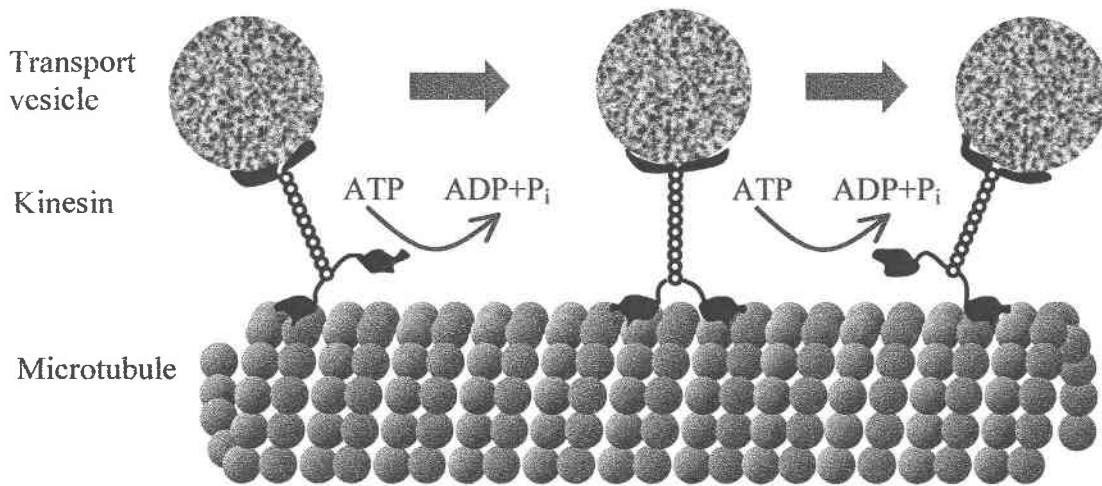


Figure 2-5: The movement of the motor protein (kinesin) along microtubules.

## 2.4 Signal Transduction

### 2.4.1 Introduction

A chromatophore cell, like all living cells, is composed of a restricted set of elements, four of which (C, H, N and O) make up nearly 99% of its weight. Living organisms synthesize only a small number of the organic molecules that they in principle can make. Cells contain just four major families of small organic molecules: the simple sugars, the fatty acids, the amino acids and the nucleotides. Each family serves a different function in the cell. Particularly relevant for the study of pigment granule movement in chromatophores are nucleotides and amino acids.

Nucleotides act as carriers of chemical energy. The triphosphate ester of adenine, ATP (Figure 2-6), participates in the transfer of energy in hundreds of individual cellular reactions. It is composed of adenine, ribose, and three phosphate groups. Its terminal phosphate is added using energy from the oxidation of foodstuffs, and this phosphate can be split off by hydrolysis to release energy that drives energetically unfavorable biosynthetic

reactions elsewhere in the cell. Also, nucleotides are used as specific signaling molecules in the cell (for example cAMP).

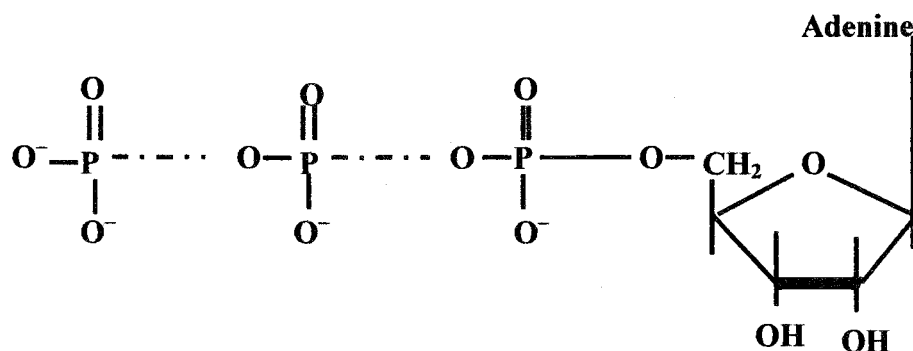


Figure 2-6: Chemical structure of ATP

Amino acids serve as subunits in the synthesis of proteins. Proteins are long linear polymers of amino acids joined by a peptide bond between the carboxylic acid group of one amino acid and the amino group of the next. They make up most of the dry mass of a cell. They have precisely engineered moving parts whose mechanical actions are coupled to chemical events.

One of the most important functions of proteins in chromatophores cells is to act as enzymes that catalyze specific biochemical reactions. Catalysts are chemicals that while helping a reaction come about, are not themselves changed. If there is any chemical reaction in chromatophores (as in any living thing) there is an enzyme that works to bring it about.

The signal transduction pathway is a cascade of biochemical reactions inside the cell. It is a method by which molecules inside the cell can be altered by molecules on the outside. In other words, it is the conversion of the reception signal, typically found at the surface of the cell, to a signal that directly facilitates a response. The original signal molecule is not physically passed along the pathway, just certain information is passed on. Very often



signal transduction involves a number of steps. At each step the signal is transduced into a different form, commonly a shape change in a protein.

There are two major intracellular signaling mechanisms that are used to control protein activity in fish chromatophores. These are signaling by a GTP-binding protein (guanine nucleotide binding protein) and signaling by phosphorylation.

Signaling by a GTP-binding protein is accomplished by phosphate addition and removal. The phosphate is not attached directly to the protein; instead it is a part of the guanine nucleotide (GTP), which binds tightly to the protein. With GTP bound to it, the protein is active. The loss of phosphate group occurs when the bound GTP is hydrolyzed to GDP in a reaction that is catalyzed by the protein itself. With GDP bound the protein becomes inactive.

Protein phosphorylation-dephosphorylation is another way to control protein activity, but this time by phosphate transfer. It represents one of the preeminent molecular mechanisms for modulating the functional properties of proteins. It takes place in all living cells. The protein phosphorylation-dephosphorylation process includes two thermodynamically favorable reactions; the water-driven hydrolysis by enzyme protein phosphatases, and high-energy compound-driven phosphorylation by enzyme protein kinase.

A phosphate group is transferred from an ATP molecule to a hydroxyl group on a serine, threonine, or tyrosine side chain of protein. A large amount of free energy is released when the phosphate-phosphate bond in ATP is broken to produce ADP. The phosphorylations catalyzed by protein kinases can be reversed by protein phosphatases which remove the phosphate (Figure 2-7).

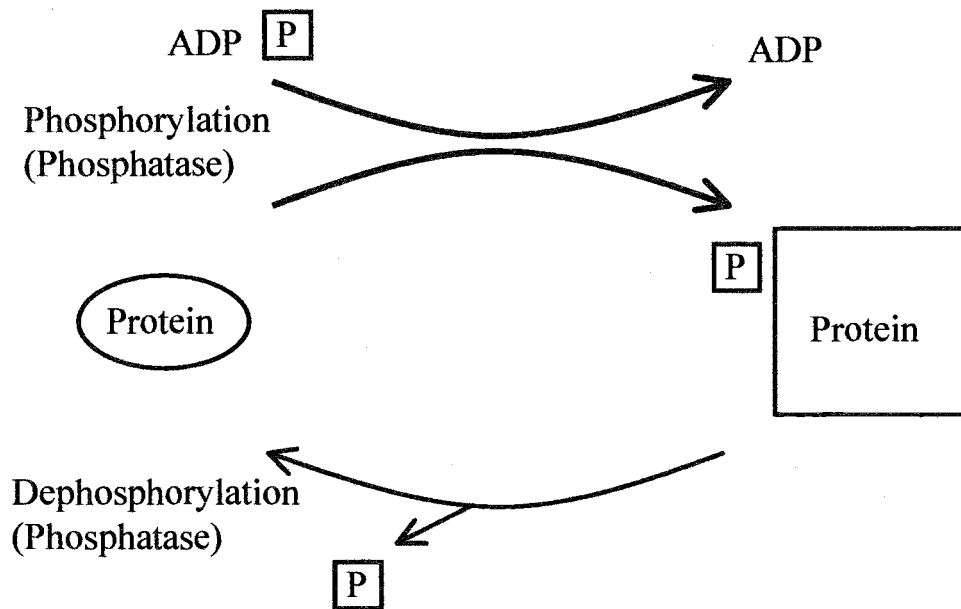


Figure 2-7: Signaling by phosphorylation/dephosphorylation.

In order to sustain reasonable target specificity among thousands of phosphoproteins, a network of hundreds of protein kinases and protein phosphatases is required.

## 2.4.2 G-protein Mediated Pathway

### 2.4.2.1 G-protein Linked Receptors

A targeted fish chromatophore cell responds to molecules of various substances. The substance molecules behave as a ligand, the term used for a small molecule that specifically binds to a larger one. Ligand binding generally causes a receptor protein to undergo a change in conformation, i.e., to change shape. This shape change directly activates the receptor in a fish chromatophore. Receptors become activated so as to generate a cascade of intracellular signals to alter the behavior of the cell. They act as signal transducers.

In fish the receptors are transmembrane proteins on the surface of the target-cell and belong to the class known as the G-protein-linked receptors. Ligands that cause aggregation of pigment in fish chromatophores bind to special type of G-protein-linked receptors, for example  $\alpha 2$ -receptors. All of the G-protein-linked receptors belong to a large superfamily of seven-pass transmembrane proteins. They consist of a single polypeptide chain that threads back and forth across the lipid bilayer seven times (Figure 2-8).

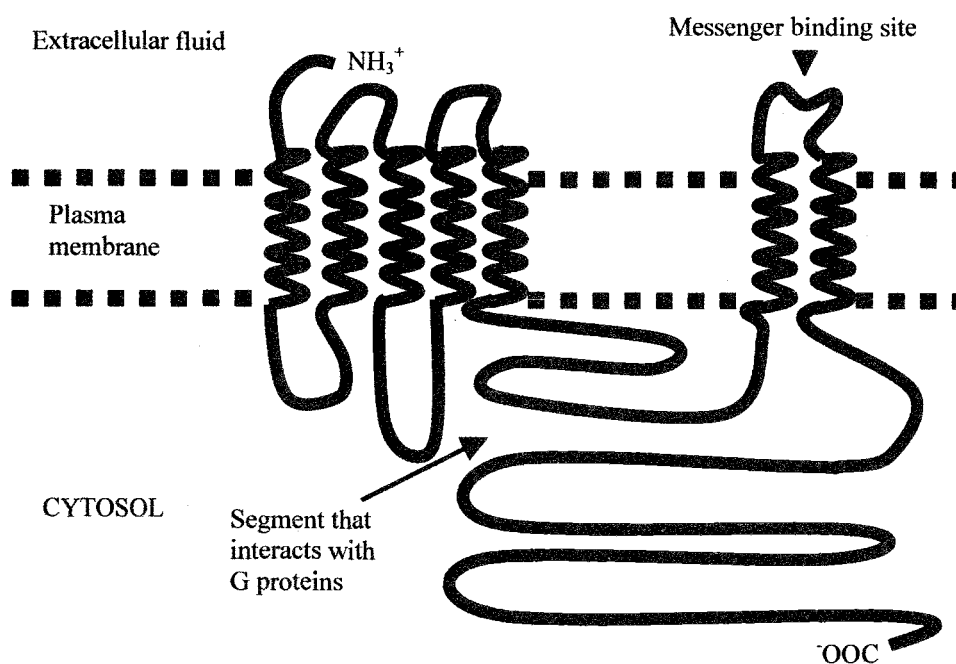


Figure 2-8: A schematic drawing of a G-protein-linked receptor.

These kinds of receptors act indirectly to regulate the activity of a separate plasma-membrane-bound target protein. In fish this membrane-bound target protein is the enzyme adenylyl cyclase.

#### 2.4.2.2 Heterotrimeric G-protein

The interaction between the receptor and the target protein is mediated by a third protein. Seven-helix receptors always act through a heterotrimeric GTP-binding regulatory protein (G-protein). GTP stands for guanosine triphosphate (Figure 2-9).

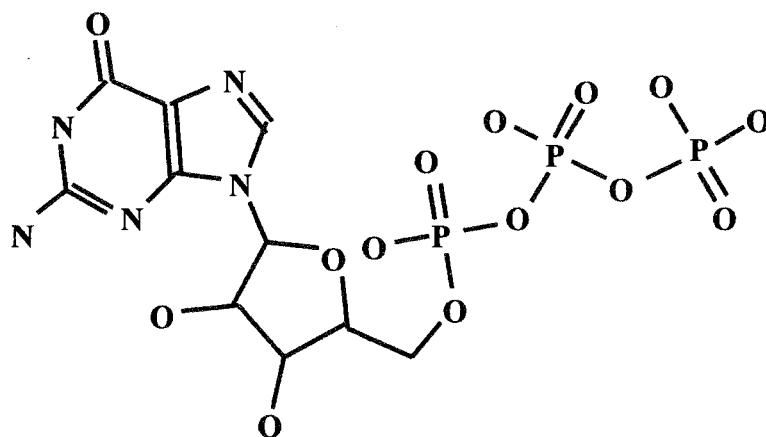


Figure 2-9: GTP (guanosine-5'-triphosphate).

G-proteins have GTP binding and GTP hydrolysis capabilities. The activated receptor changes its conformation and switches on the trimeric G proteins that associate with it causing them to eject their GDP (GDP stands for guanosine diphosphate) and replace it with GTP (Figure 2-10).

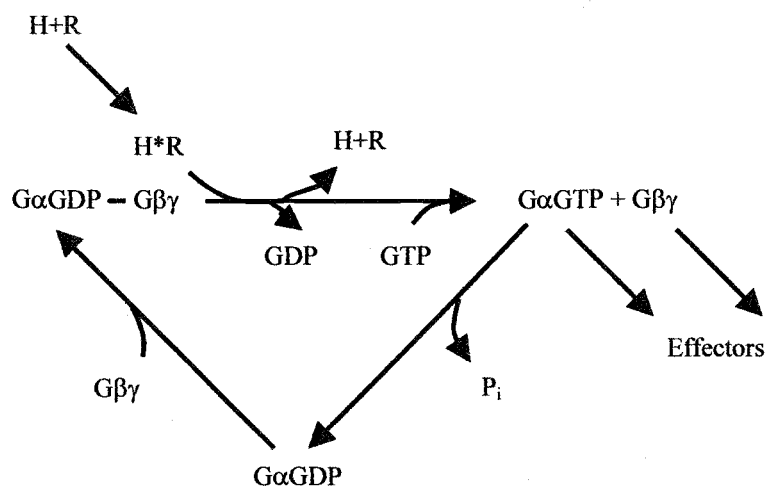


Figure 2-10: GTP-GDP exchange.

A trimeric G-protein is composed of three different polypeptide chains, called  $\alpha$ ,  $\beta$  and  $\gamma$ . The excitation signal is usually carried forward by the  $\alpha$  chain. The active protein has an opportunity to diffuse away from the receptor and deliver its message for a prolonged period to its downstream target.

The  $\alpha$  chain (subunit) of the G-protein hydrolyzes its own bound GTP to return the G-protein to the inactive form, converting it back to GDP. The proportion of G-protein in the active state is determined both by the rate of receptor-catalyzed GTP-GDP exchange and by the rate of hydrolysis of bound GTP (Figure 2-11).

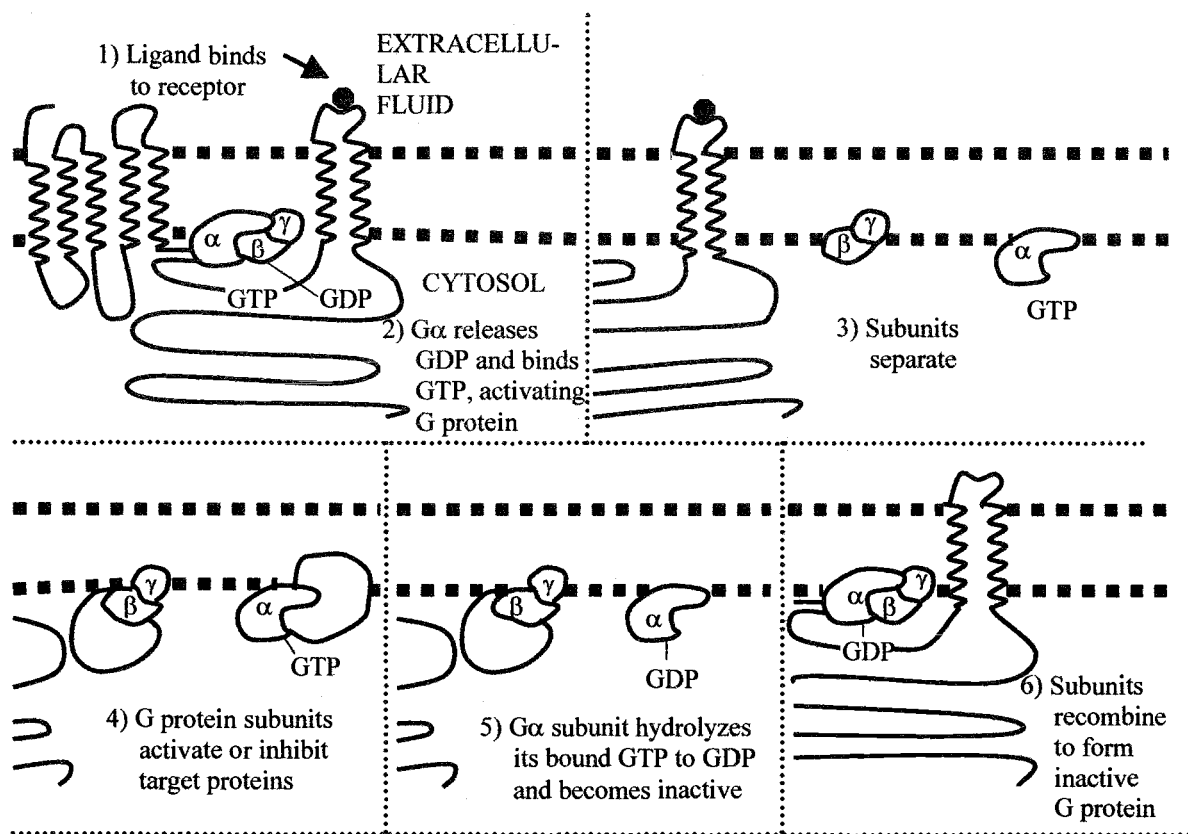


Figure 2-11: The G-protein activation/inactivation cycle.

### 2.4.2.3 Adenylyl Cyclase Enzyme

Adenylyl cyclase, or abbreviated AC, is the protein that the G-protein activates in the fish chromatophore cell. AC is a plasma-membrane-bound enzyme responsible for signal transduction.

G-protein-linked receptors activated by ligands that cause aggregation of pigment in fish chromatophores inactivate adenylyl cyclase. They act indirectly via inhibitory G-proteins ( $G_i$ -proteins).

The  $G_i$  protein is composed of  $\alpha_i$  ( $\alpha$  chain) and  $\beta\gamma$ , a tight complex formed from a  $\beta$  chain and a  $\gamma$  chain. When activated, a G-receptor binds to  $G_i$ , causing its  $\alpha_i$  polypeptide chain to bind GTP and dissociate from the  $\beta\gamma$  complex. Both the released  $\alpha_i$  and  $\beta\gamma$  contribute to the inhibition of adenylyl cyclase.  $\alpha_i$  inhibits the adenylyl cyclase indirectly, whereas  $\beta\gamma$  inhibit synthesis of one or more small intracellular signaling molecules. Synthesis of intracellular molecules can be inhibited in two ways—directly, by binding to the cyclase itself, and indirectly, by binding to any free  $\alpha_s$  subunits in the same cell, thereby preventing them from activating cyclase molecules.  $\alpha_s$  is a chain of a stimulatory G protein ( $G_s$ ). Receptors that activate adenylyl cyclase are coupled to this enzyme via trimeric  $G_s$  protein. The fish who are genetically deficient in  $G_s$  show decreased responses to certain hormones and, consequently, have metabolic abnormalities, abnormal bone development, and are mentally retarded.

Inactivation of adenylate cyclase stops the conversion of ATP to small intracellular molecules.

### 2.4.2.4 Cyclic AMP – a Second Messenger

Ligand activated G-protein-linked receptors in fish chromatophores, activate binding of G-proteins that inactivate (or activate) AC enzyme that regulate the concentration of

small intracellular molecules called cAMP. cAMP stands for a adenosine 3',5'-cyclic monophosphate (Figure 2-12).

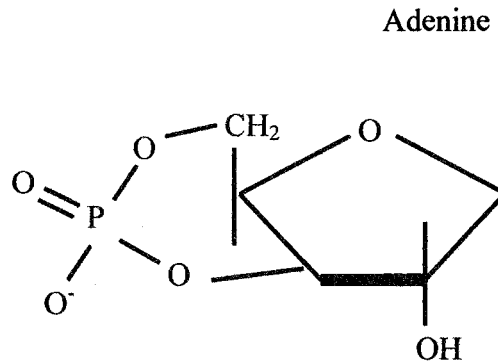


Figure 2-12: Cyclic AMP.

This cyclic nucleotide is synthesized from ATP by the AC enzyme and serves as an intracellular mediator (intracellular messenger, or second messenger). This means that these small molecules in turn pass the signal on by altering the behavior of selected cellular proteins (Figure 2-13).

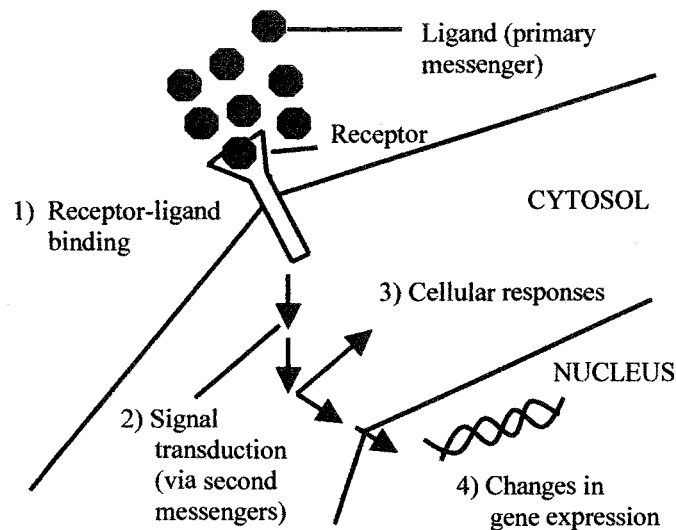


Figure 2-13: The pathway by which a G-protein-linked cell-surface receptor generates a cAMP second messenger.

Cyclic AMP concentration levels can change up to five-times in seconds. Such rapid synthesis of the molecule is balanced by rapid and continuous destruction by one or more cyclic AMP phosphodiesterases. Cyclic AMP phosphodiesterases hydrolyze cAMP to adenosine 5'-monophosphate (5'-AMP) (Figure 2-14).

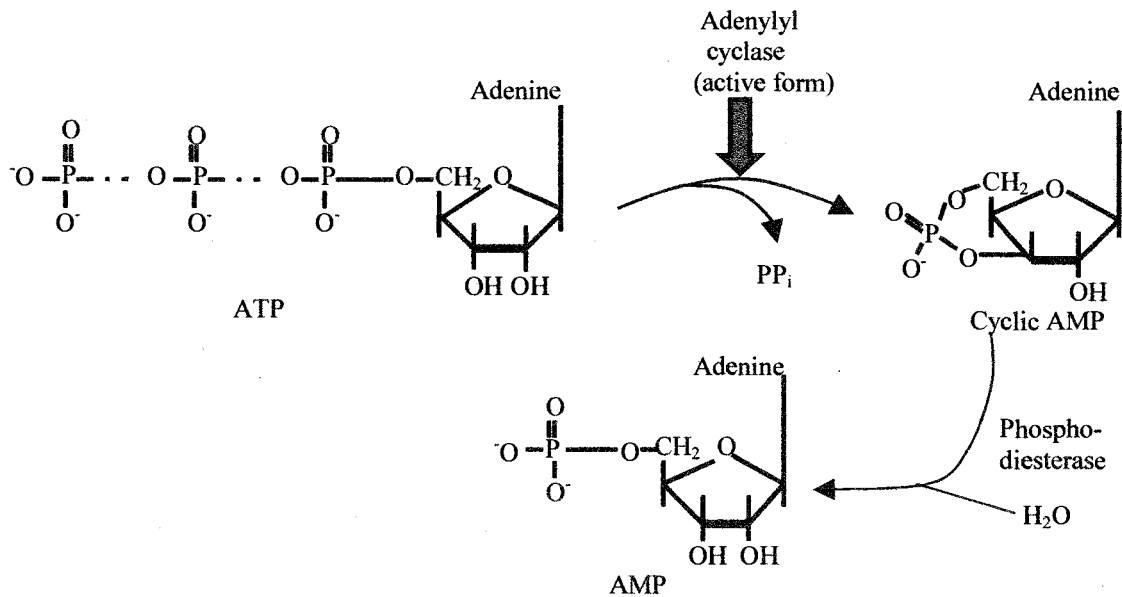


Figure 2-14: The synthesis and degradation of cAMP.

### 2.4.3 Protein Phosphorylation/Dephosphorylation

#### 2.4.3.1 Protein Kinase A – cAMP Dependent Kinase

Most effects of cyclic AMP in eukaryotic cells, to which chromatophores belong, are mediated by activation of a key enzyme – protein kinase A (PKA). The PKA enzyme is phosphoryltransferase. This means that it catalyzes the transfer of a phosphoryl group from a high-energy ATP molecule to a hydroxyl group located on the amino acid side-chain of a target protein. Acceptor sites in fish chromatophores are the hydroxyl groups of serine, threonine, and tyrosine. A large amount of free energy is released when the phosphate-phosphate bond in ATP is broken to produce ADP.



PKA is an enzyme complex. This means that it is not made as a single, giant, covalently linked molecule. Instead, it is formed by a noncovalent assembly of many preformed molecules, which are called subunits. In the inactive state, PKA consists of a complex of two catalytic subunits and two regulatory subunits. Regulatory subunits can bind cAMP which was the final product of the pathway. If this binding happens, catalytic subunits become free to bind and phosphorylate specific substrate proteins that are the next substance in the pathway (Figure 2-15).

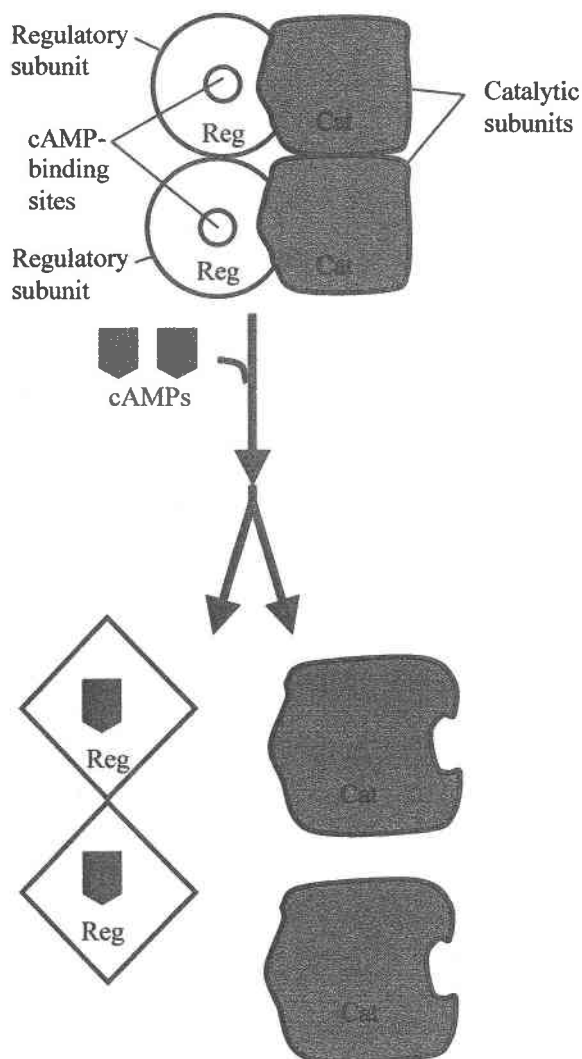


Figure 2-15: The activation of cAMP dependent PKA.

### **2.4.3.2 Protein Phosphatase**

Protein phosphatase is a second group of enzymes that can reverse the phosphorylation catalyzed by PKA. Protein phosphatases are phosphoesterases that catalyze the hydrolytic removal of a phosphate group from the hydroxylated amino acid residue of a protein. When PKA is inhibited protein phosphatase is active and dephosphorylate proteins that were phosphorylated by active PKA. The fish pigment granules aggregate.

There are stimulating substances which can activate adenylyl cyclase. In this case, cAMP levels are high, PKA activated and pigment granules disperse (Figure 2-1).

### **2.4.4 Signal Transduction in Chromatophores**

Pathways that affect pigment granule mobility include changes in the intracellular concentration of cAMP. Dispersion is activated by increase in cAMP levels while aggregation occurs when cAMP levels are depressed.

In this study of fish chromatophores, the synthetic drug clonidine ( $C_9H_9Cl_2N_3$ ) binds to a cell receptor, which interacts with heterotrimeric G-protein. Binding of clonidine to its receptor causes the exchange of GTP for GDP; the G-protein is now considered activated. In this case the G-protein is an inhibitory G-protein. When it is activated, it inhibits the enzyme AC. Active AC converts ATP to cAMP. The cAMP activates cAMP dependent protein kinase (PKA) which can phosphorylate many targets. When clonidine is added to fish chromatophores, AC is inhibited, cAMP levels drop, PKA is inhibited, and the pigment granules aggregate. It is believed that when cAMP is low, protein phosphatase is active and can dephosphorylate proteins that were phosphorylated by active PKA (Figure 2-16).

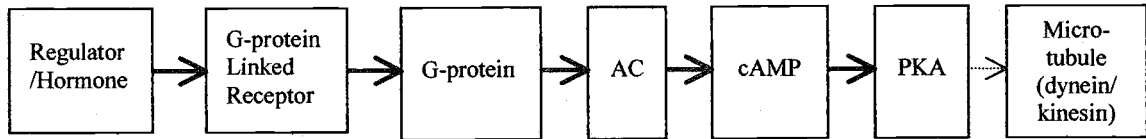


Figure 2-16: The signal transduction pathway in fish chromatophores.

## Chapter 3

### Image and Video Processing of Pigment Granule Distribution Sequences in Fish Chromatophores

#### 3.1 Introduction

In this chapter, a range of image and video processing techniques are applied to fish chromatophore image sequences. Several new analysis and modeling methods, specialized for chromatophores, are developed. Chromatophore pigment granule distributions are characterized using various parameters obtained from these methods. Figure 3-1 summarizes the methods described in the chapter and their relationships.

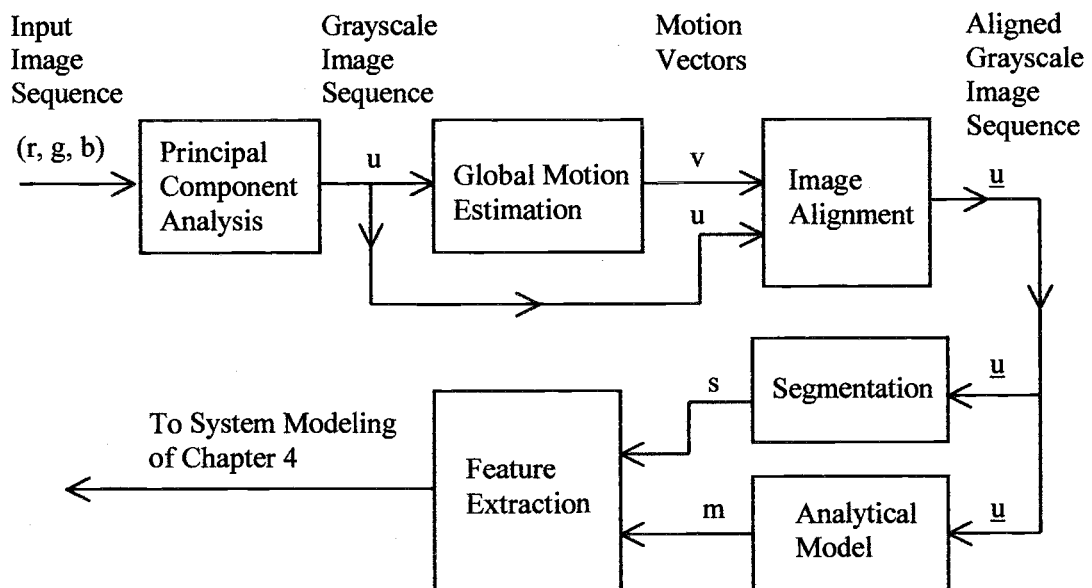


Figure 3-1: Block diagram of methods presented in Chapter 3.

### 3.2 Chromatophore Perception and Acquisition

In general, cells are small and complex. Most cells in their natural state are almost invisible under an ordinary microscope. There is little in the contents of most cells, which are 70% water by weight. It is hard to see their structure, hard to discover their molecular composition, and harder still to find how their various components function. However, the movement of pigment granules in chromatophores is easily visible by bright field microscopy.

In recent years electronic imaging systems and the associated technology of image processing have had a major impact on light microscopy. Pigment granule movement in chromatophores is observable for long periods of time when color video cameras are attached to a microscope. By using a video camera it is possible to record a sequence of pictures ("movie"). A movie consists of taking snap shots in regular intervals (e. g., every two seconds) using the video camera (Figure 3-2).

Since images produced by color video cameras are in electronic form, they can be readily digitized. In other words, they can be represented by arrays of finite length binary words. In order to be digitized, the given image is sampled on a discrete grid and each sample or picture element is quantized using a finite number of bits. The digitized image can then be processed by the computer.

Each color image frame that represents a picture of the pigment granule distribution in a chromatophore cell contains an array of  $m \times n$  picture elements (also called pixels or pels). This number of pixels per unit area, called the sampling rate, is determined by the bandwidth of the imaging system. In general, any two-dimensional function that bears information can be considered an image. The bandwidth is chosen large enough to preserve the useful information in an image that represents the pigment granule distribution.

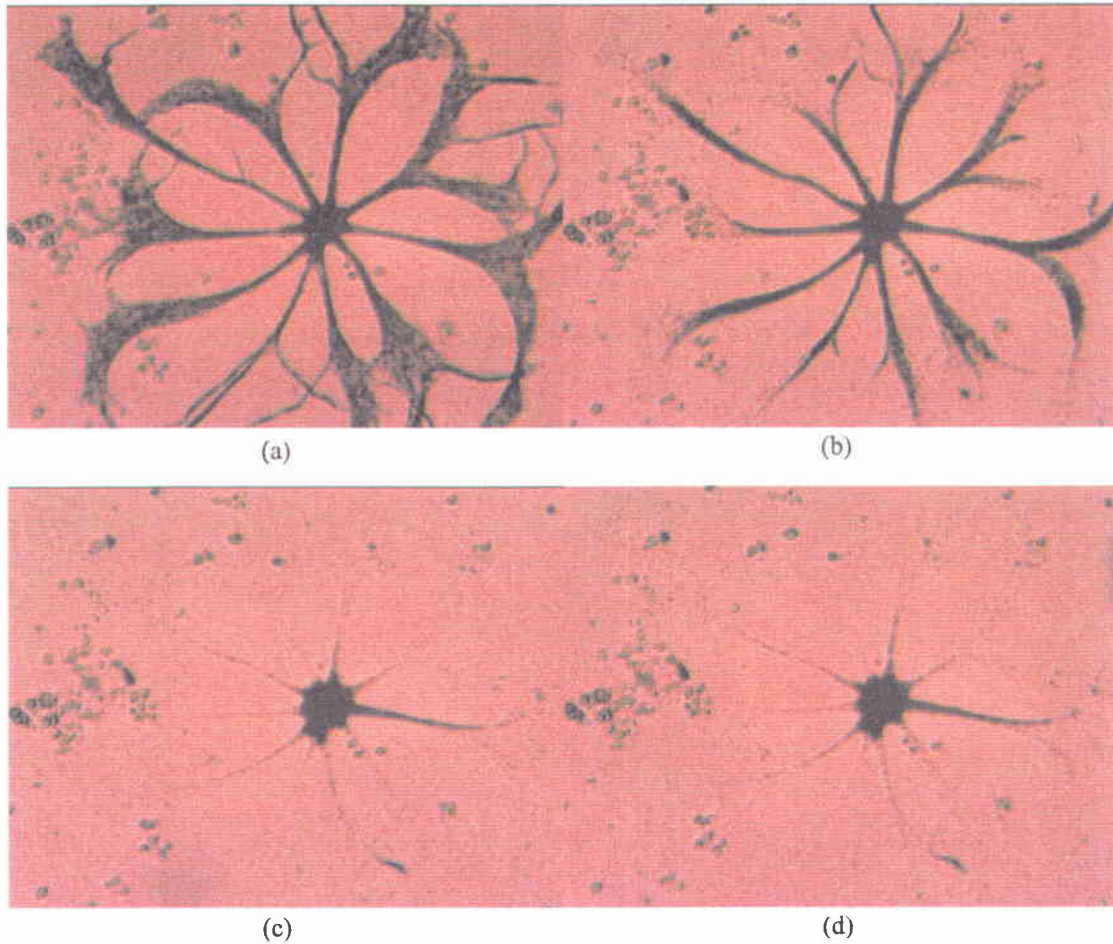


Figure 3-2: A sequence of pictures from a biological experiment that results in the movement of pigment granules in chromatophores.

In the color image frame, each pixel is defined by a three-component vector that represents a color. The human perception of color is a by-product of visual perception. The world of electromagnetic stimuli in which we are immersed has a much richer and much more varied structure than our visual system can process. We only perceive a limited range of frequencies of electromagnetic radiation, the narrow band of “visible light” which ranges in wavelength from approximately 360 nm to 660 nm. The visible wavelengths of light that are reflected from the objects in our everyday world are composed of mixtures of sometimes hundreds of separate and distinct frequencies of light. We somehow represent a distribution of frequencies of visible light as a single percept which we

call a color. In doing so we have lost a great deal of the information that was originally present in light, in fact many different distributions of visible light can produce the same subjective color percept.

The human retina (Figure 3-3) has three types of color photoreceptor cone cells, which respond to incident radiation with different spectral response curves (Figure 3-4).

Because there are exactly three types of color photoreceptors, three components are necessary and sufficient to describe a color, providing that spectral weighting functions are used. These three components are the intensities of the red, green and blue colors (RGB). The RGB color space is used to display graphics on display devices, such as the computer monitor, since for any given color, a suitable set of these three primary sources can be found (Figure 3-4).

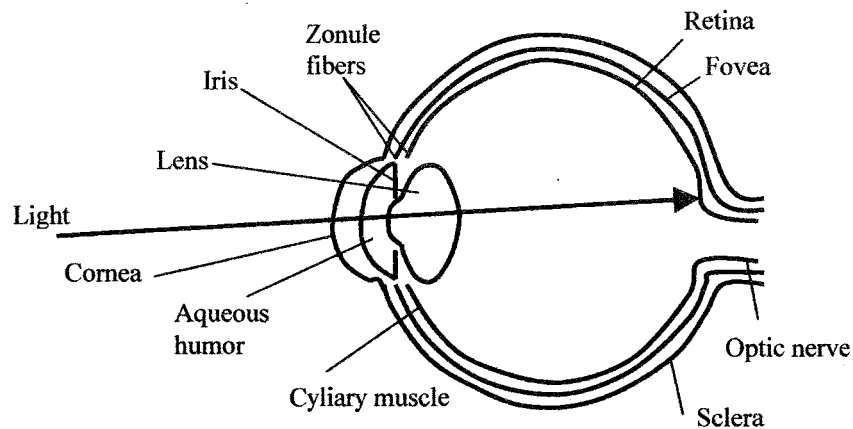


Figure 3-3: Cross-section of the human eye.

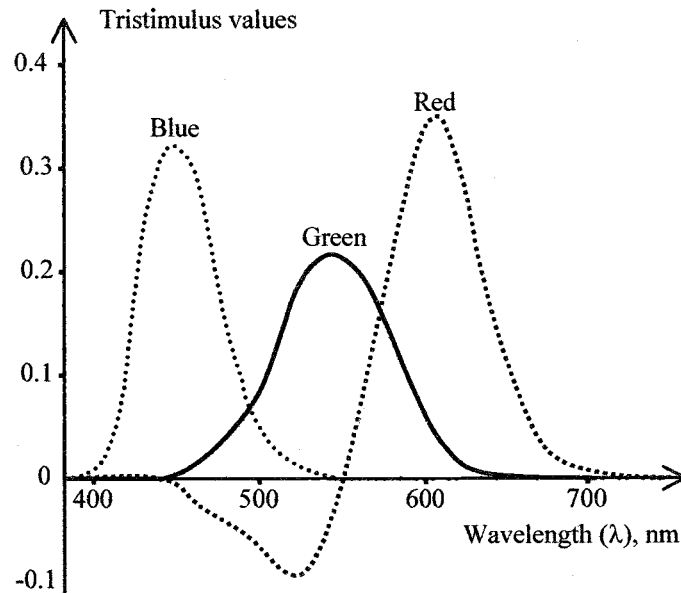


Figure 3-4: Spectral matching tristimulus curves for the CIE (the International Committee on Color Standards) spectral primary system. The negative tristimulus values indicate that the colors at those wavelengths cannot be reproduced by CIE primaries.

A sampled image is quantized to a finite number of RGB vectors. Computer images can be processed in various ways to extract latent information.

### 3.3 Color to Gray Scale Conversion Using Principal Component Analysis

The original images that are studied in this work contain various colors. Colored images contain a large amount of data that is to be manipulated for further image and video processing. Since this work is concerned with processing techniques that are practical for implementation in software or hardware form, the speed of the algorithms and the storage requirements are of major concern. Therefore, one of the requirements for the image processing part is to reduce the dimensionality of the problem.



Fortunately, it turns out that in images that represent chromatophore pigment granule distributions, the three-dimensional color information contained in each pixel can be reduced (compressed) to one variable. This is best done through a technique called principal component analysis.

Principal component analysis (PCA) is an efficient dimension reduction technique capable of transforming a set of  $p$  variables to a set of  $q$  variables, where  $q$  can be considerably smaller than  $p$ . Principal components are defined as optimal linear combinations of the original  $p$  variables, optimality meaning that a maximum of the variability of the original variables is extracted, and that the reduced  $q$  components are uncorrelated. Principal component analysis is also called the Karhunen-Loeve (KL) transform. It was first introduced by Pearson [14] who used it in a biological context. It was then developed by Hotelling [15] in work done on psychometry. It appeared once again quite independently in the setting of probability theory, as considered by Karhunen [16], and generalized by Loeve [17]. For a full treatment of principal component analysis, see, e.g., [18].

The KL transform can be applied to the images that represent pigment granule distributions in chromatophores by considering the sequence of pixels in an image as a discrete random process. It is assumed that the RGB vectors of the pixels are arrayed into a 3 by  $N$  matrix

$$\mathbf{U} = \begin{bmatrix} r_1 & r_2 & \dots & r_N \\ g_1 & g_2 & \dots & g_N \\ b_1 & b_2 & \dots & b_N \end{bmatrix}, \quad (3-1)$$

where  $(r_i, g_i, b_i)$  are the RGB components of each pixel  $i$ , and  $N$  is the total number of pixels in the color image. The autocorrelation matrix for the three colors is defined as

$$\mathbf{R}_a = E \left( \begin{bmatrix} r \\ g \\ b \end{bmatrix} \begin{bmatrix} r & g & b \end{bmatrix} \right) = E \left( \begin{bmatrix} rr & rg & rb \\ gr & gg & gb \\ br & bg & bb \end{bmatrix} \right), \quad (3-2)$$

where  $E$  is the expectation operator. The expectation is approximated as the mean over all pixels in the image. It can be shown that  $\mathbf{R}_a$  is a symmetric positive definite matrix. Its elements are a measure of correlation between the color components. For a single image, the color autocorrelation matrix can be approximated as

$$\mathbf{R} = \frac{1}{N-1} \mathbf{U} \mathbf{U}^T = \frac{1}{N-1} \begin{pmatrix} \sum_{i=1}^N r_i r_i & \sum_{i=1}^N r_i g_i & \sum_{i=1}^N r_i b_i \\ \sum_{i=1}^N g_i r_i & \sum_{i=1}^N g_i g_i & \sum_{i=1}^N g_i b_i \\ \sum_{i=1}^N b_i r_i & \sum_{i=1}^N b_i g_i & \sum_{i=1}^N b_i b_i \end{pmatrix}, \quad (3-3)$$

where  $T$  is the matrix transpose operator.

The right eigenvectors of  $\mathbf{R}$  define the principal axes. The matrix  $\mathbf{Q}$  composed of the right eigenvectors of  $\mathbf{R}$  satisfies

$$\mathbf{R}\mathbf{Q} = \mathbf{Q}\mathbf{D}, \quad (3-4)$$

where  $\mathbf{D}$  is the diagonal matrix of eigenvalues. For convenience, the eigenvalues on the diagonal of  $\mathbf{D}$  are ordered from the largest to the smallest in absolute value. According to the PCA theory, the linear KT transformation

$$\begin{bmatrix} x \\ y \\ z \end{bmatrix} = \mathbf{Q}^T \begin{bmatrix} r \\ g \\ b \end{bmatrix} \quad (3-5)$$

has the property that the transformed components  $(x, y, z)$  are uncorrelated. It is seen from (3-5) that the components  $(x, y, z)$  are the projections of the original  $(r, g, b)$  vector onto the principal axes. Another characteristic of the KL transform is that the component of the transformed vector corresponding to the largest eigenvalue carries the most information in the sense that for  $q = 1$ ,  $x$  gives the best approximation of  $(r, g, b)$ . The relative importance of the components  $(x, y, z)$  is therefore determined by the ratio of the magnitudes of the eigenvalues. Since the eigenvectors are ordered from large to small, the  $x$

component in (3-5) is the most important component and  $z$  is the least important component. By selecting  $x$  as the only variable for each pixel, a color to gray scale conversion that is optimal in the least squares sense is achieved.

Numerous experiments were carried out in the course of this work on different chromatophore images with the result that the largest eigenvalue in (3-4) is always much larger than the remaining two eigenvalues. Typical ratios of the magnitudes of the largest eigenvalue,  $\lambda_1$ , and next eigenvalue in size,  $\lambda_2$ , range from around  $|\lambda_1 / \lambda_2| = 20$  to  $|\lambda_1 / \lambda_2| = 80$ . As a result, a color image that represents pigment granules distribution in chromatophores can be reduced to a gray scale image with a negligible loss in the information content. The direction of the principal component is usually aligned with the direction of one of the image components. For erythrophores, this is the direction of the  $r$  axis and for cyanophores, it is the  $b$  axis. The direction of the principal component does not appear to have an important role on the final results. Figure 3-5 compares a color erythrophore image with its gray scale counterpart obtained by projection on the dominant principal component.

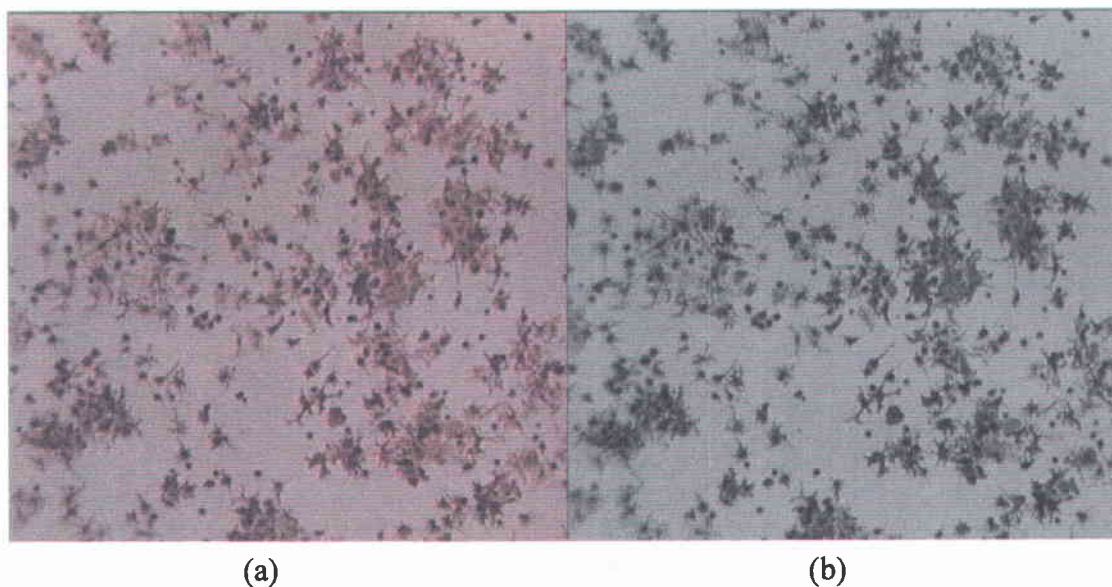


Figure 3-5: Two chromatophore images: (a) color; (b) gray scale obtained by projection on principal vector component.

## 3.4 Global Motion Estimation Using the Optical Flow Equation Model

### 3.4.1 Introduction

A chromatophore image sequence from a biological experiment that represents the distribution of pigment granules in the cell is a series of two-dimensional sequentially ordered images. Since imperfections in the biological experimental system can introduce unwanted global motion, the images in the sequence need to be stabilized or aligned. This can be done using *optical flow methods* for image motion estimation. Two dimensional (2D) optical flow methods for motion estimation are capable of estimating small non-integer frame to frame displacements accurately and efficiently.

### 3.4.2 Optical Flow Equation Methods

Optical flow equation based methods are based on solving the so called *optical flow equation* (OFE). This is a first order partial differential equation relating the components of the frame coordinate velocity vector to the partial derivatives of the image intensity. The optical flow equation is derived in the following way.

Assuming a continuous space-time distribution of the image intensity,  $s(x,y,t)$ , the image intensity will not change along a motion trajectory. On this motion trajectory we have

$$\frac{ds(x(t), y(t), t)}{dt} = 0, \quad (3-6)$$

where  $(x(t), y(t))$  is the motion trajectory. Using the chain rule of differentiation, (3-6) can be expressed as

$$\frac{\partial s(x,y,t)}{\partial x} v_x + \frac{\partial s(x,y,t)}{\partial y} v_y + \frac{\partial s(x,y,t)}{\partial t} = 0, \quad (3-7)$$

where  $v_x(x,y,t) = dx(t)/dt$ , and  $v_y(x,y,t) = dy(t)/dt$  are the components of the coordinate velocity vector. Equation (3-7) is the optical flow equation or optical flow constraint.

Using vector notation, (3-7) can be expressed as

$$\nabla s(x,y,t) \cdot \mathbf{v} + \frac{\partial s(x,y,t)}{\partial t} = 0, \quad (3-8)$$

where  $\nabla s = [\partial s(x,y,t)/\partial x, \partial s(x,y,t)/\partial y]^T$ ,  $\mathbf{v} = [v_x, v_y]^T$  and the “ $\cdot$ ” denotes the vector inner product (e.g., [20]).

From (3-8) it is seen that the OFE constrains only the component of the motion vector that is in the direction of the spatial image gradient. This is related to the fact that (3-7) represents one equation with two unknowns,  $v_x$  and  $v_y$ .

### 3.4.2.1 Limitations

In the considerations so far, it was assumed that the space and time coordinates are continuous. In practical applications both the space and time coordinates are discrete. This implies that OFE needs to be used in conjunction with appropriate spatial and temporal smoothness constraints. These constraints require the following:

1. The image intensity varies slowly over a neighborhood.
2. The image intensity varies slowly over time.
3. The displacement vector varies slowly over a neighborhood.
4. The displacement vector varies slowly over time.

### 3.4.2.2 Additional Constraints

In order to determine both components of the motion vector, additional constraints must be introduced on the components of the motion vector,  $v_x$  and  $v_y$ . Different choices of the constraints result in different OFE methods. One of the ways of introducing additional constraints on the velocity vector is to introduce a block motion model. In this model, it is

assumed that the motion of pixels remains unchanged over a particular block of pixels,  $\mathbf{B}$ . This leads to the Lucas-Kanade model [21].

### 3.4.3. Lucas-Kanade Model

This model starts by defining an error in the optical flow equation over the block of pixels  $\mathbf{B}$  as

$$E = \sum_{(x,y) \in \mathbf{B}} \left( \frac{\partial s(x,y,t)}{\partial x} v_x + \frac{\partial s(x,y,t)}{\partial y} v_y + \frac{\partial s(x,y,t)}{\partial t} \right)^2. \quad (3-9)$$

The goal of the method is to find the velocity components that minimize the above error. Computing the partial derivatives of the above expression with respect to  $v_x$  and  $v_y$  gives the following two equations for the estimated motion velocity components,  $\hat{v}_x$  and  $\hat{v}_y$ :

$$\sum_{(x,y) \in \mathbf{B}} \left( \frac{\partial s(x,y,t)}{\partial x} \hat{v}_x + \frac{\partial s(x,y,t)}{\partial y} \hat{v}_y + \frac{\partial s(x,y,t)}{\partial t} \right) \frac{\partial s(x,y,t)}{\partial x} = 0, \quad (3-10)$$

$$\sum_{(x,y) \in \mathbf{B}} \left( \frac{\partial s(x,y,t)}{\partial x} \hat{v}_x + \frac{\partial s(x,y,t)}{\partial y} \hat{v}_y + \frac{\partial s(x,y,t)}{\partial t} \right) \frac{\partial s(x,y,t)}{\partial y} = 0. \quad (3-11)$$

Solving the above two equations for the components of the estimated velocity gives

$$\begin{bmatrix} \hat{v}_x \\ \hat{v}_y \end{bmatrix} = \mathbf{A}^{-1} \mathbf{b} \quad (3-12)$$

where

$$\mathbf{A} = \begin{bmatrix} \sum_{(x,y) \in \mathbf{B}} \frac{\partial s(x,y,t)}{\partial x} \frac{\partial s(x,y,t)}{\partial x} & \sum_{(x,y) \in \mathbf{B}} \frac{\partial s(x,y,t)}{\partial x} \frac{\partial s(x,y,t)}{\partial y} \\ \sum_{(x,y) \in \mathbf{B}} \frac{\partial s(x,y,t)}{\partial x} \frac{\partial s(x,y,t)}{\partial y} & \sum_{(x,y) \in \mathbf{B}} \frac{\partial s(x,y,t)}{\partial y} \frac{\partial s(x,y,t)}{\partial y} \end{bmatrix},$$

$$\mathbf{b} = - \begin{bmatrix} \sum_{(x,y) \in \mathbf{B}} \frac{\partial s(x,y,t)}{\partial x} \frac{\partial s(x,y,t)}{\partial t} \\ \sum_{(x,y) \in \mathbf{B}} \frac{\partial s(x,y,t)}{\partial y} \frac{\partial s(x,y,t)}{\partial t} \end{bmatrix}.$$

The accuracy of the estimated motion vectors depends on a number of factors, including the type and size of the chosen blocks, as well as on the accuracy of the computed partial derivatives, i.e., the smoothness of the image.

#### 3.4.4 Shifted Chromatophore Pigment Distribution Experiment

In order to evaluate the behavior of the method for chromatophores, OFE experiments were performed on shifted chromatophore pigment distribution images. Table 3-1 summarizes the behavior of the computed motion vectors for one image using different block sizes. The computations were performed on the image shown in Figure 3-6.

It should be noted that the image of Figure 3-6 contains pigment granule distributions whose size varies considerably over the image. Some of the distribution are as small as several pixels in both dimensions and others are as large as  $100 \times 100$  pixels. This type of image is difficult to process with a single block size and therefore it represents a good test case for the proposed motion estimation algorithms.

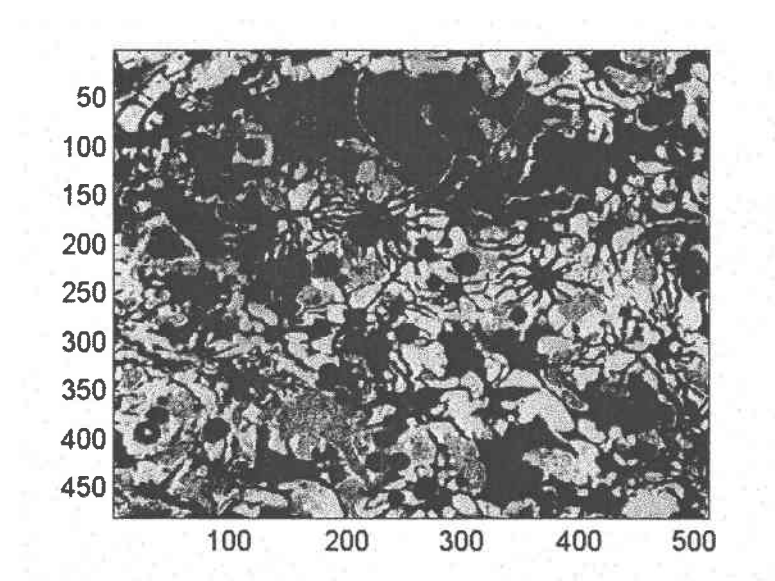


Figure 3-6: Chromatophore pigment distribution image used for Lucas-Kanade estimation with different block sizes.

Table 3-1: Lucas-Kanade results for the image of Figure 3-6 shifted by  $\mathbf{v}=(0,1)$  pixels. All motion vector results are in pixels.

Block Size	Min $v_y$	Max $v_y$	Mean $v_y$	STD $v_y$
$4 \times 4$	-3.7270	4.5358	0.5133	0.6075
$8 \times 8$	-1.2934	2.2139	0.6368	0.3362
$16 \times 16$	-0.4013	1.2710	0.7241	0.1908
$32 \times 32$	0.1905	0.9698	0.7581	0.1164

Motion vectors were computed at each image point. The min, max, mean and the standard deviation of Table 3-1 were computed over all points. It is seen from Table 3-1 that the computed motion vector improves slowly with the increase in the block size as it approaches the exact value  $v_y=1$  pixel. Modifications to the original Lucas-Kanade motion



estimation method are needed for chromatophore images in order to improve the motion estimation accuracy.

### **3.4.5 Iterative Correction**

The Lucas-Kanade motion estimation method is accurate only when the block size is large, or when the frame-to-frame displacement is small and the changes of the intensity and the motion vector are slow. The accuracy of the motion vector estimates can be improved through an iterative alignment procedure [22]. After an initial estimate of the motion is obtained, the first image is shifted towards the second to compensate for the estimated displacement. The motion estimation procedure is then repeated between the shifted first image and the original second image to obtain an estimate of any residual velocity. This shift-and-estimate procedure can be repeated.

The method was tried on unfiltered and low-pass filtered chromatophore pigment granule distribution images. It was found to be extremely effective for improving the global motion estimates of these images using a single iteration. Multiple iterations often made the result worse and were found to be unreliable. The results for global motion estimation are summarized in the following section.

### **3.4.6 Global Motion Estimation Using Corrected Lucas-Kanade Model**

The purpose of global motion estimation in this work is to compensate for random shifting or vibrations of the components in the image acquisition system. In order to evaluate the method for global estimation, the following test was performed.

#### **3.4.6.1 Test 3-1**

Image 1: 200 × 200 pixel subset of the image shown in Figure 3-6.

Image 2: 200 × 200 pixel subset of the image shown in Figure 3-7.

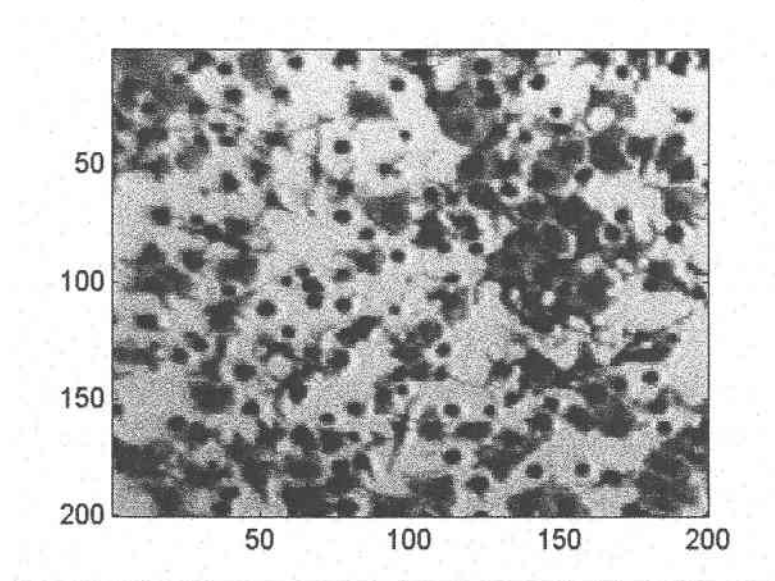


Figure 3-7: Small chromatophore pigment distribution image used for global motion estimation experiment.

The test images were filtered with a low-pass filter and the resulting images were shifted by  $(v_x, v_y) = (1, 1)$ . The global motion vector between the two filtered images was estimated using a single  $200 \times 200$  pixel Lucas-Kanade block. The filters were implemented using the Matlab `filter2` function. The size of the filter matrix was variable and the impulse response of the filter matrix was the half wave cosine function. The filter coefficients were normalized so that their sum is equal to 1.

Iterative motion vector correction using a single shift-and-estimate step was applied to the above images. The images were shifted using bilinear interpolation between the nearest four pixels. Only one iteration step was used since additional steps degraded the accuracy of the computed vectors.

### 3.4.6.2 Test 3-1 Results

Image 1 (large pigment granule distribution, little background,  $200 \times 200$ ):

- a) No filter      vx=1.0443, vy=1.0309;
- b) 3 x 3 filter   vx=1.0142, vy=1.0110;
- c) 6 x 6 filter   vx=1.0020, vy=1.0017;
- d) 9 x 9 filter   vx=1.0008, vy=1.0007.

Image 2 (small pigment granule distribution, more background, 200 × 200):

- a) No filter      vx=1.0284, vy=1.0208;
- b) 3 x 3 filter   vx=1.0086, vy=1.0085;
- c) 6 x 6 filter   vx=1.0029, vy=1.0031;
- d) 9 x 9 filter   vx=1.0017, vy=1.0022.

It is seen that the shift-and-estimate correction improves the estimated motion vectors considerably.

The methods described above are suitable for aligning pairs of images before further processing.

## **3.5 Segmentation of Chromatophore Pigment Granule Distribution Images**

### **3.5.1 Introduction**

The next image processing goal is to perform bi-level classification of the image pixels in order to reduce the complexity of the data and to simplify the recognition of the pigment granule distribution from the background. This is typically accomplished using image segmentation techniques. However, chromatophore pigment granule distribution images can contain various effects caused by variable lighting conditions and it is not always possible to perform segmentation directly. For this reason, a segmentation algorithm for gray-level, variable lighting condition images was designed in this work.

Due to inconsistent lighting conditions, a global segmentation threshold may produce incomplete segmentation of images. This is illustrated in Figure 3-8. The reason for the in-

complete segmentation is that the object (pigment granule distribution) pixels and background pixels have overlapping gray levels. Therefore, they cannot be distinguished from each other. The selection of a single threshold for these kinds of images is not possible in general. Experiments on chromatophore images show that selecting a local segmentation threshold gives much better results.

The method for segmenting gray-scale chromatophore pigment granule distribution images that is proposed in this work computes the mean intensity over selected regions of the image and uses bilinear interpolation to calculate the mean intensity at the remaining points. The procedure is recursive and adaptive. Once the mean intensity value is obtained for all image points, a threshold value is chosen for each point and the image is segmented. A simple filtering process is used afterwards to remove some of the unwanted background noise. The method can also be used for improving existing methods for badly illuminated images, such as the Z-shaped nonlinear transform (ZNT) method [23].

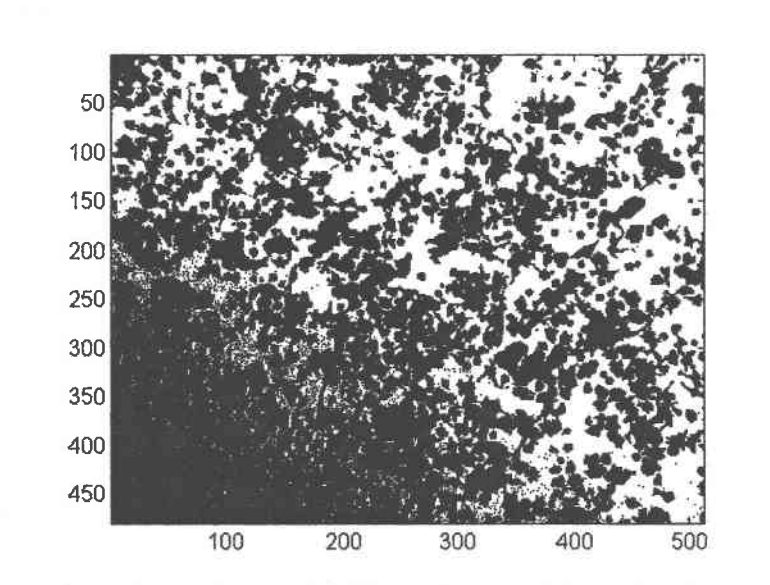


Figure 3-8: Example of chromatophore segmentation with a constant threshold.

### 3.5.2 Fundamental Ideas Behind Proposed Segmentation Approach

The segmentation approach is based on two basic ideas:

*1. The segmentation threshold should depend on the statistics of the pixel neighborhood.*

Since the threshold must change from location to location, it is logical to determine the threshold based on statistics of the neighborhood of the segmented pixel. This idea is explained further in Section 3.5.3. For computational and practical reasons it would be good if the neighborhood statistics could be described by a single parameter. If a single parameter is chosen, this parameter can be determined using the second idea, described below.

*2. The background noise in the original image should be reduced before segmentation.*

Background noise, such as variable lighting conditions, is the main reason why a single threshold cannot segment a chromatophore pigment granule distribution image well. If some of this noise can be removed from the image, better segmentation results can be expected.

Based on a large collection of chromatophore pigment granule distribution images, it has been determined that the background lighting is a slowly changing function of position in the image. It is reasonable to assume that the variable lighting effects are additive and that they affect the pigment granule areas in the same way as they affect the non-pigment granule areas. If a rectangular area of the image is observed, these assumptions lead to the conclusion that the image can be decomposed into two images:

1. Pigment granules with white background representing ideal lighting conditions;
2. A perturbation to the ideal image representing the variable lighting.

This is illustrated in Figure 3-9.

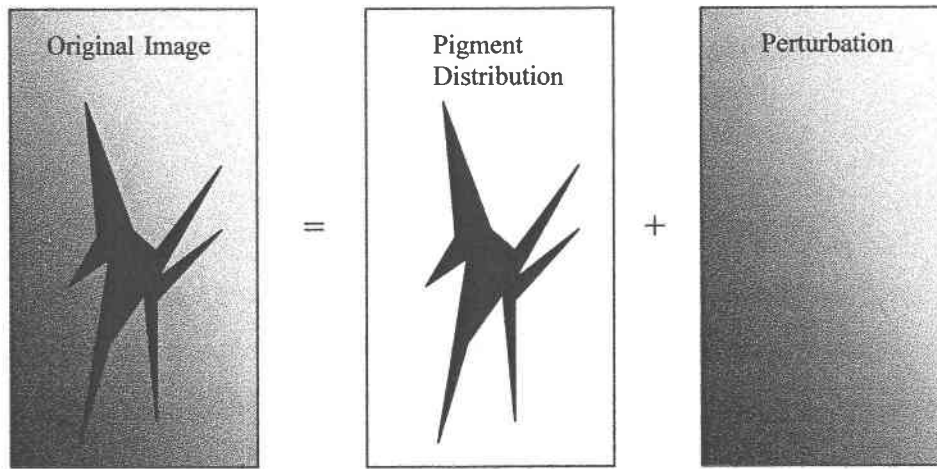


Figure 3-9: Decomposition of original image into ideal image and a variable lighting perturbation.

If the original image is processed using a linear operation that yields a scalar value (linear functional), this linear operation,  $L$ , can be decomposed into two parts:

$$L(\text{Original Image}) = L(\text{Pigment Distribution}) + L(\text{Perturbation}).$$

Two different rectangles of similar size are now chosen at different locations of the image and  $L$  is applied to each rectangle. If each rectangle contains pigment distributions of several chromatophores, it can be assumed that the effect of  $L$  on the pigment distribution part of the first rectangle is approximately the same as the effect of  $L$  on the pigment distribution part of the second rectangle. This assumption is typically satisfied for larger rectangles. For appropriately chosen linear operators this is equivalent to assuming that both rectangles contain the same percentage of similar pigment granule distributions. Subtracting the above equations for the two rectangles then gives

$$L(\text{Original Image 1}) - L(\text{Original Image 2}) = L(\text{Perturbation 1}) - L(\text{Perturbation 2}).$$

Therefore, the goal is to choose  $L$  in such a way that by capturing the change in the effect of  $L$  on the original image, the change of the effect of  $L$  on background is captured.

One more restriction on the choice of  $L$  is imposed. It is required of  $L$  that its affect on shrinking rectangles converges to the original image. All of these requirements suggest that  $L$  can be chosen as the mean pixel intensity on the rectangle.

A different way of looking at the choice of  $L$  is in terms of standard filtering techniques. The background noise represents a slowly varying (“low frequency”) noise component that can be isolated using a low-pass type filtering operation. The mean value over a large rectangle surrounding a point is one particular choice of such a low-pass filter. Subtracting the mean value over a given rectangle from the original image will reduce the variable lighting perturbation.

### **3.5.3 Proposed Segmentation Method**

The main idea behind the method used for chromatophore segmentation in this work is to use a segmentation threshold that depends on the statistics of some neighborhood of a given pixel. While computing the statistics of every point in the image can be computationally costly, the computational cost can be reduced by calculating the statistic only for certain points and by using interpolated values for the remaining points. If the number of points where the statistic is computed is kept much smaller than the number of points where the statistic is obtained by interpolation, the computational cost is dominated by the interpolation time. This time can be kept within reasonable limits. Due to the slowly varying nature of the background noise in the images, the number of points where the statistic needs to be computed can be kept relatively low.

Once the statistic of each point is known (either by direct computation or by interpolation), the threshold for each point is computed. The image is then segmented. The resulting segmented image will consist of black and white regions. The black regions correspond to the places in the image where the pigment granule distributions are located and the white regions correspond to parts of the original image that mostly contained the background (Figure 3-10 (a)). If the threshold is chosen conservatively—meaning that the

black pigment granule regions do not contain any areas that correspond to the background in the original image—it is possible to repeat the segmentation process. In the second segmentation, only the part of the original image corresponding to the background in the previous segmentation result is segmented. This newly segmented image is then combined with the previous segmentation adding parts of the pigment granule distributions that were not visible in the previous segmentation to the overall result as well as some background noise (Figure 3-10 (b)). The repetition is stopped once the newly segmented image contains a sufficient amount of background noise. Typical chromatophore pigment granule distribution images do not require more than two segmentation steps.

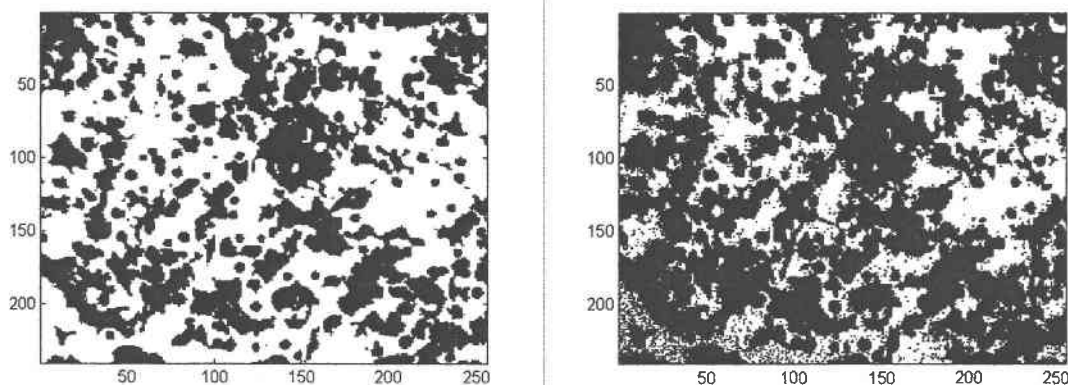


Figure 3-10: Repetitive segmentation: (a) first step; (b) second step showing more of the granule area together with background noise.

The background noise in the segmented images can be recognized as isolated regions of black pixels whose area is much smaller than the area of a typical pigment granule distribution. It is possible to filter this type of noise from the final segmented image.

### 3.5.3.1 Overview of Thresholding Procedure

The recursive procedure for determining the threshold is described below.



1. Calculate the statistical parameter(s) of each image corner (Figure 3-11):
  - Choose a minimum size rectangle near each corner and calculate the statistical parameters from the pixels in this rectangle.
  - Increase the rectangle size and recalculate the parameters.
  - Repeat the above two steps until a sufficient parameter history list is obtained.
  - Evaluate the behavior of the parameter history list and stop if the parameters satisfy the stopping criterion. Otherwise keep on increasing the rectangle until the maximal allowed size is reached.
  
2. Calculate the statistical parameter(s) at the image center:
  - Vary the size of the calculation rectangle in the manner described in Step 1 and calculate the parameters.

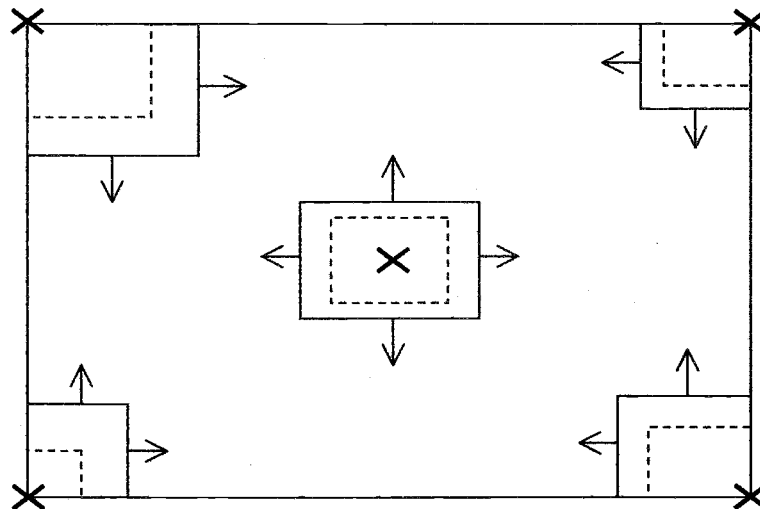


Figure 3-11: Calculation of statistical parameters at the image corners and in the center.

3. Compare the computed parameter(s) at the image center (from Step 2) with the interpolated parameter value(s) at the image center. The interpolation is done based on the parameter values(s) at the corners. If the computed and interpolated values are “close” according to some error criterion, skip to step 5.

4. Subdivide the image into 4 subimages and repeat the process for each subimage starting from Step 1.
5. Use interpolation to calculate the statistics parameter(s) for every remaining image point from the parameter values at the computed points.
6. Calculate the threshold value for every point based on the statistics parameter(s) obtained in the above steps.

Once the threshold of each point is computed, the image can be segmented.

It is important to note that the details of the threshold selection mechanism can be varied without changing the general procedure described above. Specifically, it is possible to use different statistical parameters (mean, min, max functions etc.), different interpolation functions, and different error evaluation criteria. In the following subsection a simple choice of these functions is made.

### 3.5.3.2 Statistical Parameter

The simplest approach is to have one statistical parameter,  $s$ . The threshold,  $T$ , at each point will then be a function of one parameter:  $T = T(s)$ . The first candidate for the statistical parameter,  $s$ , is the mean pixel intensity in some neighborhood of the point of interest:

$$s = \frac{1}{N} \sum_{k=1}^N u(x_k, y_k) \quad (3-13)$$

where  $u(x_k, y_k)$  is the pixel intensity of point  $(x_k, y_k)$  and  $N$  is the number of pixels in the neighborhood. The reasoning behind this choice was explained in Section 3.5.2.

### 3.5.3.3 Interpolation Function

Since the values are interpolated at every point based on the values at four corner points, a logical first candidate for the interpolation function is a function of the form:

$$f(x,y) = a_{00} + a_{10}x + a_{01}y + a_{11}xy, \quad (3-14)$$

where  $a_{00}$ ,  $a_{10}$ ,  $a_{01}$ ,  $a_{11}$  are constants determined by the requirement that  $f$  matches the known computed values at the four corner points. This corresponds to bilinear interpolation.

### 3.5.3.4 Rectangle Selection

For the rectangles used in determining the pixel neighborhood we choose squares. This removes one degree of freedom in choosing the rectangle size and simplifies the procedure. In the procedure of Section 3.5.3.1, the squares are increased in a geometric progression to improve the efficiency of the algorithm:

$$w^{(k)} = g w^{(k-1)} \quad g > 1, \quad (3-15)$$

where  $w^{(k)}$  is the width of the rectangle in the  $k$ -th iteration and  $g$  is the rectangle growth factor. A good choice for the growth factor,  $g$ , proves to be a value between  $\sqrt{2}$  and 2. Smaller growth factors often require a large number of iterations while factors larger than 2 result in rapid changes from iteration to iteration. With large growth factors it is easy to exceed the optimal square size.

### 3.5.3.5 Stopping Criterion for the Square Growth

The size of the squares that are used for computing the statistics turns out to be very important. Pixel neighborhoods that are too small are more problematic than those that are too large. The reason for this is that statistical parameters computed based on small neighborhoods do not include the characteristics of the image background. The statistic

of the background is essential in obtaining a good threshold value that will be able to isolate the pigment granule distribution from the background. Therefore, the stopping criterion needs to be very strict, requiring small monotonic variations in the computed values from one iteration to the next.

The typical behavior of the mean value as a function of square size for four corners of a chromatophore pigment granule distribution image is shown in Figure 3-12.

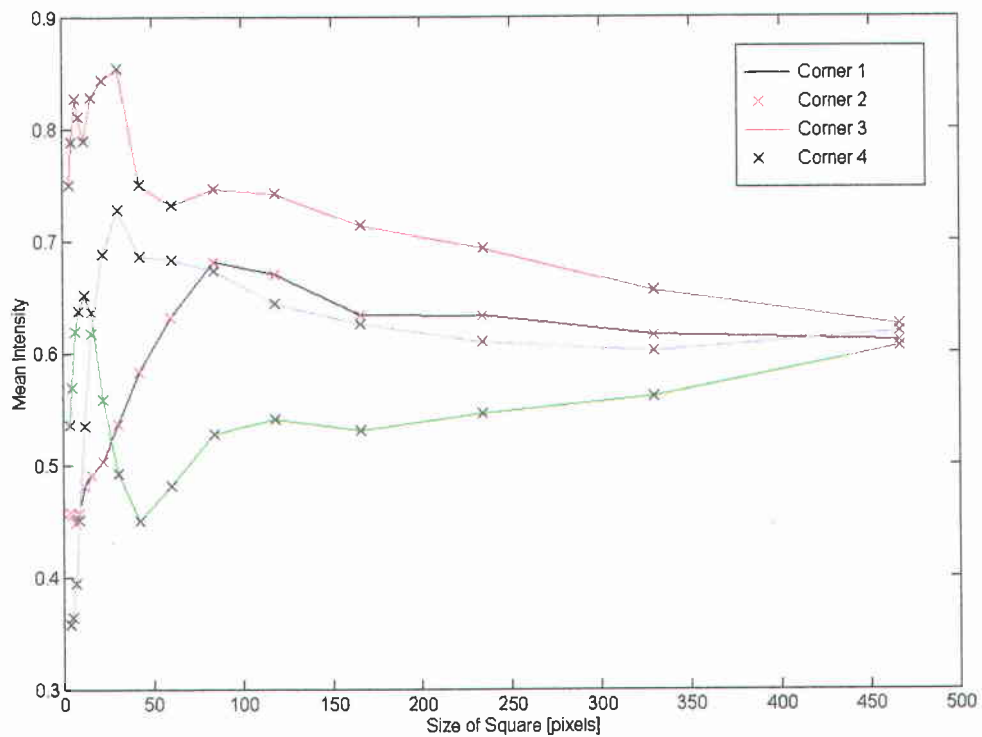


Figure 3-12: Typical behavior of mean pixel intensity as a function of square size.

It is seen from Figure 3-12 that the mean changes quickly at first and then converges to the mean value of the whole image nearly monotonically. The oscillating behavior occurs while the size of the square is smaller than or comparable to the size of the pigment granule distributions in the image. Once the square size exceeds the size of the average pig-

ment distribution, the mean value changes nearly monotonically. The growth of the squares should not be stopped before the oscillations become small. The relative amplitude of the oscillations is monitored and when it becomes sufficiently small, the growth of the squares is stopped.

### 3.5.3.6 Error Evaluation at the Image Center

At the center of the image the computed mean intensity is compared to the interpolated intensity. The relative error between the two intensities proves to be a good measure of the accuracy of our interpolation.

### 3.5.3.7 Subdivision of the Image into Smaller Images

In the procedure of Section 3.5.3.1 it may become necessary to subdivide the image into smaller images. In this case it is important that the mean values at the corners of each subimage are computed consistently. The interpolation function should be continuous over the whole image. Therefore, the computed means at the corners that are shared between two subimages should agree. This suggests that the squares used for computing means of the subdivided image must span two adjacent images. The approach is illustrated in Figure 3-13.

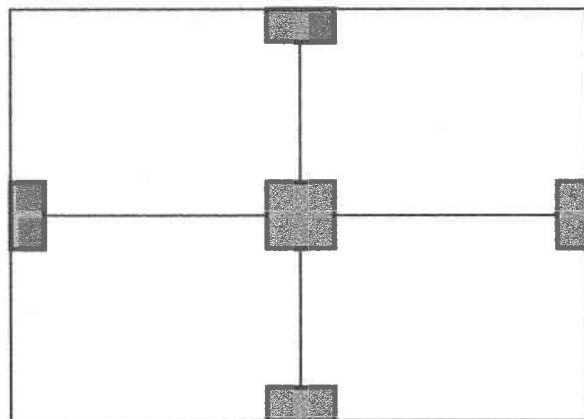


Figure 3-13: Choosing the statistical neighborhood areas when the image is divided into subimages.

### 3.5.3.8 First Segmentation

Once the interpolated mean intensity is obtained over the whole image, the segmentation threshold must be calculated. Before the segmentation threshold is chosen, we subtract the calculated mean intensities from the original image. This operation reduces the variable lighting from the image and improves the segmentation:

$$I_{AC} = I - I_m, \quad (3-16)$$

where  $I$  is the matrix of original image intensities and  $I_m$  is the calculated matrix of mean intensities. The resulting matrix  $I_{AC}$  is segmented with a threshold of 0 for each pixel. This corresponds to choosing the threshold equal to the computed mean intensity:  $T(s)=s$ .

The mean image intensity proves to be a high threshold for chromatophore pigment granule distribution images. The black areas in the resulting image will contain little or no background while the white areas will contain both the background and parts of the pigment granule distributions. We can now isolate the regions of the original image corresponding to the white areas in the segmented image and repeat the whole segmentation procedure only on this white part of the image.

### 3.5.3.9 Repeated Segmentation

The regions of the image used in the second segmentation contain mostly pigment granule distribution background but they also include parts of pigment granule distributions whose intensity is very similar to the intensity of the surrounding background. Therefore, the result of the second segmentation usually contains some black noise pixels which do not correspond to pigment granules in the original image. However, these pixels can be recognized and removed if necessary. The result of the second segmentation is combined with the result of the first segmentation to produce the resulting segmented image after each step.

In the second and subsequent steps, it is possible to vary the segmentation threshold. A higher threshold will include more pigment areas in the segmented image as well as more removable noise. Threshold values between  $-\sigma$  and 0 prove to be good choices for the final segmentation, where  $\sigma$  is the computed standard deviation of the image intensity in the region that is segmented in the last step.

### 3.5.4 Segmentation Examples

#### 3.5.4.1 Example 3-1

In the first example the image shown in Figure 3-14 is segmented using the procedure described above. Figure 3-14 is a gray scale version of an original image obtained using principal component analysis.

The image obtained after the first segmentation is shown in Figure 3-15. It is seen that some of the pigment granule parts are missing from the segmented image.

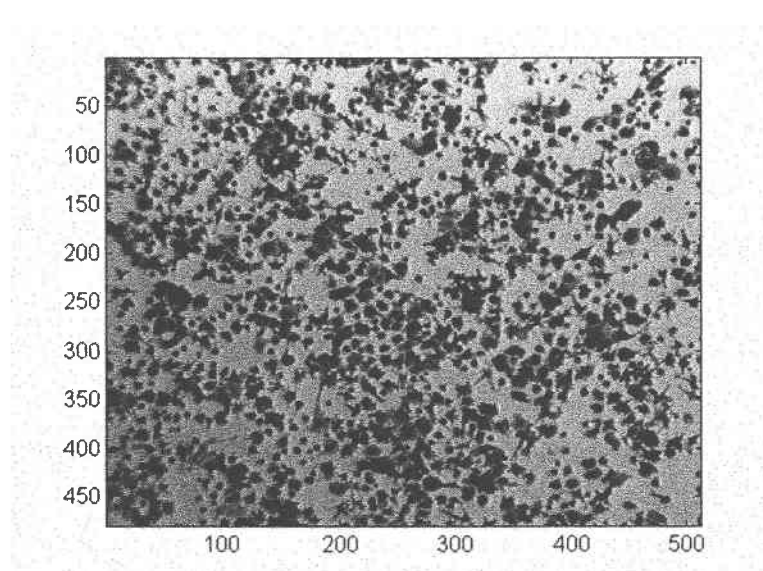


Figure 3-14: Original image 1.

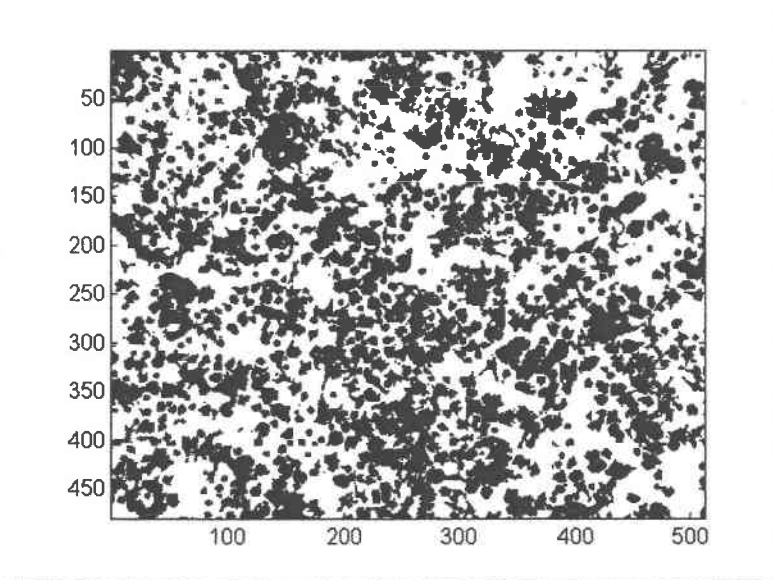


Figure 3-15: Result of the first segmentation step.

Figure 3-16 shows the combined results of the first and second segmentations. Most of the pigment granule parts are represented correctly in this image, but some background noise is contained as well.

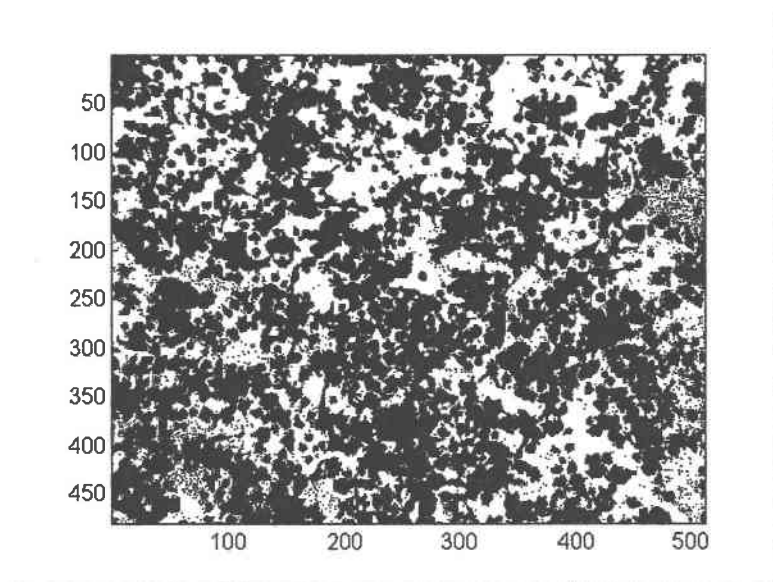


Figure 3-16: Result after the second segmentation step with a low threshold ( $-\sigma$ ).



Figures 3-17 and 3-18 show the effect of increasing the segmentation threshold in the second segmentation. The threshold is increased in steps of  $\sigma/2$  from the threshold in Figure 3-16. The figures contain much more noise. Experiments on chromatophore pigment granule distribution images show that a threshold of around  $-\sigma$  for the second segmentation gives the best results.

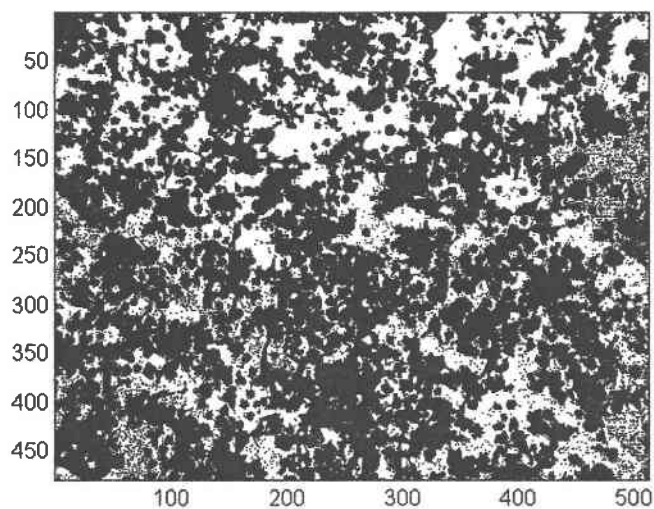


Figure 3-17: Result after the second segmentation step with a medium threshold ( $-\sigma/2$ ).

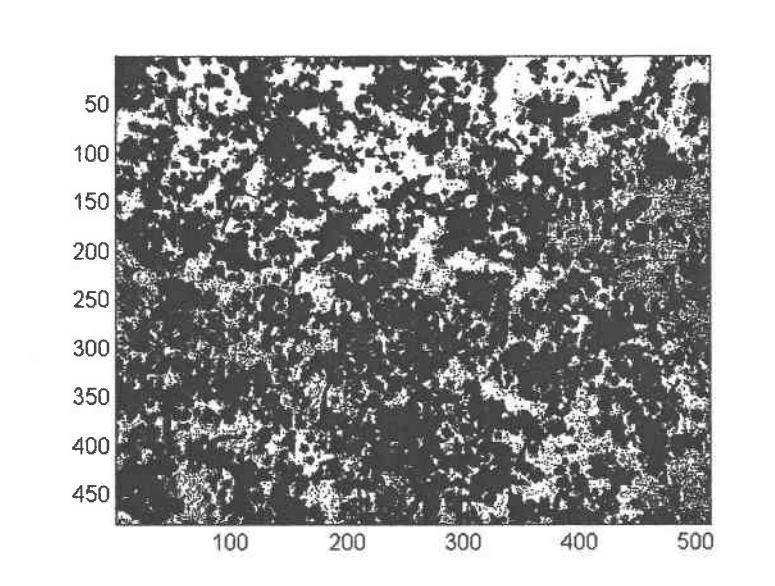


Figure 3-18: Result after the second segmentation step with a high threshold (0).

A simple filter for removing isolated patches was implemented and used for improving the segmented images. The filter is based on the idea that if the image is scanned in the horizontal, vertical, and the two diagonal directions, we can distinguish most of the background noise from the pigment granules based on the lengths of the intersected segments. The filtering procedure can be summarized as follows:

- Perform four scans through the image in the horizontal, vertical, and the two  $45^\circ$  directions.
- In each scan remove groups of black pixels whose length is smaller than  $n_w$ .

While this simple filter cannot recognize all of the background noise, it can improve the image significantly without the need of excessive computation. The computational complexity of the filter grows linearly with the number of image pixels. Therefore it is more practical than filters that would scan the neighborhood of each potential noise point for connected points. Figure 3-19 shows the filtered result for the segmented image of Figure 3-16. It is seen that most of the background noise is removed from this figure.

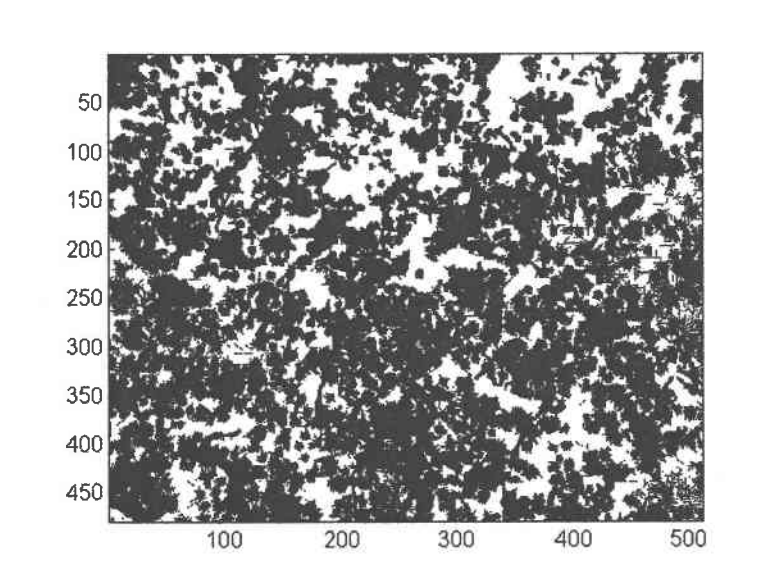


Figure 3-19: Final result after passing the segmented image of Figure 3-16 through a simple filter of isolated patches.

When the same filter is applied to the noisiest image of Figure 3-18, only a part of the noise is removed (Figure 3-20), but the resulting image still improves even the worst segmented result. This experiment shows that noise filtering of segmented images can be very useful.

When the above filtering process is applied to a hole sequence of images, even the results that contain significant background noise after the segmentation, such as those of Figure 3-20, correctly capture the dynamic behavior of pigment granules as a function of time. This is seen in Chapter 4.

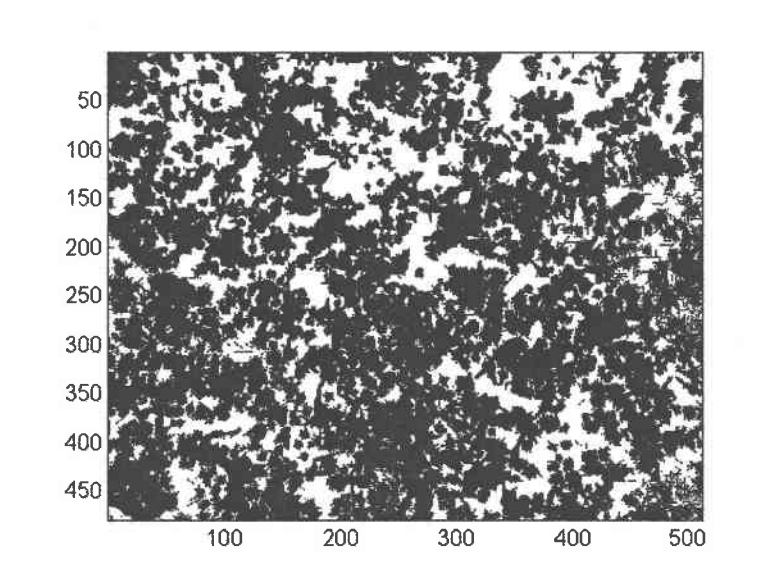


Figure 3-20: Result after filtering the noisiest segmented image of Figure 3-18.

### 3.5.4.2 Example 3-2

The original gray scale image used for the second example is shown in Figure 3-21.

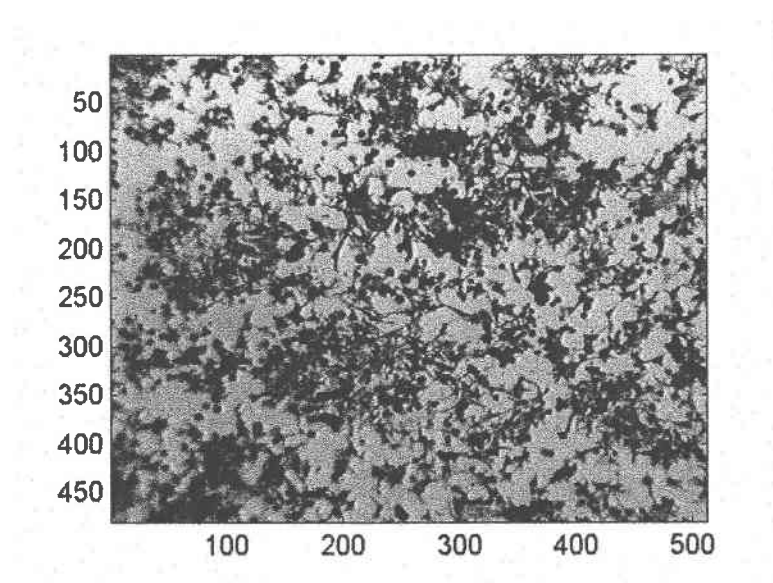


Figure 3-21: Original image 2.

The image segmented using the proposed method is shown in Figure 3-22. No filtering is required for this image since there is very little background noise in the segmented results.

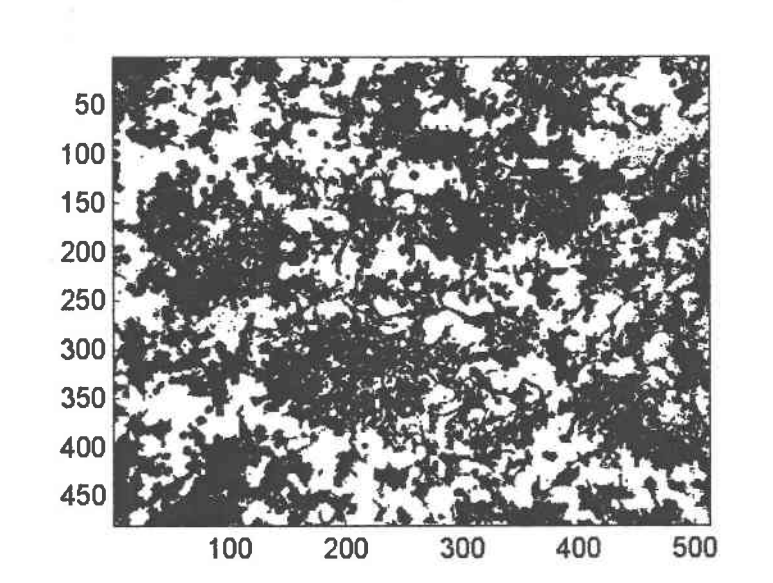


Figure 3-22: Image 2 after performing proposed segmentation without filtering.

### 3.5.4.3 Example 3-3

The chromatophores in the third example, shown in Figure 3-23, are distributed non-uniformly over the surface of the image. The image contains large areas which are densely populated with pigment granules and areas of similar size with no visible pigment granules at all.

The segmentation result for this image is show in Figure 3-24.

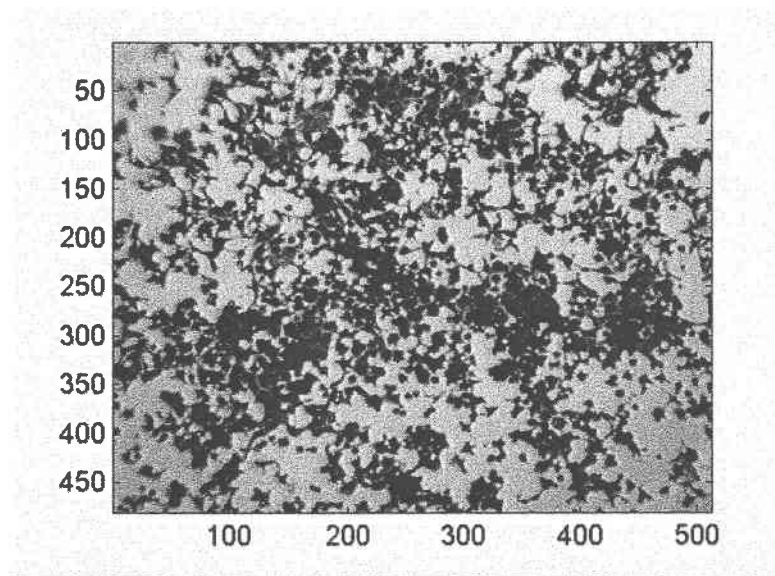


Figure 3-23: Original image 3.

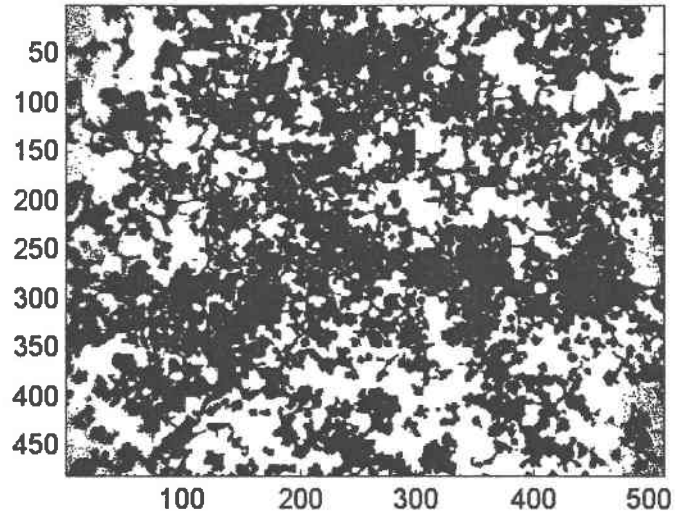


Figure 3-24: Image 3 after segmentation.

The filtered result is shown in Figure 3-25.

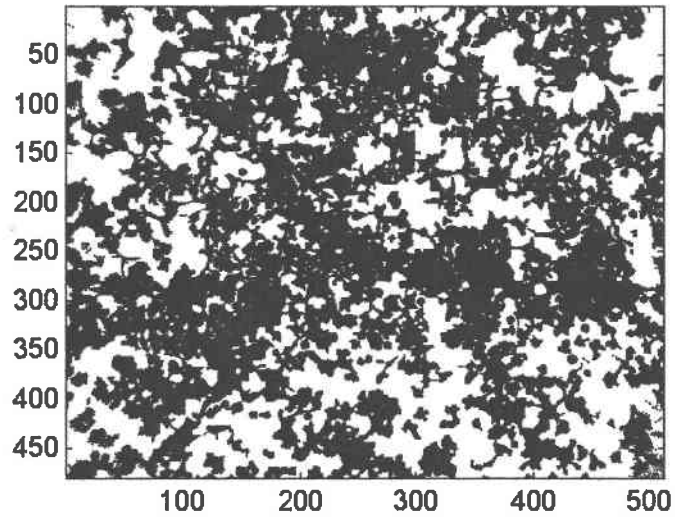


Figure 3-25: Segmented and filtered image 3.

## **3.6 Feature Extraction of Chromatophore Pigment Granule Distributions by Fitting an Analytical Model**

### **3.6.1 Introduction**

In this dissertation, one aim of chromatophore pigment granule distribution processing is to extract important features from image data. Features, such as size and gray color intensity of pigment granule distribution provide a description, interpretation, or understanding of the chromatophore's scene and aid in the identification of the pigment granule distribution object.

Chromatophore pigment granule distributions on a particular image have similar properties. These properties are shape and intensity. The idea is to capture these dominant characteristics of the chromatophore pigment granule distribution in the form of a simple analytical model. This way chromatophore pigment granule distributions are described by a small set of coefficients. The coefficients carry information about the model at each centrosome.

There are several benefits in pigment granule distribution modeling. First of all, the pigment granule distribution model is much easier to work with. Secondly, the amount of data associated with visual information is so large that its storage requires enormous storage capacity. Although the capacities of several storage media are substantial, their access speeds are usually inversely proportional to their capacity. When chromatophore pigment granule distributions are described by small sets of coefficients, the amount of information is reduced significantly, which helps processing speed.

Modeling can be considered a data compression technique for chromatophore pigment granule distribution images since the number of bits required to store or transmit images is reduced without any appreciable loss of relevant information. Furthermore, pigment granule distributions can be recognized based on their coefficients and tracked from frame to frame.



### 3.6.2 Analytical Model of Chromatophore Pigment Granule Distributions

Different gray level intensities on the image represent different concentrations of pigment granules for a chromatophore (Figure 3-26). Areas of greater concentration are represented by lower intensity levels, while areas of lower concentration are represented by higher intensity levels.

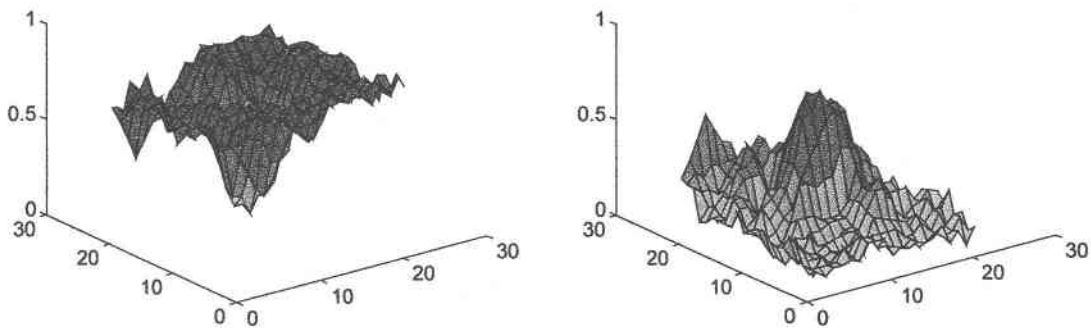


Figure 3-26: Pigment granule distribution of a single cell: (a) Intensity  $I(x,y)$ ; (b)  $1-I(x,y)$ .

The idea of analytical modeling is to find an analytical function,  $f(x,y)$ , which approximates the shape of the image intensity corresponding to a local pigment granule distribution. The analytical function should be relatively simple in the sense that it is described by a small set of coefficients. For convenience, the image intensity,  $I(x,y)$ , is inverted so that the central dark area around the centrosome has a maximum value. The resulting image,  $g(x,y)=1-I(x,y)$ , is then considered to be the image that needs to be approximated.

It is seen from Fig. 3-26 that the pigment granule distribution function  $g(x,y)$  has a bell-like shape. This suggests that it should be possible to model it with a function of the form  $f(x,y)=b/(1+a_1x^2+a_2y^2)$ , where  $a_1>0$ ,  $a_2>0$  (Figure 3-27).

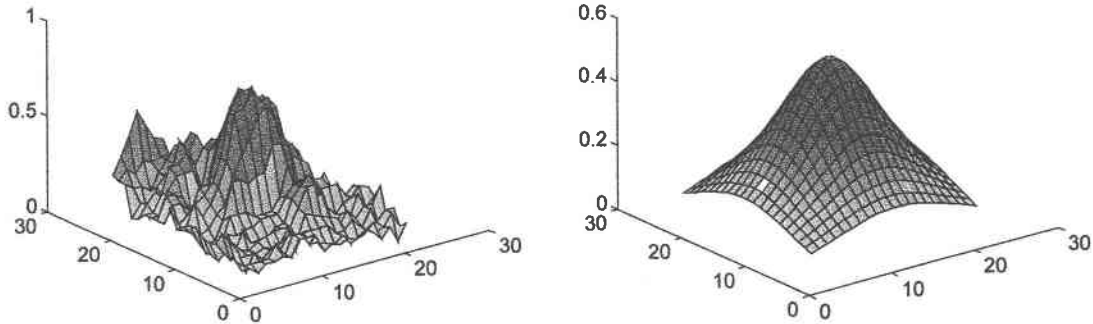


Figure 3-27: Pigment distribution function  $g(x,y)$  and its model  $f(x,y)$ .

The modeling problem consists of the following steps:

1. Find the model origin (position of the model).
2. Choose a rectangular area for fitting the model to the image.
3. Compute the coefficients  $a_1$ ,  $a_2$  and  $b$ .

### 3.6.3 Pigment Granule Distribution Modeling Equations

The equations for computing the model coefficients are derived next. The starting equation is the modeling function

$$f(x,y) = \frac{b}{1 + a_1x^2 + a_2y^2} \quad (3-17)$$

where  $x$ ,  $y$  are the local coordinates of a granule distribution point with respect to the model origin. The above function will approximate a pigment granule distribution image locally.

The first step for fitting model (3-17) to the distribution function  $g(x,y)$  is to introduce an error function. The approach used here is to choose the square of the difference between  $f$

and  $g$  for the error function and to find the coefficients that minimize the error function. This corresponds to the well known least squares approach.

The error function has the form

$$e(a_1, a_2, b) = \sum_i [f(x_i, y_i) - g(x_i, y_i)]^2 = \sum_i \left( \frac{b}{1 + a_1 x_i^2 + a_2 y_i^2} - g_i \right)^2 \quad (3-18)$$

where  $g(x_i, y_i)$  is the granule distribution to be fitted by the model and  $i$  indexes all of the points (pixels) in the fitting rectangle.

At the error minimum, the partial derivatives of the error function with respect to the coefficients  $a_1$ ,  $a_2$  and  $b$  are zero:

$$\frac{\partial e}{\partial b} = \sum_i 2 \left( \frac{b}{1 + a_1 x_i^2 + a_2 y_i^2} - g_i \right) \frac{1}{1 + a_1 x_i^2 + a_2 y_i^2} = 0, \quad (3-19)$$

$$\frac{\partial e}{\partial a_1} = \sum_i 2 \left( \frac{b}{1 + a_1 x_i^2 + a_2 y_i^2} - g_i \right) \frac{-b}{(1 + a_1 x_i^2 + a_2 y_i^2)^2} x_i^2 = 0, \quad (3-20)$$

$$\frac{\partial e}{\partial a_2} = \sum_i 2 \left( \frac{b}{1 + a_1 x_i^2 + a_2 y_i^2} - g_i \right) \frac{-b}{(1 + a_1 x_i^2 + a_2 y_i^2)^2} y_i^2 = 0. \quad (3-21)$$

The system of equations (3-19)–(3-21) is linear in  $b$  but it is nonlinear in  $a_1$  and  $a_2$ . Therefore, it cannot be solved directly. It turns out that a simpler set of equations is obtained for  $1/f$ :

$$f(x, y)^{-1} = \frac{1 + a_1 x^2 + a_2 y^2}{b}. \quad (3-22)$$

A new error function is computed between  $1/f(x, y)$  and  $1/g(x, y)$ :

$$e(a_1, a_2, b) = \sum_i \left[ \frac{1}{f(x_i, y_i)} - \frac{1}{g(x_i, y_i)} \right]^2 = \sum_i \left( \frac{1 + a_1 x_i^2 + a_2 y_i^2}{b} - (g_i)^{-1} \right)^2 \quad (3-23)$$

Taking the partial derivatives of the error function with respect to the coefficients gives

$$\frac{\partial e}{\partial b} = \sum_i 2 \left( \frac{1 + a_1 x_i^2 + a_2 y_i^2}{b} - (g_i)^{-1} \right) (1 + a_1 x_i^2 + a_2 y_i^2) \left( \frac{-1}{b^2} \right) = 0, \quad (3-24)$$

$$\frac{\partial e}{\partial a_1} = \sum_i 2 \left( \frac{1 + a_1 x_i^2 + a_2 y_i^2}{b} - (g_i)^{-1} \right) \frac{x_i^2}{b} = 0, \quad (3-25)$$

$$\frac{\partial e}{\partial a_2} = \sum_i 2 \left( \frac{1 + a_1 x_i^2 + a_2 y_i^2}{b} - (g_i)^{-1} \right) \frac{y_i^2}{b} = 0. \quad (3-26)$$

In the above system of equations, the last two are linear in  $a_1$  and  $a_2$ . The whole system of equations (3-24)–(3-26) can now be solved iteratively in the following way. Multiplication of (3-24) by  $b^3$  gives

$$\sum_i [(1 + a_1 x_i^2 + a_2 y_i^2) - b (g_i)^{-1}] (1 + a_1 x_i^2 + a_2 y_i^2) = 0 \quad (3-27)$$

from which

$$b = \frac{\sum_i [1 + a_1 x_i^2 + a_2 y_i^2]^2}{\sum_i (g_i)^{-1} [1 + a_1 x_i^2 + a_2 y_i^2]}. \quad (3-28)$$

Therefore, if the coefficients  $a_1$  and  $a_2$  are known,  $b$  can be computed directly using (3-28).

To calculate  $a_1$  and  $a_2$ , the system of linear equations (3-26)–(3-27) is rearranged. First (3-26) and (3-27) are multiplied by  $b^2$  obtaining

$$\sum_i [(1 + a_1 x_i^2 + a_2 y_i^2) - b (g_i)^{-1}] x_i^2 = 0. \quad (3-29)$$

$$\sum_i [(1 + a_1 x_i^2 + a_2 y_i^2) - b (g_i)^{-1}] y_i^2 = 0. \quad (3-30)$$

Equations (3-29) and (3-30) are then written in the form of a linear system for  $a_1$  and  $a_2$ :

$$a_1 \sum_i x_i^4 + a_2 \sum_i x_i^2 y_i^2 = \sum_i (b (g_i)^{-1} - 1) x_i^2, \quad (3-31)$$

$$a_1 \sum_i x_i^2 y_i^2 + a_2 \sum_i y_i^4 = \sum_i (b (g_i)^{-1} - 1) y_i^2. \quad (3-32)$$

The iterative solution approach then proceeds as follows:

1. Choose a starting value for  $b$  ( $b = g(\text{at model origin})$  turns out to be a good choice).
2. Solve the linear system (3-31)–(3-32) for  $a_1$  and  $a_2$ .
3. Compute the next  $b$  using (3-28).
4. Repeat steps 2 and 3 until the change in the computed coefficients is sufficiently small.

The procedure converges in a small number of iterations.

### 3.6.4 Finding the Pigment Granule Distribution Center

In order to calculate the model coefficients and also in order to recognize, select, and track individual chromatophore pigment granule distributions in an image sequence, it is necessary to define and find the positions of these distributions in the image.

As explained in Chapter 1, microtubules are long and straight hollow cylinders. The granules, which are visible in the images, are attached to microtubules, which are not

visible. However, the pigment granules provide a useful marker for the arrangement of microtubules in the cell. Microtubules are attached to the centrosome (MTOC). The pigment granules in image sequences aggregate in the centrosome. The areas in the image represented with low intensity levels correspond to the higher pigment granule distribution densities and consequently to the position of the centrosome. Therefore, the positions of the centrosome can be determined by finding a minimum intensity for a certain area of the image. However, the image intensity usually varies considerably from point to point and contains a large number of local minima within a given chromatophore distribution (Fig. 3-28 (c)). As a result, the position of the centrosome cannot be determined directly from the position of the local minima. Two approaches have been tried in this work to determine the position of the minimum:

1. Find the minimum of the mean intensity in a certain region.
2. Filter the image with a low-pass filter and then find the minimum.

Although the two approaches are similar to each other, approach 2 is more general and it has proven to be more robust for practical applications.

The behavior of the intensity levels of a more complex chromatophore image is illustrated in Fig. 3-28. It is clear from Figures 3-28 (c) and (d) why it is much easier to find the pigment distribution center on the filtered image.

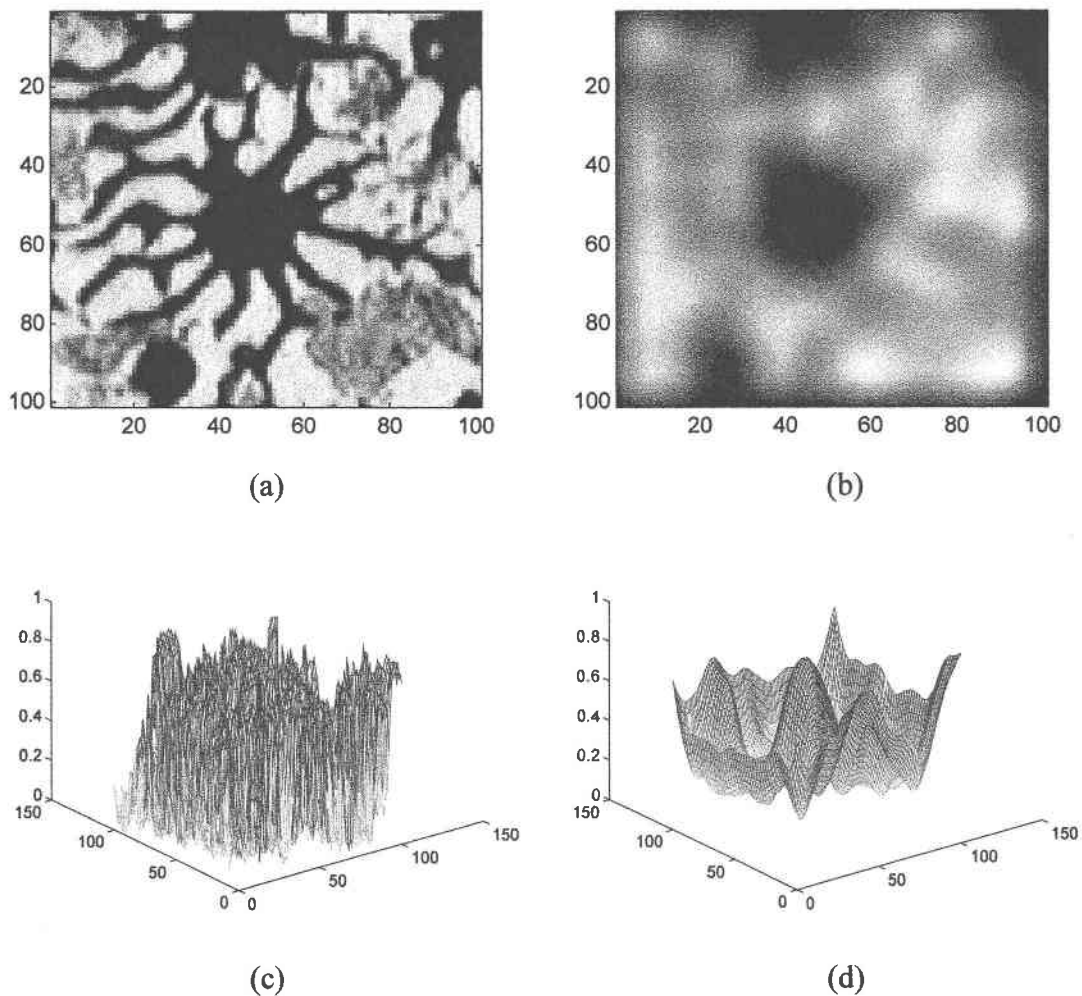


Figure 3-28: Variation of intensity  $I(x,y)$  for typical fish chromatophore: (a) original grayscale image; (b) image filtered with  $20 \times 20$  pixel half wave cosine filter,  $\text{filter}(I(x,y))$ ; (c) surface plot of  $1 - I(x,y)$ ; (d) surface plot of  $1 - \text{filter}(I(x,y))$ .

### 3.6.5 Pigment Granule Distribution Modeling Example

The approach described in Section 3.6.4 can now be used to find the positions of the pigment distributions on the image while the calculation procedure from Section 3.6.3 can be used to compute the coefficient for each distribution. The result is a collection of coefficient triplets  $(a_1, a_2, b)$ , one for each pixel. Only the triplets corresponding to pigment distribution centers (centrosomes) need to be stored. The computed coefficients can

be used to recognize, select and track desired pigment granule distributions and to characterize their behavior.

The modeling procedure is exemplified on the image shown in Fig. 3-29 (a). The position of the calculated pigment granule distribution centers is shown on Fig. 3-29 (a) with white dots. Figure 3-29 (b) shows an image plot of the  $b$  coefficient calculated for each point of the image. It is seen that the  $b$  coefficient resembles a low pass filtered version of the original image. Its value is directly related to the density of the pigment granules.

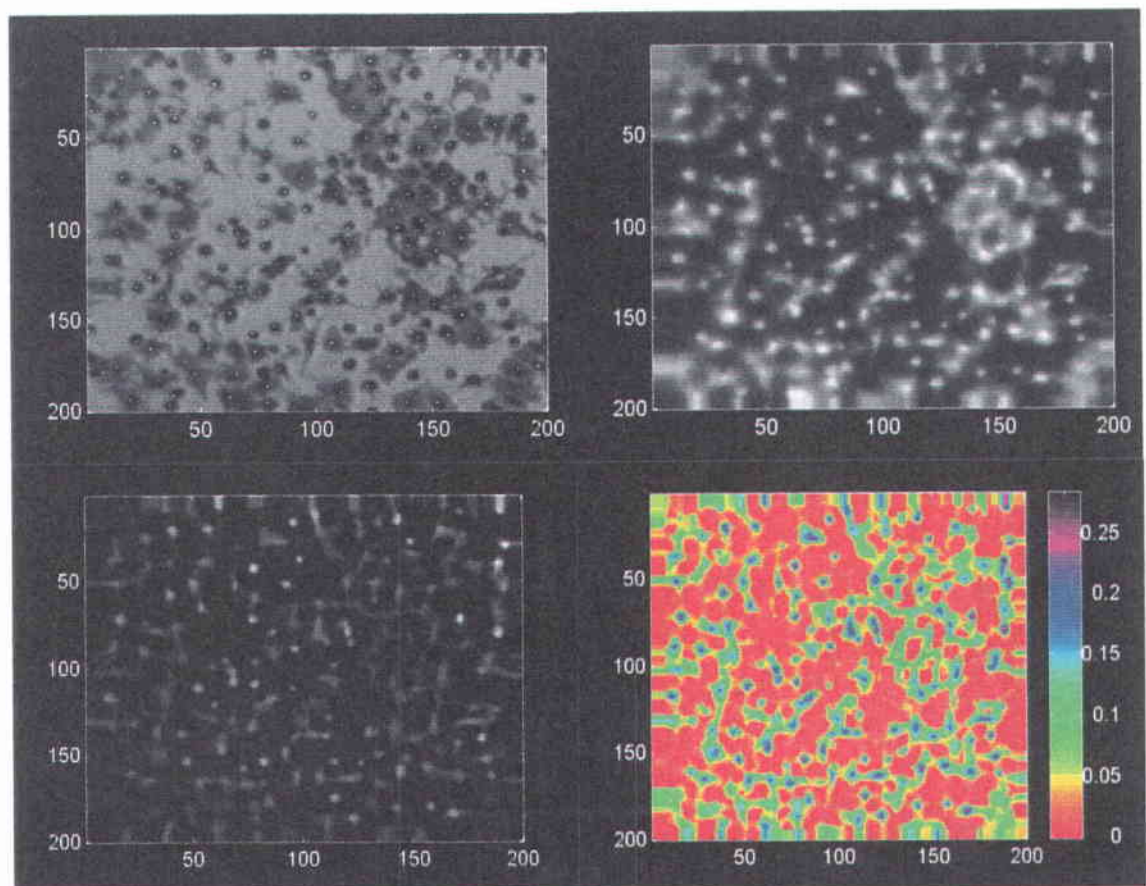


Figure 3-29: Chromatophore pigment granule distribution modeling: (a) Original image with calculated positions of pigment distribution centers shown as white dots; (b) Image plot of  $b$  coefficient calculated for every point of the image; (c) Image plot of  $a = \sqrt{a_1^2 + a_2^2}$ , (d) Image plot of  $b \sqrt{a}$ .



The calculated model coefficients can be combined to extract various features from the chromatophore image. For example, the two  $a$  coefficients can be combined into a single coefficient using the relation

$$a = \sqrt{a_1^2 + a_2^2}.$$

The resulting  $a$  coefficient characterizes the width of the pigment granule distributions. A large  $a$  means aggregated, isolated pigment granules. The behavior  $a$  of  $a$  for the image of Fig. 3-29 (a) is shown in Fig. 3-29 (c).

Useful information can also be obtained by combining the  $a$  and  $b$  coefficients. A plot of  $b\sqrt{a}$  is shown in Fig. 3-29 (d). It is seen that this combination accentuates the variation in the granule distributions of the original chromatophore image and shows details that were not visible in the original image.

## **Chapter 4**

### **Mathematical Model of the $G_s$ -AC-PKA Signal Transduction Pathway From the Chemical Reception Signal to the Image Sequence**

#### **4.1 Introduction**

This chapter proposes a mathematical model (system model) for the behavior of fish chromatophores. Current biological research in the area of cell pathway modeling is extended to include the effect of chemical reactants in the pathway on the produced visual images.

#### **4.2 Fundamentals of Chemical Reaction Modeling**

Signaling pathways inside cells represent chains of chemical reactions. An accurate and general approach for modeling chemical reactions is to model them in terms of coupled ordinary differential equations. These equations describe the time evolution of the concentrations of the chemical involved: reactants, intermediaries, catalysts and products. A wide variety of chemical reactions can be modeled this way, including cell signaling processes. Due to the fact that relatively large systems of ordinary differential equations can be solved using today's computers, extensive research is being done worldwide in applying chemical reaction modeling to biological systems.

For the sake of completeness, the methodology for modeling chemical reactions using differential equations is described here. Also, the related notation and terminology are introduced through several simple inorganic examples.

### 4.2.1 Simple Reactions

The net chemical reaction that takes place when water (H<sub>2</sub>O) is formed from hydrogen (H<sub>2</sub>) and oxygen (O<sub>2</sub>) is



The notation used to describe this reaction indicates that two molecules of hydrogen combine with one molecule of oxygen to form two molecules of water. Any chemical reaction can be described this way. For example, the net reaction for the formation of nitrogen dioxide (NO<sub>2</sub>) from nitrous oxide (NO) and oxygen (O<sub>2</sub>) is



Another example of a chemical reaction is the decomposition of hydrogen peroxide (H<sub>2</sub>O<sub>2</sub>) into water and oxygen



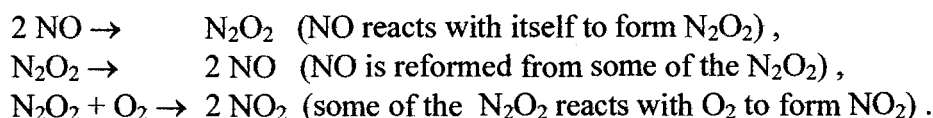
The arrow in relations (1)–(3) shows the direction of the chemical reaction. The molecules in (1)–(3) that are to the left of the arrow are called the *reactants* and the molecules on the right are the *products*.

In general, any chemical reaction of the type (4-1)–(4-3) that involves up to two reactants and up to products can be written in the form



where the symbols *A* and *B* stand for the *reactants* of the reaction and the symbols *C* and *D* stand for the *products* of the reaction. The constants *a*, *b*, *c*, and *d*, which indicate the proportions in which the reactants combine and the products are formed, are called *stoichiometric coefficients*. If any of the terms in (4-4) are missing from the original reaction, its stoichiometric coefficient is set to zero.

It is important to note that stoichiometric descriptions of reactions such as (4-4) do not explain how a reaction takes place. They only specify the net result of the reaction. Most chemical reactions have a mechanism involving the formation of intermediate products. For example, the net reaction (4-2) for the formation of nitrogen dioxide actually consists of three subreactions – all of which occur simultaneously. A believed mechanism for this reaction is:



The intermediate product of dinitrogen dioxide ( $\text{N}_2\text{O}_2$ ) does not appear in the net reaction (4-2), but it is involved in the mechanism of the reaction. Therefore, a detailed mathematical model of the reaction should take the presence of  $\text{N}_2\text{O}_2$  into account. Nevertheless, even without the detailed representation of the intermediate product, relation (4-2) correctly describes the net result. This possible simplification of chemical reactions is extremely important in the modeling of biological systems where whole sequences of yet unexplained chemical reactions can often be skipped without significantly affecting the final result.

The generalization of (4-4) to more than two reactants or more than two products is straightforward. One only needs to add more terms to (4-4). Also, chemical reactions are usually reversible, i.e., they can proceed in both directions. If the reaction involves the release of energy in one direction it will involve the absorption of energy in the opposite direction. Reversible reactions are often represented by replacing the single arrow ( $\rightarrow$ ) with two separate arrows, one above the other, or a symbol that has arrows on both ends ( $\leftrightarrow$ ). Reversible reactions really represent two different reactions with distinct characteristics.

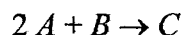
#### 4.2.2 Model Variables; Units of Measurement; Notation

The chemicals involved in a chemical reaction are characterized in terms of their quantity as a function of time. It is customary to measure the quantity of a chemical in units of

*moles*. One mole of molecules is an *Avogadro's number* of molecules. Avogadro's number is approximately  $6.022 \times 10^{23}$  molecules. Concentrations of molecules in a solution are measured in units of *molarities* (M). One molarity is one mole of solute per liter of solution. For example, a 2 M aqueous solution of sodium chloride (NaCl) is a solution consisting of two moles of NaCl per each liter of solution. The notation  $[A]$  is used to denote the concentration (in molarities) of a molecule  $A$  in a solution. For example,  $[\text{NaCl}] = 2 \text{ M}$  represents a solution of NaCl whose concentration is 2 M.

### 4.2.3 Rates of Reactions; The Rate Law

The chemical reaction (4-4) involves the combination of a set of reactants into a set of products. If there is no accumulation of intermediate products, the rate of change of the concentration of a reactant is proportional to its stoichiometric coefficient. The same is true for the rate of change of the product concentrations. For example, the simple reaction



involves the combination of two molecules of  $A$  and one molecule of  $B$  to form one molecule of  $C$ . Because there is no accumulation of intermediate products, the concentration of  $A$  decreases at twice the rate at which the concentration of  $B$  decreases. Therefore,  $d[A]/dt = 2d[B]/dt$ . Also, the concentration of  $C$  increases at the same rate at which the concentration of  $B$  decreases. Therefore,  $d[C]/dt = -d[B]/dt$ .

In general, the following relationship holds for the simple reaction of (4-4)

$$-\frac{1}{a} \frac{d[A]}{dt} = -\frac{1}{b} \frac{d[B]}{dt} = \frac{1}{c} \frac{d[C]}{dt} = \frac{1}{d} \frac{d[D]}{dt} = v(t) \quad (4-5)$$

where  $v(t)$  is defined as the *rate* of the reaction. Since the stoichiometric coefficients  $a$ ,  $b$ ,  $c$ ,  $d$  have no units,  $v$  has units of M/time. The reaction rate  $v$  is generally not a constant, because the reaction slows as the reactants are used up during the course of the reaction.

Equation (4-5) represents a system of four differential equations with five unknowns, i.e., the number of equations is one less than the number of unknown concentrations. One more equation is needed to make a determinate system out of (4-5). This last equation is provided by the *rate law* of the chemical reaction. For the homogeneous reaction (4) with the reaction rate of (4-5), the rate law is usually described by the equation

$$v(t) = k [A]^{\alpha} [B]^{\beta}. \quad (4-6)$$

Equation (4-6) is the framework on which mathematical models of chemical reactions are built. In this equation, the constant of proportionality,  $k$ , is called the *rate constant* of the reaction, and the constants  $\alpha$  and  $\beta$  are called the *order* of the reaction with respect to the reactants  $A$  and  $B$ , respectively. The constants  $k$ ,  $\alpha$ , and  $\beta$  can be determined by chemical experiments. The coefficients  $\alpha$  and  $\beta$  have no units of measurement and the units of  $k$  are determined from (4-6) as  $M^{1-\alpha-\beta} \text{ time}^{-1}$ .

#### 4.2.4 Stoichiometric Networks; Graph Representation

Chemical reactions can be represented by mathematical graphs. The construction of these graphs can proceed in different ways. Usually, the nodes of the graph are the chemicals involved in the reaction while the edges of the graph depend on the reactions. The edges are assigned the rate law while the nodes are assigned the stoichiometric constants. Representing chemical reactions by directed graphs leads to stoichiometric networks. While a direct application of graph theory and network theory is possible, the behavior of the stoichiometric network is difficult to visualize from the graph. In biological systems such as the living cell, a large number of complex chemical reactions is involved and a simpler graphical representation is required. This simpler representation consists of the chemicals involved and the directions of the chemical reactions. Figure 4-1 illustrates two simple graphical representations of the reaction (4-4). While both representations are equivalent, the second form stresses that one reactant-product pair is more important than the second pair that can be considered as a byproduct. The more important pair is

indicated with a straight line. The stoichiometric coefficients, the reaction rates, and other information that would be contained in a stoichiometric network model are omitted from this simpler biological representation, as in Fig. 2-7.



Figure 4-1: Two simplified graphical views of chemical reaction (4).

#### 4.2.5 Graphical Representation of Biochemical Reactions; Signaling Pathways

In biochemical reactions, a number of reactant compounds are transformed into a number of product compounds. Every transformation in the sequence is usually catalyzed by one or more enzymes whose names are drawn next to the direction arrow (Fig. 4-2 (a)). A pathway is a collection of reactions. The nature of a pathway is that adjacent bioreactions operate on shared compounds: the *main substrates* that lie along the backbone of the pathway. The reactions between the main substrates (along the pathway) are usually symbolized by straight arrows. The unshared compounds are the *side substrates*, they are drawn off to the side of each bioreaction with curved arrows showing whether particular side substrates are reactants or products of a reaction (Fig. 4-2 (b)).

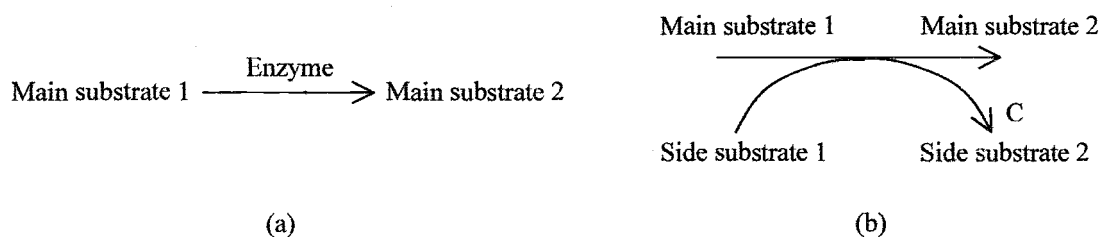


Figure 4-2: Graphical representation of biochemical reactions along pathways: (a) reaction catalyzed by an enzyme; (b) main and side substrates.

It should be noted that biochemical pathways described by the symbols of Figures 4-1 and 4-2 can also be converted into mathematical graph form. The nodes of the graph are the main and side substrates as well as the enzymes, while the edges of the graph are the straight lines that connect the main substrate as well as the curved lines that connect groups of side substrates. This representation is called the *pathway graph*.

A large amount of research is being done in cataloging biochemical pathways inside the cell as well as in automated ways of accessing this information and casting it into different representations. In this chapter, recent developments in the modeling of the fish chromatophore signal pathway of Fig. 3-7 are extended to describe the visual behavior of fish chromatophores.

### **4.3 DQCS Database**

A number of open access cellular signaling databases exist worldwide to facilitate the exchange of biological research information. One such database is the Database of Quantitative Cellular Signaling (DQCS), maintained by The National Center of Biological Sciences, Bangalore, India [10]. DQCS is a repository of models of signaling pathways which includes reaction schemes, concentrations, rate constants, as well as annotations on the models. The database provides a number of search, navigation, and comparison functions. From this database, a differential equation based model of the  $G_s$ -AC-PKA signal transduction pathway of fish chromatophores is extracted. The model is then extended to include the effect of the reactants on the chromatophore image sequence.

### **4.4 $G_s$ -AC-PKA Pathway Model**

The chromatophore pathway of greatest importance for this dissertation is the  $G_s$ -AC-PKA pathway. This pathway consists of receptor-ligand interaction, G-protein activation,



adenylyl cyclase mediated formation of cAMP, and activation of PKA. The graphical representation of the main components of the  $G_s$ -AC-PKA pathway are presented below.

#### 4.4.1 G-protein Activation

The layout of the G-protein activation pathway is shown in Fig. 4-3.

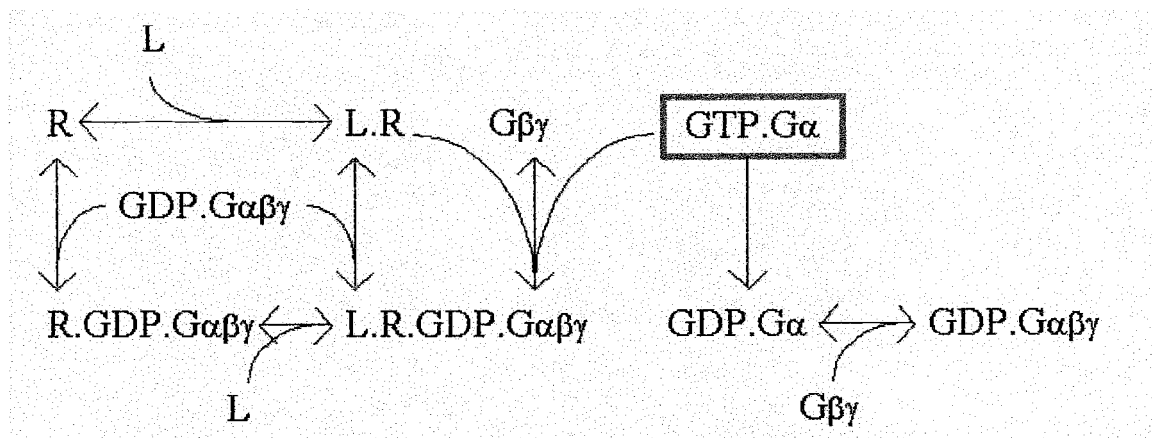


Figure 4-3: Layout of G-protein activation pathway.

It is assumed that GTP is present in fixed amounts, so it is left out of the explicit equations in the mathematical model that is explained below.

#### 4.4.2 AC Pathway

The AC pathway is shown in Fig. 4-4. Adenylyl cyclase is also known as adenylyl cyclase. There are a number of isoforms. This model includes only the canonical Gs-stimulated activity.

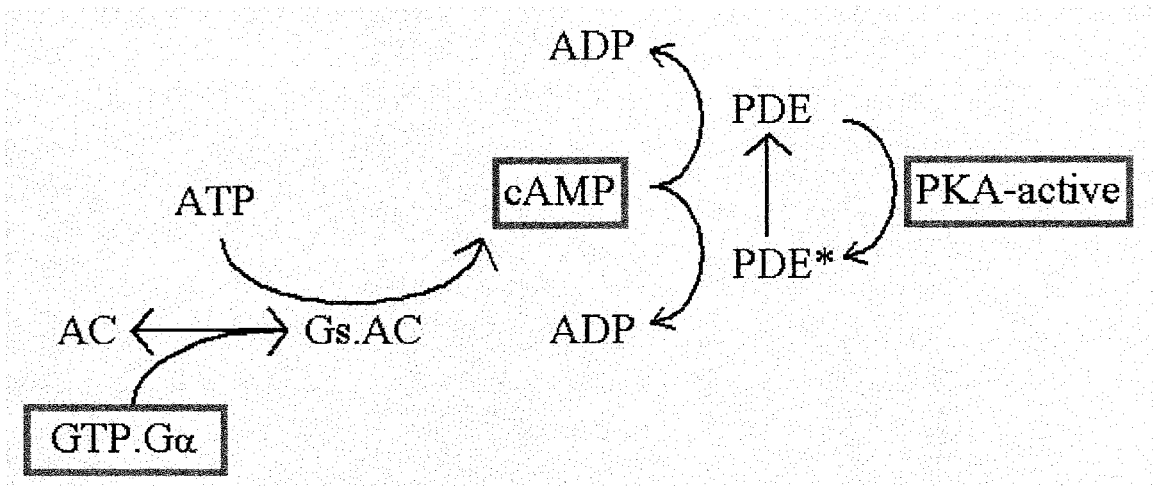


Figure 4-4: Layout of AC pathway.

#### 4.4.3 PKA Pathway

The layout of the PKA pathway is shown in Fig. 4-5.

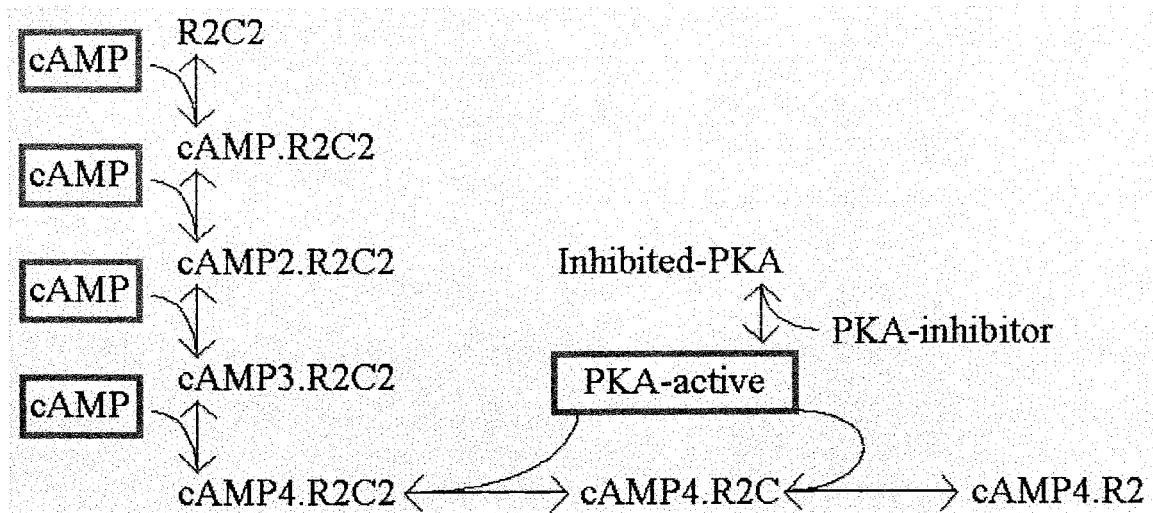


Figure 4-5: Layout of PKA pathway.

The complete G<sub>s</sub>-AC-PKA pathway is summarized in graphical form in Figure 4-6.

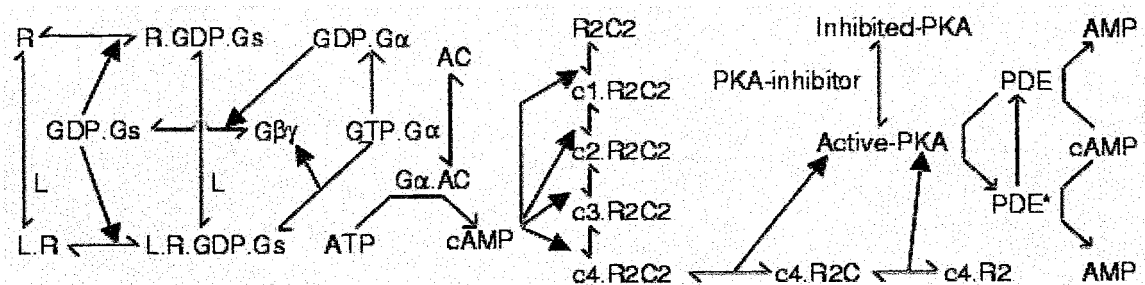


Figure 4-6: Summary of  $G_s$ -AC-PKA pathway.

## 4.5 Mathematical Model of $G_s$ -AC-PKA Pathway

A differential equation based mathematical model of the  $G_s$ -AC-PKA pathway shown in the first part of Fig. 2-16 was proposed by researchers at the National Center of Biological Sciences and it is obtainable from DQCS [10]. The model contains 27 differential equations corresponding to 27 of the 30 pathway substrates shown in the pathway graphs of Figs. 4-3 to 4-5. The concentrations of the three remaining substrates are assumed constant throughout the chemical reaction. These are the buffered molecules. For the purpose of this dissertation, the initial ligand concentration is considered to be the input of the model. Since the same model is intended to describe many different types of chromatophores and many different types of ligands, the input to the model is scaled depending on the actual chromatophore and the actual ligand used.

### 4.5.1 $G_s$ -AC-PKA Pathway Differential Equations and Nonzero Initial Conditions

The net behavior of the  $G_s$ -AC-PKA pathway is described by concentrations of 30 substrates. These are the model variables. There are 27 coupled ordinary differential equations relating the 30 pathway variables. All of the reactions are modeled by the first order rate law. Most of the initial conditions are chosen as zero. Those initial conditions that are nonzero are given below. All concentrations are given in  $\mu\text{M}$  and the time is in seconds.

*Initial conditions of unbuffered molecules:*

1. [AC] = 0.015
2. [cAMP-PDE] = 0.5
3. [GDP.Gabc] = 1
4. [PKA-inhibitor] = 0.25
5. [R] = 0.083333
6. [R2C2] = 0.5

*Concentrations of buffered molecules:*

1. [AMP] = 1000
2. [ATP] = 5000
3. [L] = Scaled model input.

*Differential Equations:*

1.  $d[AC]/dt = - 500[AC][GTP.Ga] + 1[Gs.AC]$
2.  $d[cAMP]/dt = - 75[cAMP2.R2C2][cAMP] + 110[cAMP3.R2C2] - 75[cAMP][cAMP3.R2C2] + 32.5[cAMP4.R2C2] - 54[R2C2][cAMP] + 33[cAMP.R2C2] - 54[cAMP.R2C2][cAMP] + 33[cAMP2.R2C2] - 2.5200342724661[cAMP][cAMP-PDE] + 40[cAMP-PDE\_PDE\_complex] - 5.0400685449322[cAMP][cAMP-PDE*] + 80[cAMP-PDE*\_PDE*\_complex] + 18[Gs.AC\_cyclase\_complex]$
3.  $d[cAMP-PDE]/dt = + 0.1[cAMP-PDE*] - 6[cAMP-PDE][PKA-active] + 36[PKA-active\_phosph-PDE\_complex] - 2.5200342724661[cAMP][cAMP-PDE] + 50[cAMP-PDE\_PDE\_complex]$
4.  $d[cAMP-PDE*]/dt = - 0.1[cAMP-PDE*] + 9[PKA-active\_phosph-PDE\_complex] - 5.0400685449322[cAMP][cAMP-PDE*] + 100[cAMP-PDE*\_PDE*\_complex]$
5.  $d[cAMP.R2C2]/dt = - 54[cAMP.R2C2][cAMP] + 33[cAMP2.R2C2] + 54[R2C2][cAMP] - 33[cAMP.R2C2]$
6.  $d[cAMP2.R2C2]/dt = - 75[cAMP2.R2C2][cAMP] + 110[cAMP3.R2C2] + 54[cAMP.R2C2][cAMP] - 33[cAMP2.R2C2]$
7.  $d[cAMP3.R2C2]/dt = - 75[cAMP][cAMP3.R2C2] + 32.5[cAMP4.R2C2] + 75[cAMP2.R2C2][cAMP] - 110[cAMP3.R2C2]$
8.  $d[cAMP4.R2]/dt = + 60[cAMP4.R2C] - 18[PKA-active][cAMP4.R2]$

9.  $d[\text{cAMP4.R2C}]/dt = - 60[\text{cAMP4.R2C}] + 18[\text{PKA-active}][\text{cAMP4.R2}] + 60[\text{cAMP4.R2C2}] - 18[\text{PKA-active}][\text{cAMP4.R2C}]$
10.  $d[\text{cAMP4.R2C2}]/dt = - 60[\text{cAMP4.R2C2}] + 18[\text{PKA-active}][\text{cAMP4.R2C}] + 75[\text{cAMP}][\text{cAMP3.R2C2}] - 32.5[\text{cAMP4.R2C2}]$
11.  $d[\text{Gbg}]/dt = - 6[\text{GDP.Ga}][\text{Gbg}] + 0.025[\text{L.R.GDP.Gabc}]$
12.  $d[\text{GDP.Ga}]/dt = - 6[\text{GDP.Ga}][\text{Gbg}] + 0.066667[\text{GTP.Ga}]$
13.  $d[\text{GDP.Gabc}]/dt = - 10[\text{GDP.Gabc}][\text{L.R}] + 0.1[\text{L.R.GDP.Gabc}] - 0.2[\text{GDP.Gabc}][\text{R}] + 0.1[\text{R.GDP.Gabc}] + 6[\text{GDP.Ga}][\text{Gbg}]$
14.  $d[\text{Gs.AC}]/dt = + 500[\text{AC}][\text{GTP.Ga}] - 1[\text{Gs.AC}]$
15.  $d[\text{GTP.Ga}]/dt = - 500[\text{AC}][\text{GTP.Ga}] + 1[\text{Gs.AC}] - 0.066667[\text{GTP.Ga}] + 0.025[\text{L.R.GDP.Gabc}]$
16.  $d[\text{inhibited-PKA}]/dt = + 60[\text{PKA-active}][\text{PKA-inhibitor}] - 1[\text{inhibited-PKA}]$
17.  $d[\text{L.R}]/dt = - 10[\text{GDP.Gabc}][\text{L.R}] + 0.1[\text{L.R.GDP.Gabc}] + 0.025[\text{L.R.GDP.Gabc}] + 0.1[\text{R}][\text{L}] - 0.1[\text{L.R}]$
18.  $d[\text{L.R.GDP.Gabc}]/dt = - 0.025[\text{L.R.GDP.Gabc}] + 5[\text{L}][\text{R.GDP.Gabc}] - 0.1[\text{L.R.GDP.Gabc}] + 10[\text{GDP.Gabc}][\text{L.R}] - 0.1[\text{L.R.GDP.Gabc}]$
19.  $d[\text{PKA-active}]/dt = - 60[\text{PKA-active}][\text{PKA-inhibitor}] + 1[\text{inhibited-PKA}] + 60[\text{cAMP4.R2C2}] - 18[\text{PKA-active}][\text{cAMP4.R2C}] + 60[\text{cAMP4.R2C}] - 18[\text{PKA-active}][\text{cAMP4.R2}] - 6[\text{cAMP-PDE}][\text{PKA-active}] + 45[\text{PKA-active\_phosph-PDE\_complex}]$
20.  $d[\text{PKA-inhibitor}]/dt = - 60[\text{PKA-active}][\text{PKA-inhibitor}] + 1[\text{inhibited-PKA}]$
21.  $d[\text{R}]/dt = - 0.1[\text{R}][\text{L}] + 0.1[\text{L.R}] - 0.2[\text{GDP.Gabc}][\text{R}] + 0.1[\text{R.GDP.Gabc}]$
22.  $d[\text{R.GDP.Gabc}]/dt = - 5[\text{L}][\text{R.GDP.Gabc}] + 0.1[\text{L.R.GDP.Gabc}] + 0.2[\text{GDP.Gabc}][\text{R}] - 0.1[\text{R.GDP.Gabc}]$
23.  $d[\text{R2C2}]/dt = - 54[\text{R2C2}][\text{cAMP}] + 33[\text{cAMP.R2C2}]$
24.  $d[\text{Gs.AC\_cyclase\_complex}]/dt = 4.5[\text{ATP}][\text{Gs.AC}] - 90[\text{Gs.AC\_cyclase\_complex}]$
25.  $d[\text{cAMP-PDE\_PDE\_complex}]/dt = 2.5200342724661[\text{cAMP}][\text{cAMP-PDE}] - 50[\text{cAMP-PDE\_PDE\_complex}]$
26.  $d[\text{cAMP-PDE*\_PDE*\_complex}]/dt = 5.0400685449322[\text{cAMP}][\text{cAMP-PDE*}] - 100[\text{cAMP-PDE*\_PDE*\_complex}]$
27.  $d[\text{PKA-active\_phosph-PDE\_complex}]/dt = 6[\text{cAMP-PDE}][\text{PKA-active}] - 45[\text{PKA-active\_phosph-PDE\_complex}]$

### 4.5.2 $G_s$ -AC-PKA Pathway Response

The system of ordinary differential equations describing the  $G_s$ -AC-PKA pathway can be readily integrated to yield the response of all the pathway substrate concentrations. For the purpose of illustrating the pathway behavior, three example responses are given. The initial ligand concentration is used as the input to the model. It is normalized with respect to a reference ligand concentration  $L_0 = 1$  pM. This reference ligand concentration corresponds to a very small value below which the model is typically not used. The time responses of two substrate concentrations (cAMP and Active PKA) that are positioned near the output of the pathway is shown in Figures 4-7 to 4-9.

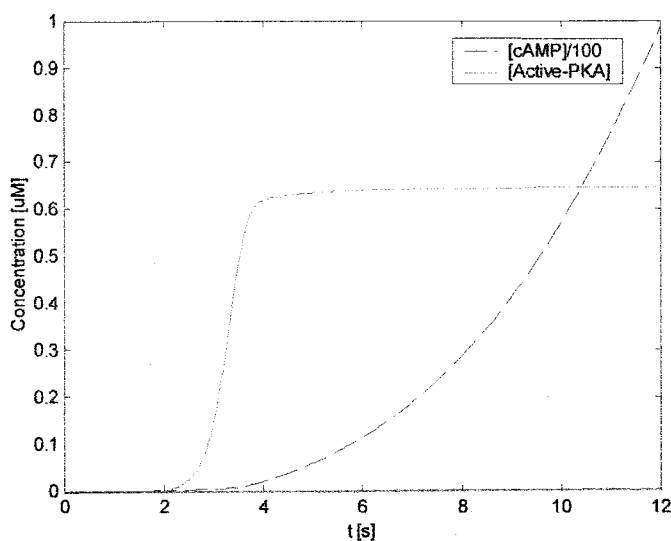


Figure 4-7: Pathway model response for input ligand concentration  $10^5 L_0$ .

It is seen from Figures 4-7 to 4-9 that the main effect of the change in the input ligand concentration is in the change of the time constants of the response curves. Higher ligand concentrations result in faster responses. Also, for high ligand concentrations, large changes of the ligand produce small changes in the time constants. At low ligand concentrations, the time constants are more sensitive to the relative change in the ligand concentration. It is also seen that the PKA curves lag the cAMP curves indicating that the change of PKA concentration is a consequence of the change in the cAMP concentration.

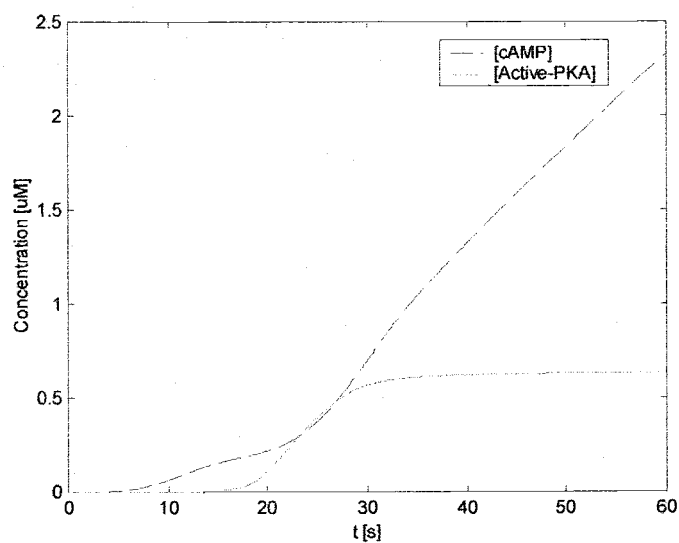


Figure 4-8: Pathway model response for input ligand concentration of  $10^2 L_0$ .

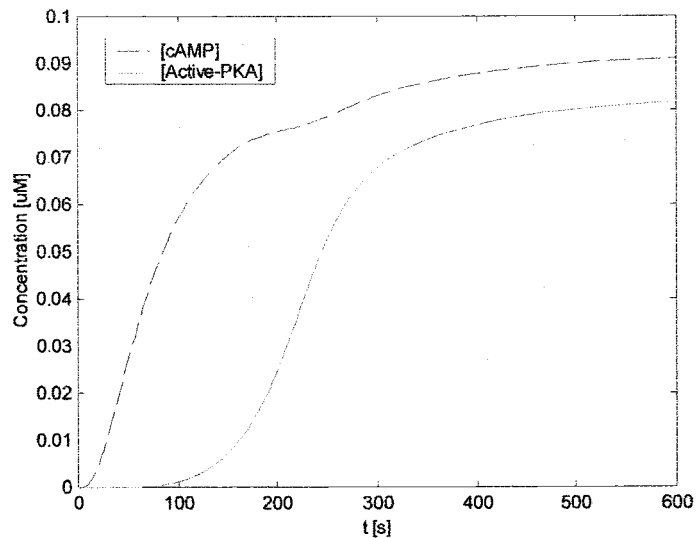


Figure 4-9: Pathway model response for input ligand concentration of  $L_0$ .

The input ligand concentrations in Figures 4-7 to 4-9 were chosen on purpose to cover a large range of concentrations. The actual input ligand concentrations used in the models of the following sections fall in the range bounded by Figures 4-8 and 4-9.

## 4.6 Link Between Pathway and Visual Image

The differential equation based model gives the concentrations of the various substrates as a function of time for a given input ligand concentration. The next step in the modeling of fish chromatophores is to link the chemical concentrations to the obtained visual image. This link is established based on a physical model of pigment granule motion along the microtubules.

It is believed that the pigment granules are carried along the microtubules by two motor protein families: kinesins and dyneins. However, the exact chemical reactions linking the kinesins and dyneins to the  $G_s$ -AC-PKA pathway are unknown to this date. Instead of trying to build the missing link from the  $G_s$ -AC-PKA pathway to the kinesins and dyneins, a link based on active PKA is proposed in this dissertation. There are two reasons for the choice of active PKA as the link to the granule motion: (1) its response to an input ligand lags the response of cAMP which is known to be linked to pigment motion, i.e., it is further along the pathway; (2) numerical experiments on measured image sequences performed for this work show that the simplest and the best model is obtained when active PKA is used as the link to granule motion. Active PKA is therefore used to form the output from the chemical reaction pathway model.

The differential equations for the  $G_s$ -AC-PKA pathway model the dispersion of pigment granules. In reality, pigment granules can either aggregate or disperse with the application of a ligand, depending on which receptor the ligand binds to. In order to model aggregation with the dispersion model, it is necessary to modify the model output. For aggregation, the model output is taken to be

$$[\text{PKA-active}](t_{\text{FINAL}}) - [\text{PKA-active}](t) \quad (4-7)$$

where  $[\text{PKA-active}](t_{\text{FINAL}})$  is the final concentration of active PKA at saturation.



#### 4.6.1 Model of Pigment Granule Motion: Average Cell Approach

It is believed that the motion of pigment granules occurs primarily along the microtubules. Microtubules generally stretch outwards from the centrosome forming curved lines. Although the exact shape of the pigment granule distribution varies from cell to cell, for modeling purposes it is reasonable to assume that the pigment granule distribution has a regular shape. This is equivalent to modeling an average cell in large collection of individually varying cells. Since there is no preferred direction in the average cell, it is also assumed that the granule distribution of the average chromatophore is of circular shape and that the microtubules are straight radial lines. The model of the pigment granule distribution for the average cell is shown in Fig. 4-10 (a) together with a few selected pigment granules. The pigment granules that are shown in Fig. 10 (a) and (b) are the outermost granules which define the outer boarder of the visible pigment distribution.

After a time  $\Delta t$ , the pigment granules shown in Fig. 4-10 (a) will move radially towards the center by a distance  $v(t) \Delta t$  along the microtubules, where  $v(t)$  is the speed of motion of a pigment granule at the time  $t$ . The position of the new pigment boarder is shown in Fig. 4-10 (b).

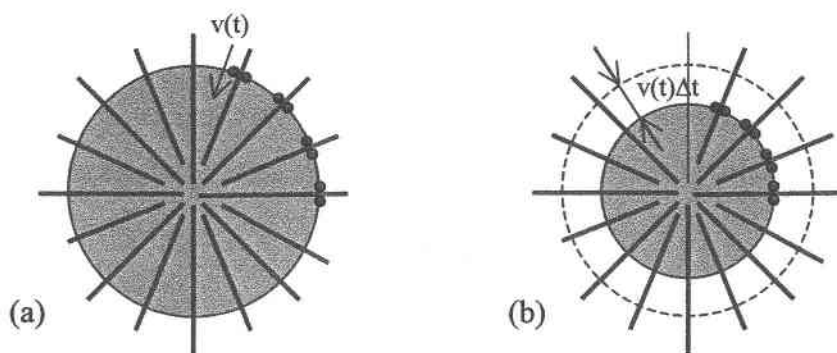


Figure 4-10: Model of average pigment granule distribution with selected pigment granules marking the outer boarder of the visible pigment distribution: (a) at the time  $t$ , (b) at  $t+\Delta t$ .

Assuming that the colored region of the average chromatophore is a circle of radius  $r(t)$ , a relationship between the area,  $A(t)$ , of the colored circle and the speed  $v(t)$  can be derived.

The area of the circle is

$$A(t) = r(t)^2 \pi = (r(0) - \int_0^t v(\tau) d\tau)^2 \pi \quad (4-8)$$

where  $r(0)$  is the radius at the start time  $t = 0$ . The speed  $v(t)$  is taken to be positive when the pigment granule is moving towards the center. If the initial radius of the pigment distribution,  $r(0)$ , is expressed in terms of the initial area,  $A(0)$ , (4-8) becomes

$$A(t) = \left( \sqrt{\frac{A(0)}{\pi}} - \int_0^t v(\tau) d\tau \right)^2 \pi \quad (4-9)$$

The next step is to determine the relationship between the speed of the granules and the concentration of the chemical that directly or indirectly causes the motion along the microtubule. As a first approximation the speed of granule motion in the radial direction is assumed proportional to the output concentration from the differential equation model,  $u(t)$ :

$$v(t) = k u(t). \quad (4-10)$$

where  $k$  is the unknown proportionality constant and  $u(t)$  is either

$$u(t) = [\text{PKA-active}](t). \quad (4-11)$$

for chromatophores and ligands that result in pigment dispersion with time or

$$u(t) = [\text{PKA-active}](t_{\text{FINAL}}) - [\text{PKA-active}](t) \quad (4-12)$$

for the case of pigment aggregation with time.

Equations (4-9), (4-10) and (4-11) or (4-12), together with the 27 differential equations for the chemical concentrations, complete the model. Only three constants remain to be

determined from experimental data on a given type of chromatophore: (1) the initial pigmented area,  $A(0)$ , of (4-9); (2) the proportionality constant  $k$  of (4-10) and (3) the input ligand proportionality constant that multiplies  $[L]$  in the differential equations of the pathway. The first one of these unknown coefficients represents the initial condition of the model while the remaining two coefficients are the model parameters. Determining the two unknown model parameters for a given type of chromatophore and for a given ligand represents the calibration of the model.

#### 4.6.1.1 Model Initial Conditions

The unknown model coefficients are determined from an experimentally obtained calibration image sequence in the following way. First, the average initial pigmented area needs to be determined from the first image of the sequence. This is the initial condition for the model. The average pigmented area for a cell can be determined by computing the total pigmented area and dividing by the total number of cells on the image. However, since the average pigmented area is just proportional to the total area, the model can also be formulated in terms of the total area. This way there is no need to find the number of cells on the image. The total pigmented area,  $A(0)$ , is now computed by segmenting the images using the techniques described in the previous chapter.

#### 4.6.1.2 Model Calibration

Once the initial pigmented area,  $A(0)$ , is determined using segmentation, the remaining two coefficients are computed iteratively from the following two conditions:

1. The final area,  $A(t_{\text{FINAL}})$ , predicted by the model must match the total pigmented area on the last image of the calibration sequence.
2. Given the above requirement, the least square error between the predicted area and the actual pigmented area on the calibration sequence should be minimal.

The first requirement gives the coefficient  $k$  in terms of the first and last areas in the calibration sequence as

$$k = \frac{\sqrt{\frac{A(0)}{\pi}} - \sqrt{\frac{A(t_{FINAL})}{\pi}}}{\int_0^{t_{FINAL}} u(\tau) d\tau} \quad (4-13)$$

The input ligand proportionality constant can then be determined by iterating between (4-13) and requirement 2.

#### 4.6.2 Modeling Example 4-1: Average Cell Approach

The modeling approach described in Section 4.6.1 is validated on a chromatophore image sequence consisting of 150 images. The images were taken at intervals of 4 seconds for a total duration of 10 minutes. Clonidine was used as the input ligand. It was applied in a concentration of 5  $\mu\text{M}$  (initial concentration). The first, middle and last images from the 150 image sequence are shown in Figs. 4-11 to 4-13.

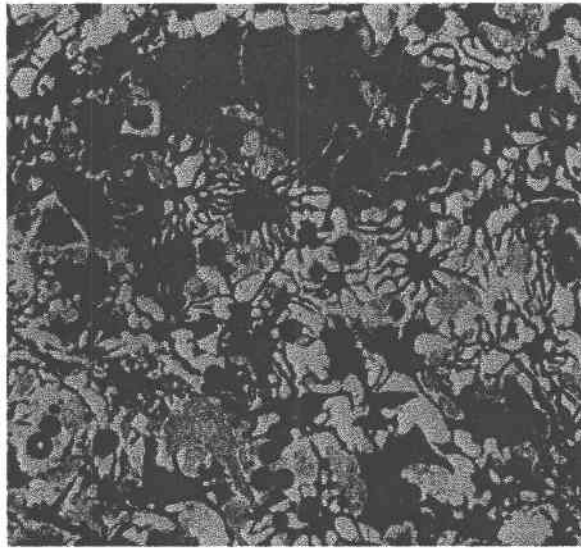


Figure 4-11: First image in 150 image sequence of Example 4-1.

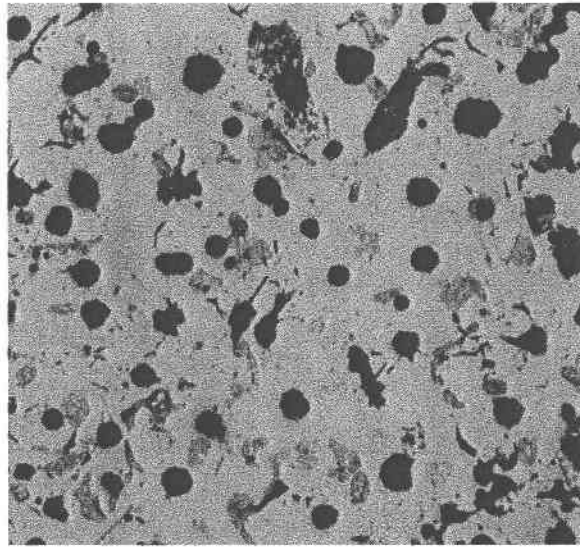


Figure 4-12: Middle image in 150 image sequence of Example 4-1.

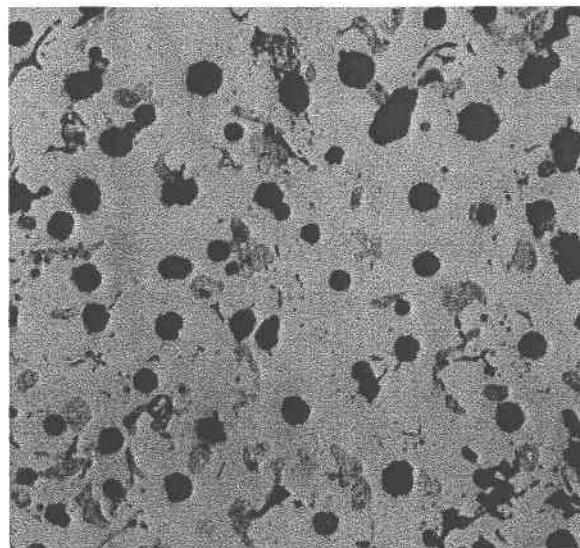


Figure 4-13: Last image in 150 image sequence of Example 4-1.

The 150 images were converted to grayscale and segmented using the approach described in Chapter 3. The total colored area of each image was calculated from segmented experimental data. This area corresponds to the curve labeled “From Measurement” in Fig. 4-14. The results obtained by the modeling approach described in Section 4.6.1 are

also shown in Fig. 4-14. The agreement between measured and simulated results is remarkably good considering the simplicity of the physical model and the fact that only two model parameters were calculated from measured data.

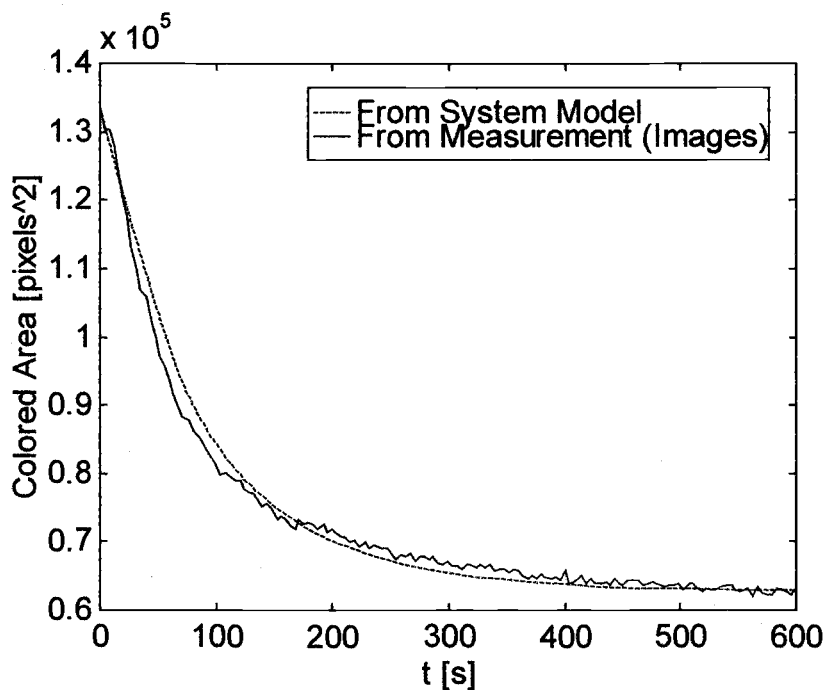


Figure 4-14: Area of pigment granules from pathway model and from measurement.

Since the pigment granules in the experiment aggregate with time, (4-12) was used for the pathway output,  $u(t)$ , in (4-10). The chemical response of the signaling pathway corresponding to the model of this experiment is illustrated in Fig. 4-15. Several chemicals near the output of the pathway are shown.

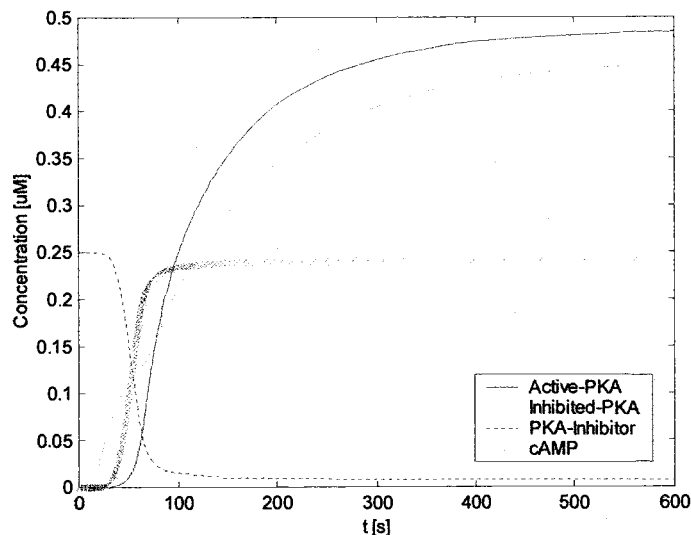


Figure 4-15: Pathway substrate response for Example 4-1.

### 4.6.3 Model of Pigment Granule Motion: Individual Cell Approach

In the previous chapter, chromatophore pigment granule distributions of each cell were modeled by fitting bell-like surfaces to the chromatophore image. This individual cell modeling approach is now linked to the signaling pathway. The end result is a system model for an individual cell from the input ligand to the mathematical surface describing the pigment distribution.

Starting from a particular cell, a surface  $f(x,y)$  of the form

$$f(x,y) = \frac{b}{1 + a_1 x^2 + a_2 y^2} \quad (4-14)$$

is assigned to the cell using the methods of Chapter 3. The coefficients  $a_1$  and  $a_2$  in the denominator of (4-14) are related to the width of the pigment distribution and they change with time. The width of the distribution (4-14) in one direction, e.g., the  $y$  direction, can be determined by integrating  $f(x,y)$  from  $-\infty$  to  $\infty$ :

$$\begin{aligned}
 I(x) &= \int_{y=-\infty}^{\infty} f(x,y) dy = b \int_{y=-\infty}^{\infty} \frac{dy}{c(x) + a_2 y^2} = \frac{b}{\sqrt{a_2}} \int_{u=-\infty}^{\infty} \frac{du}{c(x) + u^2} = \\
 &= \frac{b}{\sqrt{a_2} c(x)} \arctan \frac{y}{c(x)} \Big|_{-\infty}^{\infty} = \frac{b}{\sqrt{a_2} c(x)} \left( \frac{\pi}{2} - \left( -\frac{\pi}{2} \right) \right) = \frac{b \pi}{\sqrt{a_2} c(x)} \quad (4-15)
 \end{aligned}$$

where  $c(x) = 1 + a_1 x^2$ . The area of (4-15) is maximal for  $x = 0$ . Introducing the effective width of the curve  $f(0,x)$  as the width of the rectangle whose area is equal to  $I(0)$  (Fig. 4-16) gives

$$w_{\text{eff}} = \frac{I(0)}{b} = \frac{\pi}{\sqrt{a_2}}. \quad (4-16)$$

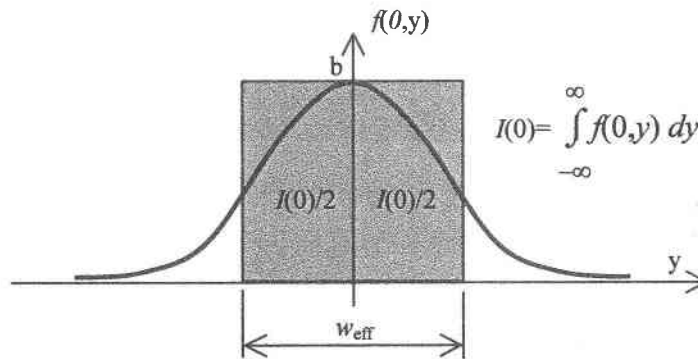


Figure 4-16: Definition of effective width of  $f(0,y)$ .

The effective half-width of (4-14) is linked to the signaling pathway using ideas similar to the average cell approach of the previous sections. Due to the motion of the pigment granule the effective half-width will change with time according to the relation

$$w_{\text{eff}}(t)/2 = w_{\text{eff}}(0)/2 - \int_0^t v(\tau) d\tau, \quad (4-17)$$



where  $v(t)$  is the speed of granule motion towards the distribution center. Using (4-16) for the effective width in (4-17) leads to

$$\frac{1}{\sqrt{a_2(t)}} = \frac{1}{\sqrt{a_2(0)}} - \frac{2}{\pi} \int_0^t v(\tau) d\tau . \quad (4-18)$$

Assuming that the motion of the granules towards the distribution center is proportional to the output reactant concentration  $u(t)$  according to  $v(t) = k_y u(t)$ , gives

$$\frac{1}{\sqrt{a_2(t)}} = \frac{1}{\sqrt{a_2(0)}} - \frac{2}{\pi} \int_0^t k_y u(\tau) d\tau , \quad (4-19)$$

where  $k_y$  is the unknown constant of proportionality. A similar relationship holds for the granule motion in the  $x$  direction:

$$\frac{1}{\sqrt{a_1(t)}} = \frac{1}{\sqrt{a_1(0)}} - \frac{2}{\pi} \int_0^t k_x u(\tau) d\tau . \quad (4-20)$$

In general,  $k_x$  and  $k_y$  can be different. However, the model calibration is simplified significantly if the two coefficients  $a_1$  and  $a_2$  are combined into one coefficient,  $a$ , according to

$$a(t) = \sqrt{a_1(t)^2 + a_2(t)^2} . \quad (4-21)$$

Equations (4-19) and (4-20) can now be replaced by one equation containing a single unknown coefficient  $k$ :

$$\frac{1}{\sqrt{a(t)}} = \frac{1}{\sqrt{a(0)}} - \frac{2}{\pi} \int_0^t k u(\tau) d\tau . \quad (4-22)$$

Equation (4-22) can be used together with the differential equations of the signaling pathway to form a complete input-output model of the system. The resulting model is

calibrated in a similar manner as in the average cell approach. First, the initial coefficient  $a(0)$  is computed from the first image in the sequence. This determines the initial condition for the model. Next, the remaining two unknown coefficients,  $k$  and the input ligand proportionality constant, are determined from the requirements:

1. The final  $a$  coefficient predicted by the system model,  $a(t_{\text{FINAL}})$ , agrees with the corresponding coefficient calculated from the last image in the calibration sequence.
2. The difference between the predicted  $a$  coefficient and  $a(t)$  computed from the calibration sequence is minimal in the least square sense.

The first of these requirements gives  $k$  as

$$k = \frac{\frac{\pi}{2\sqrt{a(0)}} - \frac{\pi}{2\sqrt{a(t_{\text{FINAL}})}}}{\int_0^{t_{\text{FINAL}}} u(\tau) d\tau} \quad (4-23)$$

Equation (4-23) is used iteratively together with requirement 2 to find the ligand proportionality constant that gives the best model.

#### 4.6.4 Modeling Example 4-2: Individual Cell Approach

The approach described in the previous section has been validated on the image sequence of Example 4-1. Figures 4-17 to 4-19 show a small area around a selected cell from the image sequence of Example 4-1. The locations of the distribution center that was found using the methods described in Chapter 4-1 are shown as white dots on the figure. The image sequence was first low-pass filtered with a  $20 \times 20$  pixel two dimensional convolution filter in the shape of a half wave cosine function. It was then processed to find the model coefficients.

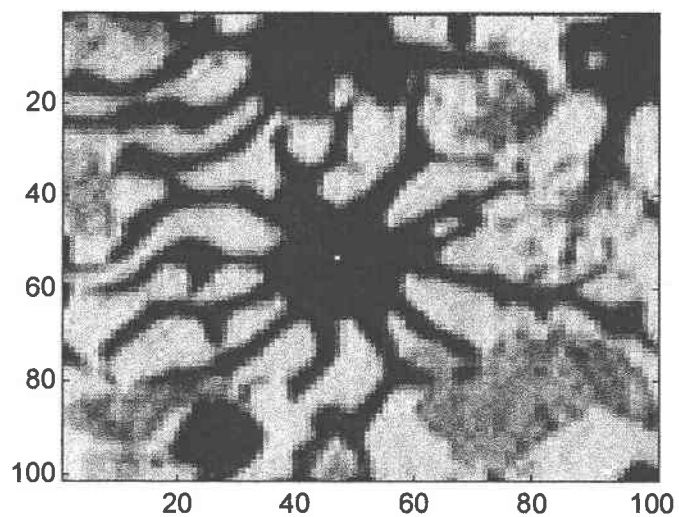


Figure 4-17: Image for calibrating individual cell model ( $t = 0$  s).

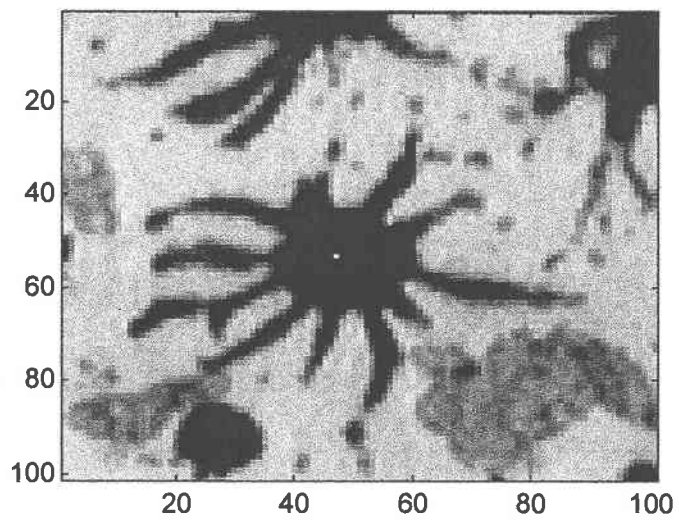


Figure 4-18: Image for calibrating individual cell model ( $t = 59$  s).

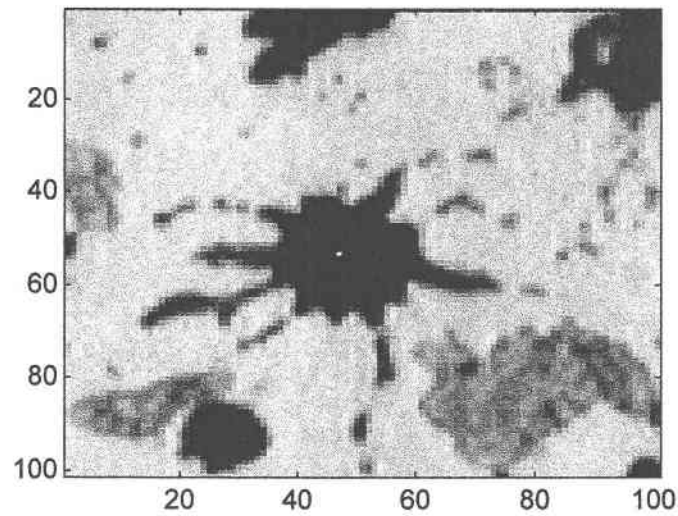


Figure 4-19: Image for calibrating individual cell model ( $t = 103$  s).

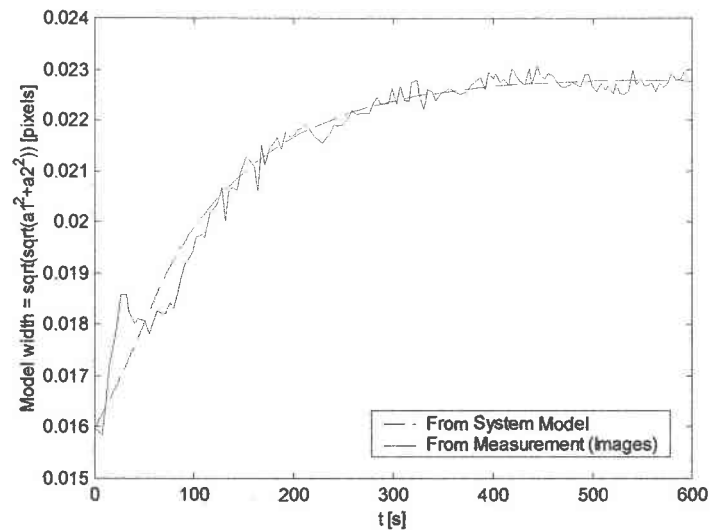


Figure 4-20: Comparison of model widths predicted by pathway model (system model) and computed directly from the image sequence (measured).

Figure 4-20 compares the  $a$  coefficient predicted by the system model with the corresponding coefficient calculated directly from the image sequence. It is seen that the agreement is better at later times than near the initial time. This is related to the fact that

the rectangle used to compute the  $a$  coefficient does not vary with time. Its size is much smaller than optimal initially and becomes optimal near the middle of the simulation. It is likely that the model prediction could be improved using time varying rectangles in the computation of model coefficients.

#### 4.6.5 Average Cell Modeling Approach Applied to Single Cell

The average cell modeling approach described in Section 4.6.1 makes use of the total pigmented area for constructing the system model. As such it is very general, and it works on image sequences which contain only one pigment granule distribution. To illustrate this, the method is applied to the image sequence of Figures 4-17 to 4-19. A comparison between the time evolution of pigmented areas predicted by the system level model and extracted directly from the image sequence is shown in Fig. 4-21.

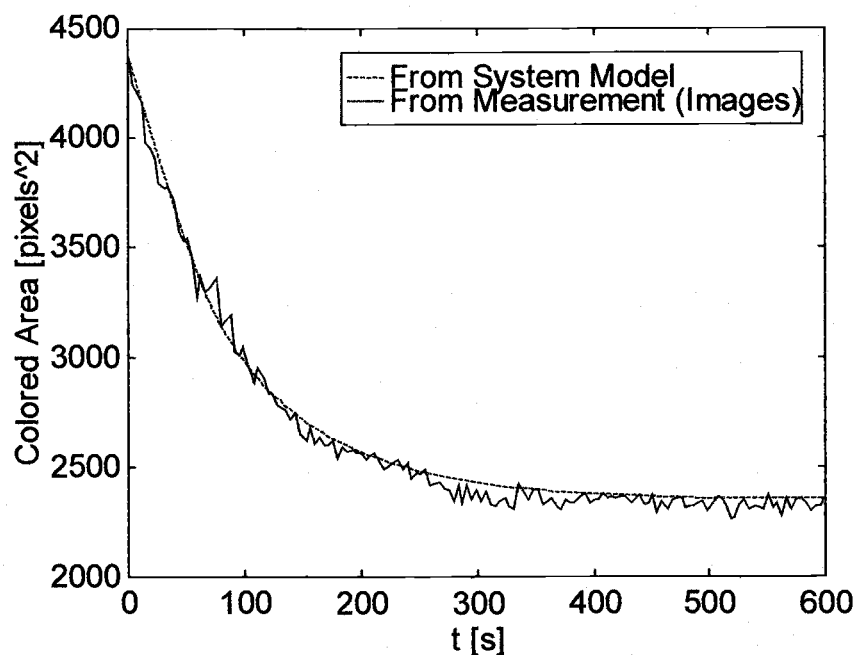


Figure 4-21: Comparison of pigmented areas predicted by pathway model (system model) and computed directly from the image sequence (measured).

## Chapter 5

### Conclusion

In this dissertation, a link between the biological aspect of chromatophores and digital image/video processing techniques developed for sequences of chromatophore microscope images has been established. The link makes it possible to model the complete chromatophore signal transduction pathway which is believed to be involved in pigment granule motion. Two system level models have been developed. Both models begin with the input ligand and end in extracted image features. The two models differ in the type of features extracted and in their applicability. While the first model predicts areas of arbitrary groups of pigment distributions, the second model treats individual pigment distributions and predicts coefficients of an analytical function. The whole modeling process makes use of image and video processing algorithms which have been adapted or developed for this purpose. To the best of the author's knowledge, this is the first full chromatophore  $G_s$ -AC-PKA-granule motion-image feature system level model of this type.

The proposed model has the following possibilities:

- It can be used in both directions:
  - The type and concentration of the applied ligand can be determined based on the aggregation or dispersion of pigment granules.
  - The time evolution of the chromatophore pigment granule areas can be predicted for a given initial ligand concentration.

- Since the model includes detailed information about the concentrations of intermediary substances, it is also possible to predict their concentration from known microscope images.
- The model is determined by only two coefficients. Therefore, it significantly compresses the information needed to describe a particular ligand–chromatophore pair.
- Since the model is determined by only two coefficients, it is practical to build lookup tables of models for a given type of ligand and a given type of chromatophore.

It is the author's belief that the developed model has important potential applications. The applications include:

- Development of intelligent biosensors capable of recognizing the type of applied chemical and its concentration based on easily obtainable low resolution cell images.
- Development of experiments that will lead to a better understanding of the Gs–AC–PKA–granule motion pathway in chromatophores and other cells.

All of the above areas represent opportunities for further study and refinement of the model.

Additional items for future exploration and research include:

- Mathematical reduction of the model's system of differential equations.
- Error estimation for principle component analysis .
- Investigation of the robustness of segmentation.
- Local motion estimation for non-integer movement of small objects.
- The effect of noise on the motion vectors estimates.
- Develop other relationships between cell biology and image/video processing.

- Electromagnetic biosensors (lower frequency of EM waves than visible light).
- Research the effect of brain cells in the control of cell organelle movement.



## Bibliography

- [1] Celia M. Henry, "Systems biology," CENEAR, vol. 81, No. 20., pp. 45–55, May, 2003.
- [2] H. Kitano, "Systems biology: a brief overview," *Science*, vol. 295, pp. 1662–1664, 2002.
- [3] Bruce Alberts, Dennis Bray, Julian Lewis, Martin Raff, Keith Roberts, and James D. Watson, *Molecular Biology of the Cell*, Garland Publishing, 1994.
- [4] Annika Karlsson, *Signaling for color change in melanophores and a biosensor application*, Ph.D. Thesis, Linköping University, 2001.
- [5] Bjorn S. Skalhegg and Kjetil Tasken, "Specificity in the cAMP/PKA signaling pathway. Differential expressions, regulation, and subcellular localization of subunits of PKA," *Frontiers in Bioscience* 2, pp. 331-342, 1997.
- [6] A. R. Reilein, I. S. Tint, N. I. Peunova, G. N. Enikolopov, V. I. Gelfand, "Regulation of organelle movement in melanophores by protein kinase A (PKA), protein kinase C (PKC), and protein phosphatase 2A (PP2A)," *J. Cell Biology*, vol. 142, no. 3, pp. 803–813, Aug., 1998.
- [7] N. Uchida-Oka, M. Sugimoto, "Norepinephrine induces apoptosis in skin melanophores by attenuating cAMP-PKA signals via alpha2-adrenoceptors in the medaka, *Oryzias latipes*," *Pigment Cell Res.*, vol. 14, no. 5, pp. 356–361, Oct. 2001.
- [8] Gabor C. Temes, Un-Ku Moon, Frank Chaplen, Wojtek Kolodziej, Thirumalai Rengachari, Vivek Sharma, and Cheng-Yan Peng, "Research on Electronic Cytosensors Progress Report for 2002," [www.catalystfoundation.org/Recipients/Projects/Oregon02Rep.pdf](http://www.catalystfoundation.org/Recipients/Projects/Oregon02Rep.pdf)
- [9] Stephen L. Rogers, Irina S. Tint, Philip C. Fanapour, and Vladimir I. Gelfand, "Regulated bi-directional motility of melanophore pigment granules along microtubules in vitro," *Proc. Natl. Acad. Sci. USA, Cell Biology*, Vol. 94, pp. 3720-3725, April 1997.
- [10] Database of Quantitative Cellular Signaling, The National Center of Biological Sciences, Bangalore, India, <http://doqcs.ncbs.res.in>.
- [11] M., Adami, I. Zolfino, S. Fenu, D. Nardelli, C. Nicolini, "Potentiometric alternating biosensing toxicity tests on cell population", *J. Biochem. Biophys. Methods*, vol. 32, pp. 171–181, 1996.
- [12] Lubert Stryer, *Biochemistry*, W. H. Freeman and co., 1995.

- [13] Sally E. Nyquist and Kathryn Brady Toner, "Pigment granule transport in chromatophores," [www.zoo.utoronto.ca/able/volumes/vol-18/8-nyquist.pdf](http://www.zoo.utoronto.ca/able/volumes/vol-18/8-nyquist.pdf).
- [14] K. Pearson, "On lines and planes of closest fit to systems of points in space," *Philos. Mag.*, 6(2): pp. 559–572, 1901.
- [15] H. Hotelling, "Analysis of a complex of statistical variables into principal components," *Journal of Educational Psychology*, 24, pp. 417–441, pp. 498–520, 1933.
- [16] K. Karhunen, "Über lineare methoden in der wahrscheinlichkeitsrechnung," *Amer. Acad. Sci., Fennicade, Ser. A, I*, 37: 3–79, 1947. (English translation: RAND Corporation, Santa Monica, California, Rep. T-131, Aug. 1960).
- [17] M. Loeve, "Fonctions aleatoires de seconde ordre," in P. Levy, *Processus Stochastiques et Mouvement Brownienne*, Paris, France: Hermann, 1948.
- [18] R. A. Johnson and D. W. Wichern, *Applied Multivariate Statistical Analysis*, Prentice Hall, Englewood Cliffs, New Jersey, 1992.
- [19] B. Kögl, *Principal Curves: Learning, Design, and Applications*, Ph.D. Thesis, Concordia University, Montreal, Canada, 1999.
- [20] Murat A. Telkap, *Digital Video Processing*, Prentice Hall, 1995.
- [21] Bruce D. Lucas and Takeo Kanade, "An iterative image registration technique with an application to stereo vision," *Proc 7<sup>th</sup> Intl Joint Conf. on Artificial Intelligence (IJCAI)*, Vancouver, British Columbia, pp. 674–679, August 24–28, 1981.
- [22] James R. Bergen, Peter J. Burt, Rajesh Hingorani, and Shmuel Peleg, "A three-frame algorithm for estimating two-component image motion," *IEEE Transactions on Pattern Analysis and Machine Intelligence*, vol. 14, no. 9, September 1992.
- [23] A. Dumitras, A. Jerbi, and F. Kossentini, "A segmentation method for still images using a Z-shaped nonlinear transform," Proposal for the International Organisation for Standardization ISO/IEC JTC1/SC29/WG11 Coding of Moving Pictures and Audio, Lancaster, UK, February 1998.
- [24] J. R. Parker, *Algorithms for Image Processing*, John Wiley & Sons, Inc, New York, 2000.
- [25] A. K. Jain, *Fundamentals of Digital Image Processing*, Prentice Hall, Englewood Cliffs, NJ, 1989.
- [26] G. Sharma, H. J. Trussell, "Digital color imaging," *IEEE Trans. Image Processing*, vol. 6, no. 7, pp. 901–931, July, 1997.

- [27] H. J. Trussell, "DSP solutions run the gamut for color systems," *IEEE Signal Processing Magazine*, pp. 8–23, April 1993.
- [28] S. F. Ellermeyer and L. L. Combs, Tutorial on Chemical Reactions, Kennesaw State University, 2000.